AD-A031 071 BATTELLE COLUMBUS LABS OHIO F/G 11/6
INITIAL DEVELOPMENT OF A FATIGUE-CRACK-RETARDATION MODEL.(U)
JAN 76 M F KANNINEN, C E FEDDERSEN N62269-74-C-0618
UNCLASSIFIED BATT-G-2920 NADC-76076-30 NL

1 OF 2
AD
A031071

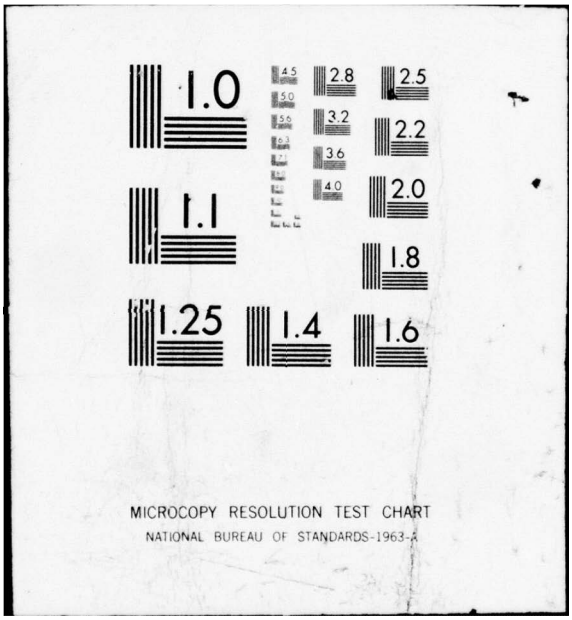
1.0
1.1
1.25
1.4
1.6
1.8
2.0
2.2
2.5
2.8
3.2
3.6
4.0
4.5
5.0
5.6
6.3
MICROCOPY RESOLUTION TEST CHART
NATIONAL BUREAU OF STANDARDS-1963-A

NADC-76076-30

INITIAL DEVELOPMENT OF A FATIGUE-CRACK-RETARDATION MODEL

M. F. Kanninen
C. E. Feddersen
BATTELLE
Columbus Laboratories
505 King Avenue
Columbus, Ohio 43201

C. Atkinson
Imperial College
London, England

31 January 1976

Final Report for Period 18 June 1974 - 31 December 1975

Prepared for

NAVAL AIR DEVELOPMENT CENTER
Warminster, Pennsylvania 18974

NADC-76076-30

INITIAL DEVELOPMENT OF A FATIGUE-CRACK-RETARDATION MODEL

M. F. Kanninen
C. E. Feddersen
Battelle
Columbus Laboratories
505 King Avenue
Columbus, Ohio 43201

C. Atkinson
Imperial College
London, England

31 January 1976

Final Report for Period 18 June 1974 - 31 December 1975

Approved for public release; distribution unlimited.

Prepared for

NAVAL AIR DEVELOPMENT CENTER
Warminster, Pennsylvania 18974

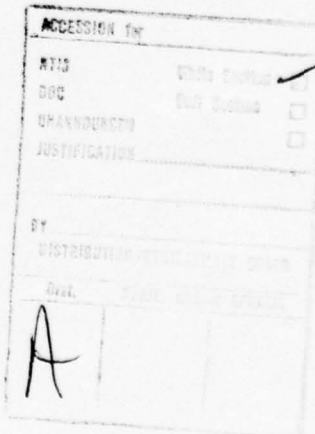

Unclassified

SECURITY CLASSIFICATION OF THIS PAGE (When Data Entered)

(19) REPORT DOCUMENTATION PAGE

READ INSTRUCTIONS BEFORE COMPLETING FORM

(18) 1. REPORT NUMBER: NADC-76076-30

2. GOVT ACCESSION NO.

3. RECIPIENT'S CATALOG NUMBER

(6) 4. TITLE (and Subtitle): Initial Development of a Fatigue-Crack-Retardation Model.

5. TYPE OF REPORT & PERIOD COVERED: Final--18 June 1974 - 31 December 1975

6. PERFORMING ORG. REPORT NUMBER: G-2920

(10) 7. AUTHOR(S): M. F. Kanninen, C. E. Feddersen, C. Atkinson

(15) 8. CONTRACT OR GRANT NUMBER(s): N62269-74-C-0618 NEW

9. PERFORMING ORGANIZATION NAME AND ADDRESS
Battelle's Columbus Laboratories
505 King Avenue
Columbus, Ohio 43201

10. PROGRAM ELEMENT, PROJECT, TASK AREA & WORK UNIT NUMBERS
Task WR02303001
W.U. DG-602

11. CONTROLLING OFFICE NAME AND ADDRESS
Naval Air Development Center
Warminster, Pennsylvania 18974

(11) 12. REPORT DATE: 31 January 1976

13. NUMBER OF PAGES: 119

14. MONITORING AGENCY NAME & ADDRESS (if different from Controlling Office)
DCASO, Columbus
Building 1, Section 1
Defense Construction Supply Agency
Columbus, Ohio 43215

(12) 123p.

15. SECURITY CLASS. (of this report): Unclassified

15a. DECLASSIFICATION/DOWNGRADING SCHEDULE

16. DISTRIBUTION STATEMENT (of this Report)

~~Approved for public release; distribution unlimited.~~

(9) Final rept. 18 Jun 74 - 31 Dec 75,

17. DISTRIBUTION STATEMENT (of the abstract entered in Block 20, if different from Report)

Approved for public release; distribution unlimited.

(14) BATT-G-2920

18. SUPPLEMENTARY NOTES

(16) WR02-303 (17) WR02-303-001

19. KEY WORDS (Continue on reverse side if necessary and identify by block number)

Fatigue-crack retardation
Fatigue-crack propagation
Ti-6Al-4V

20. ABSTRACT (Continue on reverse side if necessary and identify by block number)

A fatigue-crack-propagation model is developed by reducing crack-tip plasticity to a single pair of enlarged dislocations, termed superdislocations, whose response is equivalent to that of the aggregate plastic zone. The crack-tip damage or deformation and accompanying incremental crack advance resulting from each loading cycle are accumulated in a single super-superdislocation pair for residual interaction on the next loading cycle. Key features of this development are that the required material parameters are

DD FORM 1 JAN 73 1473 EDITION OF 1 NOV 65 IS OBSOLETE

407080

Unclassified

SECURITY CLASSIFICATION OF THIS PAGE (When Data Entered)

20. are limited to the shear modulus, Poisson's ratio, and tensile-yield strength, and that crack-surface closure is accommodated. A significant simulation of the fatigue-crack-propagation process along with a promising correlation with experimental results are achieved.

SUMMARY

A fatigue-crack-propagation model is developed by reducing crack-tip plasticity to a single pair of aggregate dislocations, termed superdislocations, whose response is equivalent to that of the entire plastic zone. The crack-tip damage or deformation and accompanying incremental crack advance resulting from each loading cycle are accumulated in a single superdislocation pair for residual interaction on the next loading cycle. Key features of this development are that the required material parameters are limited to the shear modulus, G, Poisson's ratio, ν, and tensile-yield strength, Y, and that crack-surface closure is accommodated. A significant simulation of the fatigue-crack-propagation process along with a promising correlation with experimental results are achieved.

At its present stage of development, this model provides a useful characterization of the fatigue-crack-propagation process. Substantial indications of its success include

(1) A constant crack-growth rate under uniform cyclic loading.

(2) Predicted crack-growth rates which are remarkably close to the experimentally determined values for two different materials--an aluminum alloy and a titanium alloy. The predictions for the case R = 0.5 are particularly outstanding.

(3) Predictions from fundamentally correct considerations without the use of empirical parameters of any kind. The only parameters that are required are the ordinary mechanical properties G, ν, and Y.

(4) An automatic inclusion of the crack-closure phenomenon.

Areas requiring further improvement and refinements include (1) the effect of varying the stress ratio, R, (2) adequate overload perturbation on the steady-state-growth rate, and (3) reduction in the computational time required. Recommendations for the next stage of development and the future work required are presented in the report.

PREFACE

This research program has been conducted by the Structures and Mechanics Research Department, Battelle's Columbus Laboratories, Columbus, Ohio, under Contract No. N62269-74-C-0618. This contract was initiated under Work Unit No. DG-602 of basic AIRTASK No. WR02303001. The program was administered by the Air Vehicle Technology Department, Naval Air Development Center, Warminster, Pennsylvania, with Mr. Paul Kozel providing technical liaison. This report summarizes work performed during the period June 18, 1974, through December 31, 1975.

The experimental portions of this research program were accomplished by James F. Wood and Henry J. Malik of the Structural Engineering Laboratories. The metallographic appraisals contained in this report were contributed by Richard A. Wood. The survey of microstructural influences was prepared by Dr. Alan R. Rosenfield.

CONTENTS

LIST OF ILLUSTRATIONS

LIST OF ILLUSTRATIONS

LIST OF TABLES

1. INTRODUCTION

Fatigue-crack-propagation rates can be predicted with reasonable accuracy using empirical relations when simple constant-amplitude cyclic loading is applied. The load interaction phenomenon occurring in variable-amplitude loading has not yet been properly analyzed, however. This precludes the accurate prediction of fatigue-crack-growth rates under the spectrum (service) loadings that act on aircraft and other engineering structures. To provide a quantitative formulation for fatigue-crack growth under arbitrary load sequences, a fundamentally sound analysis technique must be developed. At the same time, to be useful for routine engineering analyses, the required analysis procedure must remain as simple as possible.

The goal of the research described here is to develop an accurate computational procedure for the prediction of fatigue-crack propagation that can be used in engineering applications. To achieve this goal

(1) The model must be capable of handling load cycles that vary arbitrarily from cycle to cycle while taking the load interaction effects properly into account.

(2) The material properties required by the model in calculating crack-growth rates for given cyclic load histories must be based upon well-established mechanical properties that are independent of the particular load spectrum under consideration.

(3) The computational procedure evolved must be efficient enough to enable calculations to be carried out over load histories corresponding to actual service conditions.

To meet these criteria, a unique approach leading to a mathematical predictive model for fatigue-crack propagation based on the "inclined-strip-yield-super-dislocation" representation of crack-tip plasticity has been devised. The model represents an effective compromise between approaches that sacrifice some of the basic aspects of fatigue-crack propagation in the interest of simplicity and a completely rigorous (and, consequently, exceedingly cumbersome) approach.

The basis of the model, together with some verifications obtained by comparison with established results in fracture and fatigue, is given in this

report. Also, an experimental program on Ti-6Al-4V designed to implement the development of the model and, ultimately, to verify its predictions is described. Comparisons between the predictions of the model and experimental results are then given. Finally, the present state of work is summarized and recommendations for further work given. For the convenience of the reader, the bulk of the mathematical and experimental details have been omitted from the main body of the report and appear in appendices.

2. GENERAL DESCRIPTION OF THE MATHEMATICAL MODEL

There is currently no complete agreement on the fundamental mechanisms that control fatigue-crack propagation. Nevertheless, there are several features of the problem that are generally accepted as playing an essential role in the process. These must be taken into account in a proper analysis. They include

- The interaction between the plastic deformation produced by the current load and the residual plasticity created in previous load cycles.
- The connection that exists between the local deformation at the crack tip--as characterized by the crack-tip-opening displacement--and the crack-growth increment.
- The closure of the crack faces during the unloading portion of the load cycle prior to reaching the minimum load level.

While analytical models have been developed from one or another of these basic effects, no previously developed analysis rigorously incorporates them all. This includes models employing a finite-element method which are impractical beyond a few load cycles.

The fatigue-crack-propagation model described in this report is based on the well-established fact that macroscopic plasticity can be considered in terms of dislocation arrays. Figure 2.1 illustrates how this basic concept has evolved into the fatigue model being developed here. The following discussion elaborates on the conceptual picture given by Figure 2.1 and, in addition, delineates the individual roles played in this work by the various components (e.g., the superdislocation concept) of the complete cycle-by-cycle fatigue-crack-propagation model.

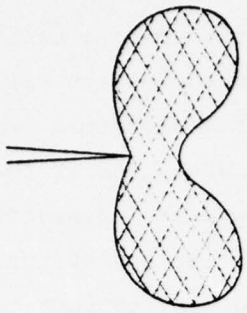

(a) Plane strain plastic deformation at the tip of a crack under fixed load

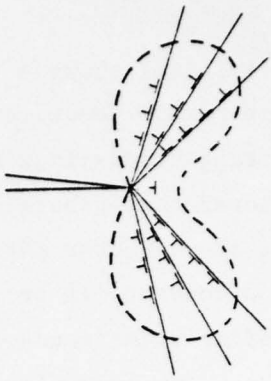

(b) Representation of crack-tip plasticity by dislocation arrays

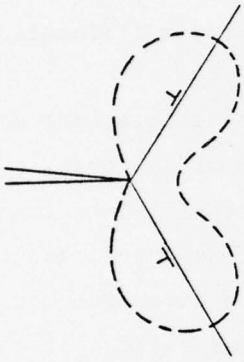

(c) Representation of crack-tip plasticity by a superdislocation pair confined to slip planes emanating from the crack tip

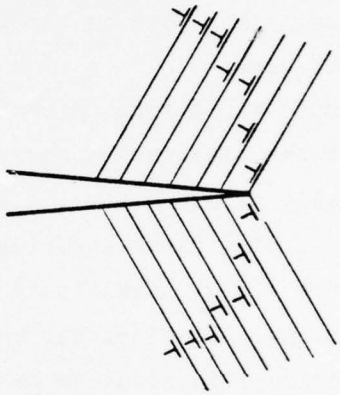

(d) Representation of crack-tip plasticity during fatigue by superdislocations

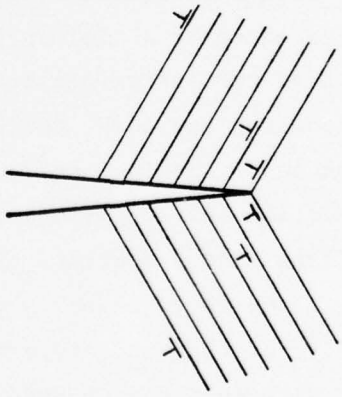

(e) Representation of crack-tip plasticity during fatigue by combination of superdislocations and super-superdislocations

FIGURE 2.1. EVOLUTION OF A FATIGUE-CRACK-GROWTH MODEL USING THE INCLINED-STRIP-YIELD SUPERDISLOCATION REPRESENTATION OF CRACK-TIP PLASTICITY

Figure 2.1(a) shows a typical plastic enclave surrounding a crack tip under plane-strain conditions. Figure 2.1(b) shows an equivalent way of characterizing crack-tip plasticity through the use of dislocation arrays. It might be noted that generally there is no significant advantage of the dislocation point of view over the conventional continuum approach. However, the dislocation concept can be reduced to a simpler way of looking at the problem that can offer significant computational advantages in applications to fracture and fatigue. In particular, by representing crack-tip plasticity by planar (one-dimensional) dislocation arrays in a "strip-yield-zone" model, considerable mathematical simplification can be obtained without sacrificing too much accuracy. This fact is the prime motivation for adopting a dislocation-based approach here.

Strip-yield-zone characterizations of crack-tip plasticity are most easily made if the dislocation array is confined to the plane of the crack. While reasonably accurate for the plane-stress conditions existing in a thin section, this is a poor representation for plane-strain conditions where, as indicated in Figure 2.1(a), plasticity tends to spread out in the direction normal to the crack plane. To characterize the latter case, Bilby and Swinden [1]* took the dislocation slip plane to be inclined to the crack plane. But, they were then able to obtain only an approximate numerical solution. The work of Atkinson [2-4] circumvented the mathematical difficulties in the "inclined-strip-yield" model by introducing the idea of a superdislocation. As shown in Figure 2.1(c), the superdislocation is considered to be a dislocation of arbitrary strength that represents the net effect of the entire dislocation array on the given slip plane. By the superdislocation approach, the problem is reduced to two algebraic equations in two unknowns. It is important to recognize that, although this simple representation has its limitations (e.g., in predicting the plastic zone size), it offers a very accurate prediction of the crack-tip opening displacement. This will be shown later in this report.

The mathematical simplicity of the superdislocation representation of crack-tip plasticity combined with an accurate prediction of the state of deformation at the crack tip gives this approach a strong appeal for use in a fatigue-crack-propagation model. In fact, this is the basis of the model described in this report. That is, the several crack-tip-connected phenomena

---

* References are listed on page 65.

that are generally accepted as playing an essential role in the fatigue-crack-growth process, namely (1) the interaction between the plastic deformation produced by a load and the residual plasticity created in previous load cycles; (2) the connection that exists between the deformation at the crack tip and the crack-growth increment; and (3) the fact that the crack faces can impinge during the unloading portion of the load cycle prior to reaching the minimum load level can all be taken into account with the superdislocation on an inclined-slip-plane idea.

At this point, it will be useful to identify and distinguish between the two complementary computational approaches that are being pursued in this work. The first is the complete or cycle-by-cycle fatigue-crack-growth model in which one superdislocation pair is generated and retained in the computation for each load cycle considered. This is shown in Figure 2.1(d). The second approach is the super-superdislocation idea shown in Figure 2.1(e). In the latter case, the residual plasticity is represented by lumping two or more superdislocations together to reduce the computational effort required. While the intention is to integrate them eventually, they are being pursued separately at present. Therefore, their relative advantages and disadvantages will be discussed here individually.

The complete cycle-by-cycle fatigue-crack-growth model employing the inclined strip-yield-superdislocation representation of crack-tip plasticity has now been substantially developed. This model is believed to be uniquely capable of providing the basis for meeting the objectives of this research as stated in the Introduction. Substantial indications that the model will be successful already exist. As described in more detail later in this report, these are as follows:

(1) After a transient period, the model produces a constant crack-growth rate under uniform cyclic loading. Because there is nothing built into the model that will force this to happen, this can be taken as one verification of the procedure.

(2) The predicted crack-growth rates for the uniform cyclic loading are remarkably close to the experimentally determined values for two different materials: an aluminum alloy and a titanium alloy. The predictions for the case R = 0.5 are particularly outstanding.

(3) The model can be used to make predictions from fundamentally correct considerations without the use of empirical parameters or "fudge factors" of any kind. The only parameters that are required are the ordinary mechanical properties G, ν, and Y.

(4) The much-discussed crack-closure phenomenon is automatically taken into account in the model. This is done both simply and accurately without requiring any ad hoc empirical approximations. This is accomplished via the singularity canceling equation which, when satisfied, assures that the crack forces will close smoothly at the crack tip.

However, the present cycle-by-cycle model suffers from the following disadvantages:

(1) The effect of increasing R while holding ΔK constant causes a modest decrease in the predicted growth rate. The experimentally observed result is a marked increase in growth rate.

(2) While an overload cycle perturbs the steady-state growth rate for a time, the observed crack-growth retardation phenomenon in which the crack-growth rates can be reduced by two orders of magnitude is not reproduced.

(3) The computer time required to perform many successive load cycles, while not unduly costly for research purposes, is prohibitive for engineering use.

While each of these may appear to be a formidable barrier to the successful development of the model, a number of alternatives have been identified which may provide a means of circumventing them. These are described in the concluding section of this report.

The use of the inclined-strip-yield-superdislocation representation of crack-tip plasticity in a mathematical predictive model for fatigue-crack propagation has suggested the use of a simpler lumped or super-superdislocation model. With this approach, the following verifications have been obtained.

(1) A prediction of the crack-tip crack-opening displacement under fixed load that compares very well with highly precise finite-element computations.

(2) A prediction of a steady-state fatigue-crack-propagation rate that is in good qualitative agreement with experimental results.

(3) A prediction of the crack-growth retardation in a uniform cyclic loading interrupted by a peak overload that approximates the observed effect reasonably well.

In the first of these verifications, there is no difference between the superdislocation and the super-superdislocation models. In the latter two cases, the super-superdislocation represents the aggregate effect of the residual plasticity associated with a multiplicity of superdislocations that were created over a large number of load cycles.

It may be useful to further amplify the distinction between the computational models based on the superdislocation and super-superdislocation concepts that are used in the work described in this report. The ultimate goal of the work is to develop a computational model that can be applied to predict fatigue-crack-growth rates in real service conditions. This calls for a mathematical model that is versatile enough to accept essentially random changes in the cycle-to-cycle applied loadings while remaining simple enough to enable it to be applied to lengthy load histories. The work reported here has progressed far enough to make it clear that a cycle-by-cycle superdislocation model can satisfy the first of these requirements, but not the second. However, a modification to lump the effect of possibly ten superdislocations into one or more single degrees of freedom super-superdislocations can allow the model to achieve the second criterion. The number of these super-superdislocations that are required will, of course, depend upon the complexity of the load spectrum being considered. Nevertheless, it is conceivable that the total number of degrees of freedom (superdislocations plus super-superdislocations) need not exceed ten. If borne out by subsequent work, this will allow the model to display both the versatility and efficiency that it must have to qualify as a basic engineering tool.

While the prime purpose of the super-superdislocation concept is as described, it has also been put to a secondary use. The secondary use is in constructing simple models for steady-state fatigue with and without interruption by an overload. These models are not intended to replace the cycle-by-cycle computational model in any sense. Rather, the intent is to have a basis for testing the various concepts and computational options that are being considered for incorporation into the complete model. The linearized super-superdislocation fatigue models permit this; first, without the necessity for using computer time (because simple closed form relations can be obtained in

this case) and, second, because an interpretation can be obtained in a clean-cut manner. Thus, these models complement the complete cycle-by-cycle model. They do not compete with it but, instead, act as auxiliary aids to assist in its development.

To help make this essential point clearer, the above description is essentially repeated in Table 2.1. In the table, each level of the model is given together with its purpose, its strengths, and its weaknesses in order of ultimate usefulness.

3. GENERAL DESCRIPTION AND RESULTS OF THE EXPERIMENTAL PROGRAM

To refine and confirm a large quantity of experimental data obtained on previous NADC-sponsored programs [5,6], selected fatigue-crack-propagation experiments on center-cracked specimens of Ti-6Al-4V alloy plate were conducted to provide more positive substantiation of the specific analytical developments of this research program. Included were the generation of fatigue-crack-propagation data under conditions of constant cyclic stress-intensity-factor range (i.e., constant ΔK), the study of the overload effects on crack-growth retardation, the calibration of specimen compliance, and observations of crack-closure effects.

In general, for basic fatigue-crack-propagation characterization, data are generated under constant-amplitude loading. However, in this program, to permit a more definitive description of crack behavior, fatigue-crack-propagation data were generated under conditions of constant cyclic stress-intensity factor range, ΔK, achieved by decrementing the load with increasing crack length in the center-cracked specimen. This approach has the advantage of allowing the dependency of fatigue-crack-propagation rate, da/dN, on K or ΔK to be more clearly established as well as permitting a large number of overload combinations to be studied over a range of crack lengths in one specimen.

Both mill-annealed (½-inch thick) and beta-processed (5/16-inch thick) Ti-6Al-4V titanium alloy material were evaluated. The basic experimental details of this research program are presented in Appendix B. Descriptions of test specimens, materials, and experimental details of this research program are presented in Appendix B. Descriptions of test specimens, materials, and experimental procedures are included.

TABLE 2.1. HIERARCHY OF THE COMPUTATIONAL MODELS USED IN THIS WORK

Model	Basic Purpose	Strong Point	Weak Point
Super-superdislocation representation of crack-tip plasticity (linearized)	Provides testing ground for concepts and computational procedures without resorting to the computer	Gives qualitative guidance on effect of various factors influencing growth rates	Cannot give quantitative predictions of crack-growth rates from first principles
Cycle-by-cycle superdislocation representation of crack-tip plasticity	Provides quantitative predictions of fatigue-crack-propagation for simple load histories	Gives accurate predictions of crack-growth rates from first principles	Cannot accommodate a large number of previous load cycles
Superdislocation representation of "near trip" crack-tip plasticity with super-superdislocation representation of residual plasticity	Provides quantitative prediction of fatigue-crack propagation with arbitrarily varying load histories	Gives accurate predictions of crack-growth rates in realistic amounts of computer time	Cannot accommodate wild fluctuations in cycle-to-cycle load history

In general, the results were quite consistent with previously generated data. Of surprise, however, was the lower fatigue-crack-propagation-rate behavior observed in the beta-processed material. A comparative summary of these and previously generated rate data is shown in Figure 3.1. Other significant results included

(1) Fatigue-crack-growth curves generated under constant stress-intensity-factor range (ΔK) conditions exhibited a linear behavior until the crack exceeded half the specimen width confirming the dominance of ΔK as a primary variable.

(2) The beta-processed material exhibited a much coarser macroscopic surface texture than the mill-annealed material for equivalent testing conditions.

(3) Overloads provided definitive retardation (i.e., more than 10,000 cycles of retarded growth) only when the overload exceeded the nominal maximum cyclic stress by a factor of 2 (i.e., 100 percent overload).

(4) Compliance response of the specimen was consistent with the analytically derived values.

(5) Crack closure, although elusive to evaluate quantitatively, was a very detectable phenomenon.

4. BASIC DESCRIPTION OF THE COMPUTATIONAL MODEL AND THE ANALYSIS PROCEDURE

Preliminary Discussion

The mathematical derivation of the basic equations for the cycle-by-cycle predictive model for fatigue-crack growth under arbitrary spectrum loading is given in Appendix A of this report. For this reason, it will only be outlined here.

The essential idea upon which the model is based is that microscopic crack-tip plasticity generally can be represented by dislocation arrays. To simplify the mathematics for fatigue-crack propagation, it is further assumed that the plastic deformation created by a cycle of load can be adequately represented by a single superdislocation. That is, the plastic deformation symmetric with respect to the crack plane is represented by a single pair of

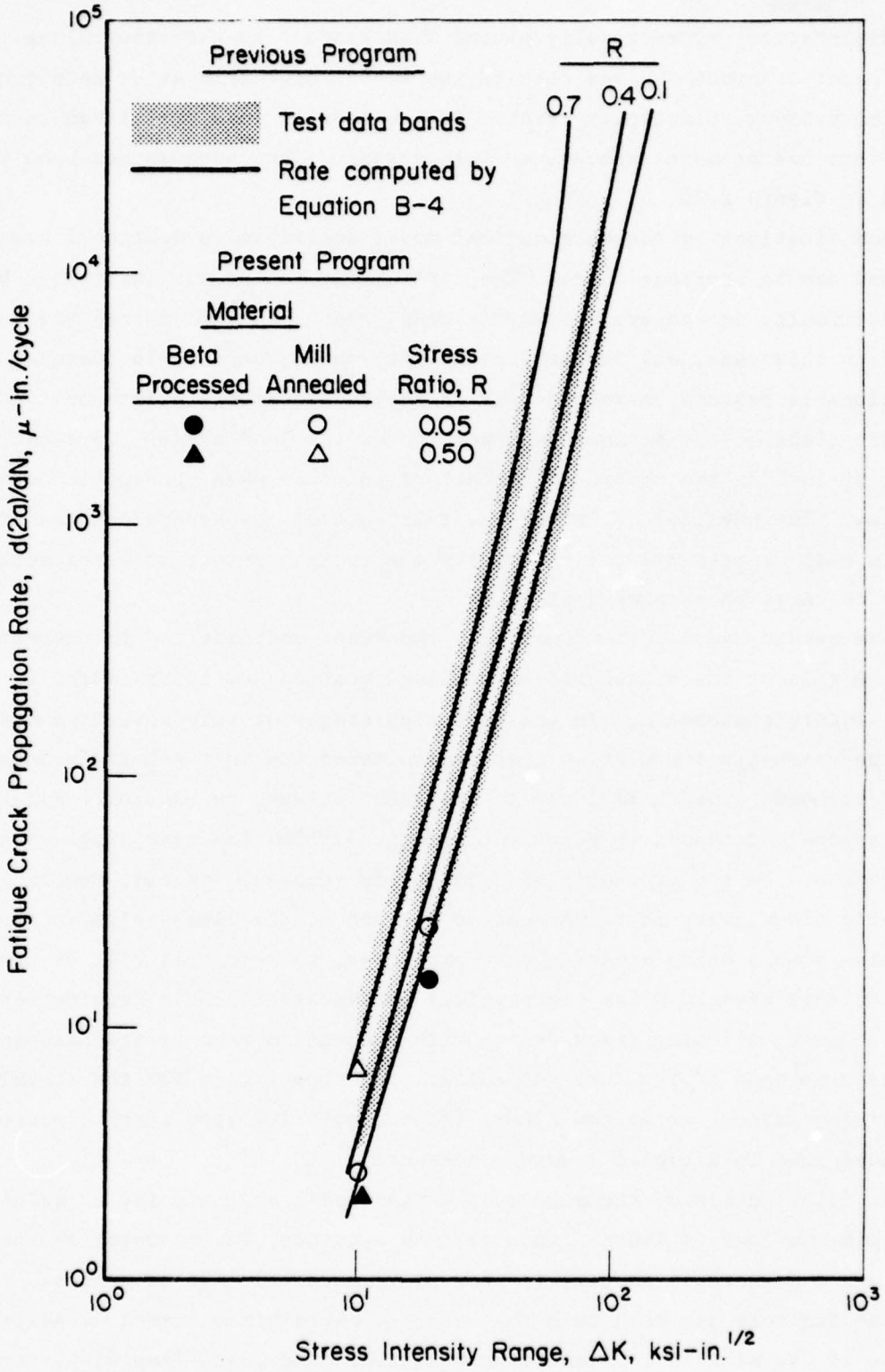

FIGURE 3.1. COMPARISON OF PRESENT AND PREVIOUS DATA
(See Appendix B also)

superdislocations symmetrically placed with respect to the crack plane. A final major assumption gives rise to the super-superdislocation model; namely, that the residual plasticity created in a series of load cycles can be aggregated into one or more super-superdislocations. This process has been illustrated in Figure 2.1.

Modifications to the mathematical model described in Section 2 have been made and can be mentioned here. The first modification was instituted because of a difficulty in the cycle-by-cycle model when the minimum load was set to zero. In this case, all residual plasticity could vanish. To overcome this objectionable feature, a second pair of superdislocations exists on the crack-tip slip plane on the minimum load portion of the load cycle. This has the effect of locking the nascent dislocations in place when the applied stress vanishes. The physical basis for the existence of the second pair is crack closure which represents the plasticity due to the contact stresses acting on the crack faces where they impinge.

The second and more fundamentally important modification is connected with the role of the singularity-canceling equation and its relation to the crack-closure phenomenon. In the beginning stages of this work, the notion that the crack-tip singularity must be abolished (as in the Dugdale model) was not questioned. Eventually, two inconsistencies were recognized. First, the dislocations introduced to represent plastic deformation have singular points that remain when the crack-tip singularity is removed. Second, removing the crack-tip singularity is tantamount to setting $\mathcal{J}$, the linear-elastic fracture-mechanics strain energy-release rate parameter, to zero. As will be shown later in this report, $\mathcal{J}$ has the physical interpretation of a driving force for crack advance, allowing crack growth with $\mathcal{J}$ equal to zero is inconsistent with the basic notions of fracture mechanics. The proper role for the singularity-canceling equation, it is now clear, is in connection with crack closure under a reduced load in a cyclic loading sequence.

An illustration of the superdislocation model at the point at which the first minimum load is imposed in a loading sequence, during which the crack has grown a measurable amount, is shown in Figure 4.1. It is supposed that the load sequence has been such that crack closure has occurred necessitating the use of the singularity-canceling equation. The crack-face displacements would then be roughly as shown (NB, the figure is not drawn to scale). Please

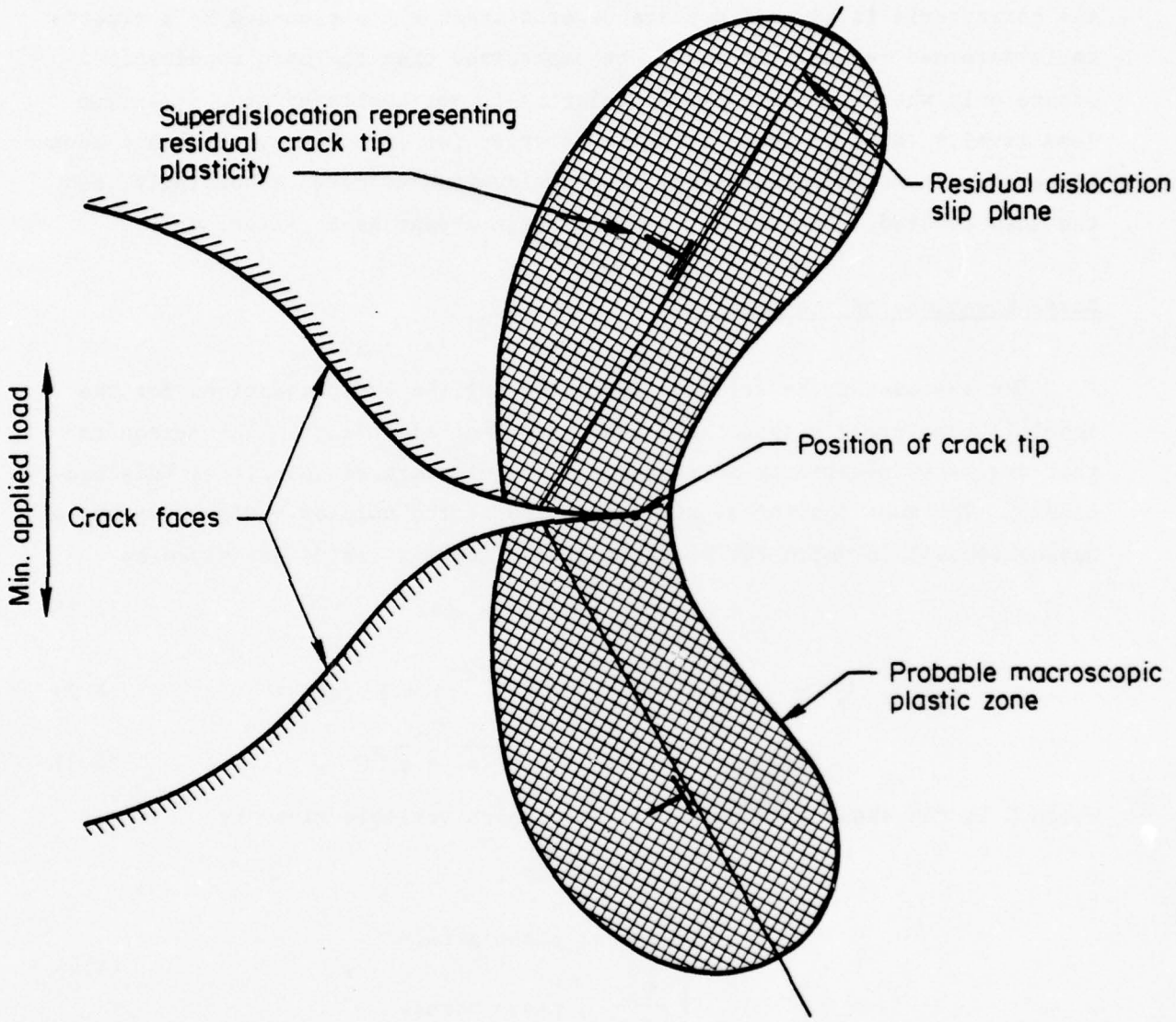

FIGURE 4.1. ILLUSTRATION OF SUPERDISLOCATION REPRESENTATION OF CRACK-TIP PLASTICITY SHOWING CRACK CLOSURE AT MINIMUM LOAD LEVEL IN A CYCLIC LOADING SEQUENCE

note that the plastic zones portrayed in this and the following figures are not computed in the model. They are shown only to clarify the way in which the superdislocation idea can represent crack-tip plasticity.

The situation when the load is increased to a maximum level is illustrated in Figure 4.2. Here the crack tip is assumed to be open and to have the characteristic blunted appearance of a crack tip surrounded by a plastically deformed region. It should be emphasized that the open appearance occurs only when the crack-tip singularity is not abolished at the maximum load level.* Having the equilibrium solution for this state, the crack advance increment can be calculated, the superdislocation adjusted accordingly, and the load reduced. The crack tip would again appear as in Figure 4.1.

Basic Equations of the Model

The approach to be followed in developing the basic equations for the model is completely within the linear theory of elasticity. The reason is that crack-tip plasticity is represented by discrete singularities (dislocations). The most convenient representation is the complex variable method of Muskhelishvili in which the stress and displacement fields are given by

$$\sigma_{xx} + \sigma_{yy} = 4 \text{ Re } \{\phi'(z)\} , \tag{4.1}$$

$$\frac{1}{2}(\sigma_{yy} - \sigma_{xx}) + i\tau_{xy} = \bar{z}\,\phi''(z) + \psi'(z) , \tag{4.2}$$

$$2G\,(u+iv) = \kappa\phi(z) - z\,\overline{\phi'(z)} - \overline{\psi(z)} . \tag{4.3}$$

where G is the shear modulus, z is the complex variable given by

$$z = x + iy ,$$

$$\kappa = \begin{cases} 3-4\nu , \text{ plane strain} \\ \dfrac{3-\nu}{1+\nu} , \text{ plane stress} \end{cases} , \tag{4.4}$$

and ϕ and ψ are functions of a complex variable that depend on the boundary conditions.

---

* Circumstances could be envisioned in which the crack would remain closed even at maximum load. It is possible that crack arrest following a large overload occurs in this way.

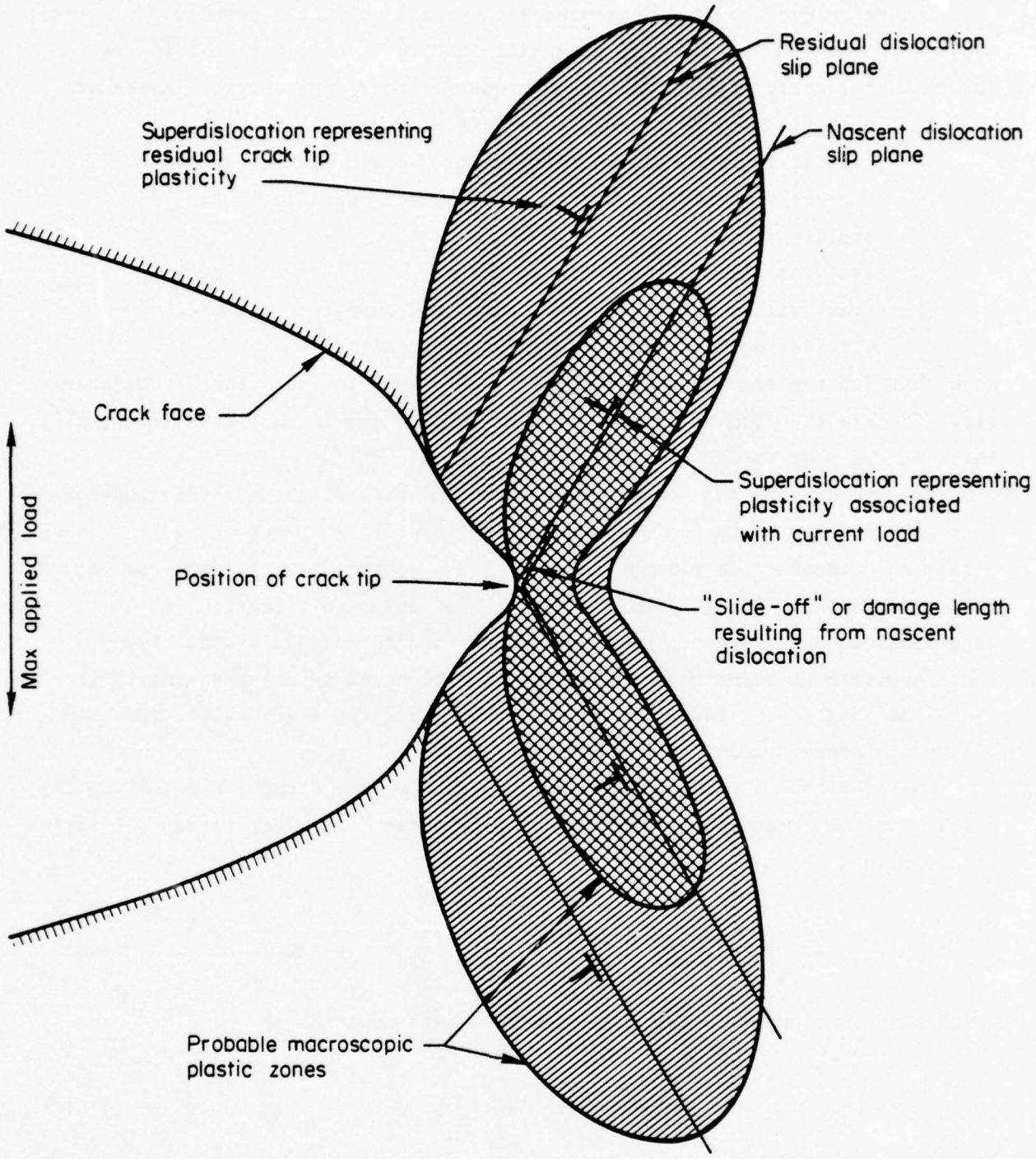

FIGURE 4.2. ILLUSTRATION OF SUPERDISLOCATION REPRESENTATION OF CRACK-TIP PLASTICITY SHOWING CRACK OPENING AT MAXIMUM LOAD LEVEL IN A CYCLIC LOADING SEQUENCE

The technique used for determining the solution to the problem of interest employs linear superposition of potential junctions valid for an infinite domain that satisfy the boundary conditions for four subproblems. These are

(1) Remotely applied uniform stress (e.g., uniaxial tension, biaxial tension, shear) for infinite domain without cracks

(2) A crack with surface tractions equal and opposite to the applied stress

(3) Isolated dislocation pairs

(4) Crack with surface tractions equal and opposite to the stresses arising from the dislocation pairs.

Note that Subproblems (2) and (4) give rise to singular behavior at the crack tip. Because the form of the singularity is the same in each case (i.e., $r^{-\frac{1}{2}}$), these can be made to cancel, if desired.

The key element in the approach is the use of a single superdislocation pair (in the case where the deformation is symmetric with respect to the crack plane) to represent the plastic zone in each load cycle. This requires only two new unknowns, strength and the position of a superdislocation, to be determined in each load cycle. The unknowns are determined by satisfying a force equilibrium relation for a superdislocation and imposing a singularity-canceling equation at the crack tip to insure that the crack closes smoothly without interpenetration at the tip.

Consider that a tensile loading is applied in the direction normal to the crack plane and that plane-strain conditions exist. Then the force equilibrium equation is

$$\tau_n = \sigma h_n + \frac{G}{4\pi(1-\nu)} \sum_{j=1}^{M} b_j \, (g_{jn} + k_{jn}) \, , \quad n = 1, 2, \ldots M \, , \qquad (4.5)$$

while the singularity-canceling or crack-closure equation is

$$\sigma a = \frac{G}{4\pi(1-\nu)} \, b_j \, f_j \, , \qquad (4.6)$$

where σ = applied tensile stress

a = half crack length

M = number of load cycles imposed

b_j = strength of the dislocation created in the $j^{\underline{th}}$ load cycle

G = shear modulus

ν = Poisson's ratio .

with the remaining undefined quantities in Equations (4.5) and (4.6) being known functions of the dislocation position in terms of the complex variable representation given by

$$Z_j = a_j + \ell_j e^{i\theta} \quad , \quad j = 1 , 2 , .. \ M \ ,$$

where θ = angle between the crack plane and slip plane (constant)

a_j = crack length at the time that the j^{th} dislocation was emitted

ℓ_j = distance from the crack plane along the slip plane to the j^{th} dislocation.

Before writing out these expressions explicitly, it may be useful to point out their physical interpretation. Note that the symbol => is taken to mean "is associated with" in these definitions

f_n => contribution to the singularity-canceling equation due to dislocation pair generated in the n^{th} load application (dimensionless).

g_{jn} => stress acting along the slip plane at the position occupied by the dislocation generated in the n^{th} load application (first quadrant) due to the surface tractions that abolish the crack face stresses caused by the dislocations generated in the j^{th} load application (dimensions of reciprocal length).

h_n => stress acting along the slip plane at the position occupied by the dislocation generated in the n^{th} load application (first quadrant) due to the applied stress (dimensionless).

k_{jn} => stress acting along the slip plane at the position occupied by the dislocation generated in the n^{th} load application (first quadrant) due to the stress field of the dislocations generated in the j^{th} load application (dimensions of reciprocal length).

Omitting the details involved in their derivation, the quantities defined on the preceding page are found to be as follows:

$$f_n = 4 \sin\theta \left[\mathrm{Re} \left\{ \frac{\left(Z_n^2 - a^2\right)^{\frac{1}{2}}}{Z_n - a} \right\} + a \ \ell_n \ \mathrm{Re} \left\{ \frac{e^{i\theta}}{(Z_n - a)\left(Z_n^2 - a^2\right)^{\frac{1}{2}}} \right\} \right] \quad (4.7)$$

$$h_n = \sin\theta \left[\cos\theta + a^2 \ \ell_n \ \mathrm{Re} \left\{ \frac{e^{2i\theta}}{\left(Z_n^2 - a^2\right)^{\frac{3}{2}}} \right\} \right] \quad (4.8)$$

$$k_{jn} = \begin{cases} -\frac{1}{\ell_n}\cos 2\theta & j = n \\ -\mathrm{Re}\left\{ e^{2i\theta}\left[\frac{e^{i\theta}(\bar{Z}_j - \bar{Z}_n) + e^{-i\theta}(Z_j - Z_n)}{(Z_j - Z_n)^2} - \frac{e^{i\theta}(\bar{Z}_j - Z_n) + e^{-i\theta}(Z_j - \bar{Z}_n)}{(\bar{Z}_j - Z_n)^2} \right] \right\} & j \neq n \end{cases} \tag{4.9}$$

$$g_{jn} = 2\ell_j \sin^2\theta\, \mathrm{Re}\left[\frac{e^{2i\theta}}{(Z_j^2 - a^2)^{\frac{1}{2}}} \left\{ -\frac{2Z_j^2 + a^2}{2(Z_j^2 - a^2)^{\frac{3}{2}}} + \frac{Z_j(\bar{Z}_j^2 - a^2)^{\frac{1}{2}}}{(Z_j^2 - a^2)(Z_j - \bar{Z}_j)} + \frac{(\bar{Z}_j^2 - a^2)^{\frac{1}{2}} - (Z_j^2 - a^2)^{\frac{1}{2}}}{(Z_j - \bar{Z}_j)^2} \right\} + \frac{\ell_j e^{2i\theta}}{(Z_j^2 - a^2)^{\frac{1}{2}}} \left\{ -\frac{a^2 Z_j e^{i\theta}}{(Z_j^2 - a^2)^{\frac{3}{2}}} + \frac{e^{-i\theta}}{(Z_j - \bar{Z}_j)^2 (\bar{Z}_j^2 - a^2)^{\frac{1}{2}}} \left[\frac{a^2(Z_j - \bar{Z}_j)}{Z_j^2 - a^2} + 2\frac{(Z_j^2 - a^2)^{\frac{1}{2}}(\bar{Z}_j^2 - a^2)^{\frac{1}{2}} + a^2 - Z_j\bar{Z}_j}{Z_j - \bar{Z}_j} \right] \right\} \right] \qquad j = n$$

$$g_{jn} = 2\ell_n \sin^2\theta\, \mathrm{Re}\left[\frac{e^{2i\theta}}{(Z_n^2 - a^2)^{\frac{1}{2}}} \left\{ \frac{(Z_j^2 - a^2)^{\frac{1}{2}} - (Z_n^2 - a^2)^{\frac{1}{2}}}{(Z_n - Z_j)^2} + \frac{(\bar{Z}_j^2 - a^2)^{\frac{1}{2}} - (Z_n^2 - a^2)^{\frac{1}{2}}}{(Z_n - \bar{Z}_j)^2} + \frac{Z_n}{Z_n^2 - a^2}\left[\frac{(Z_j^2 - a^2)^{\frac{1}{2}}}{Z_n - Z_j} + \frac{(\bar{Z}_j^2 - a^2)^{\frac{1}{2}}}{Z_n - \bar{Z}_j} \right] \right\} + \frac{\ell_j e^{2i\theta}}{(Z_n^2 - a^2)^{\frac{1}{2}}} \left\{ \frac{e^{i\theta}}{(Z_n - Z_j)^2 (Z_j - a^2)^{\frac{1}{2}}} \left[\frac{a^2(Z_n - Z_j)}{Z_n^2 - a^2} + 2\frac{(Z_n^2 - a^2)^{\frac{1}{2}}(Z_j^2 - a^2)^{\frac{1}{2}} + a^2 - Z_j Z_n}{Z_n - Z_j} \right] + \frac{e^{-i\theta}}{(Z_n - \bar{Z}_j)^2 (\bar{Z}_j^2 - a^2)^{\frac{1}{2}}} \left[\frac{a^2(Z_n - \bar{Z}_j)}{Z_n^2 - a^2} + 2\frac{(Z_n^2 - a^2)^{\frac{1}{2}}(\bar{Z}_j^2 - a^2)^{\frac{1}{2}} + a^2 - \bar{Z}_j Z_n}{Z_n - \bar{Z}_j} \right] \right\} \right] \qquad j \neq n \tag{4.10}$$

The manner in which individual superdislocation pairs are assembled into a complete cycle-by-cycle model governed by the above equations is illustrated in Figure 4.3.

It is considered that the material provides an intrinsic resistance to the movement of the superdislocation. This parameter is denoted τ_i (for internal) and is related to Y, the tensile yield stress by

$$\tau_i = Y/\sqrt{3} \ . \tag{4.11}$$

The equations of force equilibrium that are the basis for the mathematical model are formed by setting the right-hand side of Equation (4.5) equal to τ_i for each of the M superdislocations in the problem.

An expression for the crack-opening displacements can also be determined. Again omitting the details, the result is found to be

$$\Delta v = \frac{\sigma(K+1)}{2G} (a^2 - x^2)^{\frac{1}{2}} + \sin\theta \sum_{j=1}^{M} b_j d_j \ , \tag{4.12}$$

where Δv is the crack-opening displacement at a position $x \leq a$. In Equation (4.12), x is measured from the center of the crack and d_j is the function given by

$$\begin{aligned} d_j = {} & 2\delta(a_j - |x|) - \frac{4}{\pi} \ell_j (a^2 - x^2)^{\frac{1}{2}} \operatorname{Re}\left\{ \frac{Z_j e^{i\theta}}{(Z_j^2 - a^2)^{\frac{1}{2}} (Z_j^2 - x^2)} \right\} \\ & + \frac{1}{\pi} \operatorname{Im}\left\{ \log\left[\frac{a^2 - xZ_j + i (Z_j^2 - a^2)^{\frac{1}{2}} (a^2 - x^2)^{\frac{1}{2}}}{a^2 - xZ_j - i (Z_j^2 - a^2)^{\frac{1}{2}} (a^2 - x^2)^{\frac{1}{2}}} \right] \right. \\ & \left. + \log\left[\frac{a^2 + xZ_j + i (Z_j^2 - a^2)^{\frac{1}{2}} (a^2 - x^2)^{\frac{1}{2}}}{a^2 + xZ_j - i (Z_j^2 - a^2)^{\frac{1}{2}} (a^2 - x^2)^{\frac{1}{2}}} \right] \right\}, \end{aligned} \tag{4.13}$$

where $\delta(x) = \begin{cases} 0, & x \neq 0 \\ 1, & x = 0 \end{cases}$ is the Dirac Delta function.

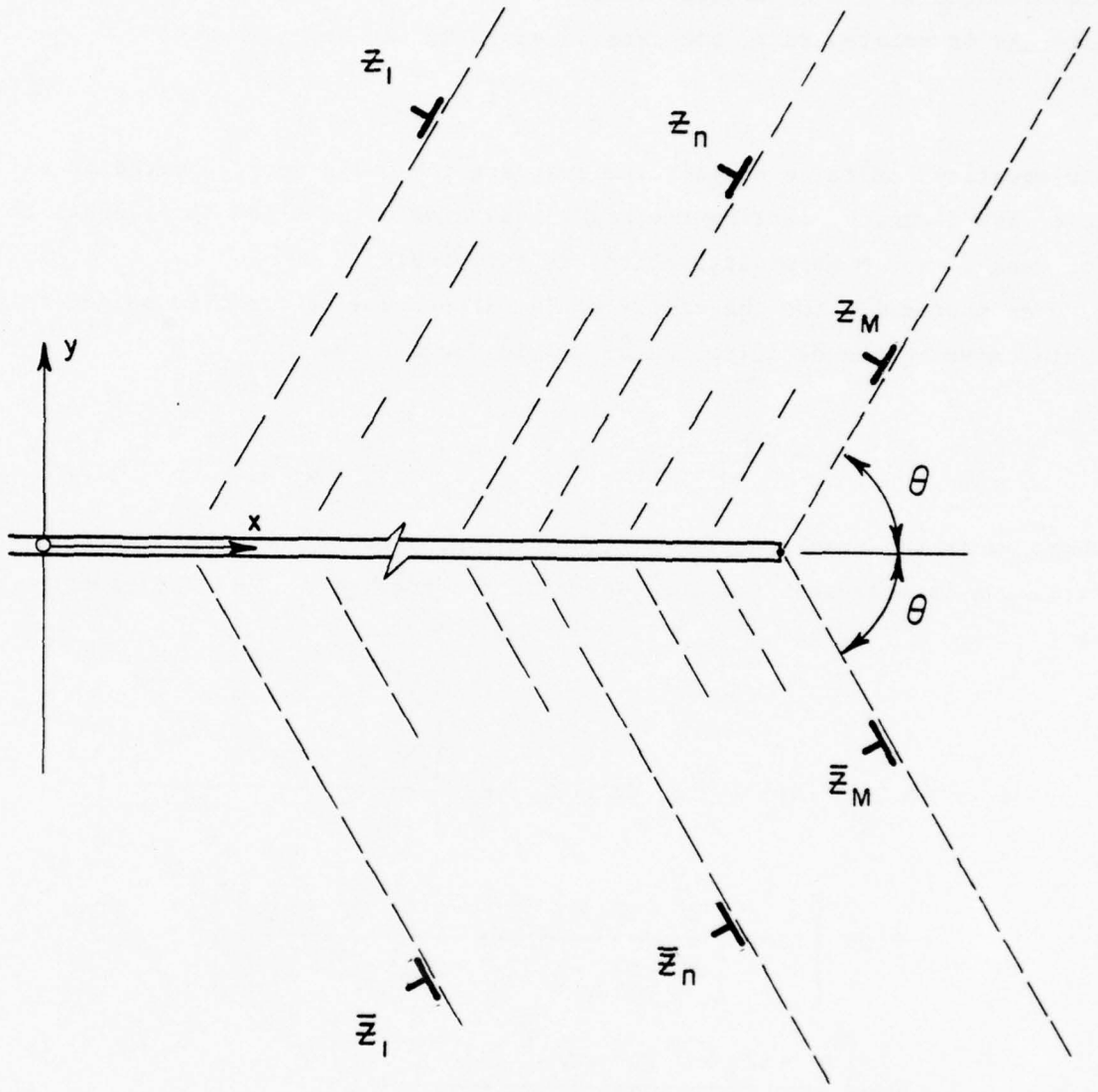

FIGURE 4.3. DISLOCATION POSITIONS FOR MULTICYCLE LOADING

Linearized Model for Fixed-Load Problem

In this section, the problem illustrated by Figure 4.4(a) will be considered. Because a single superdislocation pair suffices, the subscripts will be omitted. The notation is then as shown in Figure 4.4(b).

The governing equations are for the force equilibrium of one of the dislocations (only one needs to be considered because of symmetry) and the singularity-calceling equation. The unknowns are the superdislocation strength, b, and the position, ℓ. Setting $\tau = \tau_i$ in Equation (4.5), it is found that

$$\frac{Y}{\sqrt{3}} = \sigma h(\ell) + \frac{Gb}{\pi(\kappa+1)}\left[g(\ell) + k(\ell)\right], \tag{4.14}$$

and

$$\sigma = \frac{Gb}{\pi(\kappa+1)a} f(\ell) . \tag{4.15}$$

In the case of small-scale yielding where $\ell \ll a$, Equations (4.7) - (4.10) reduce to

$$\begin{aligned} f(\ell) &= 6\left(\frac{2a}{\ell}\right)^{\frac{1}{2}} \sin\theta \cos\frac{\theta}{2} \\ g(\ell) &= -\frac{1}{\ell}(1 - \cos 2\theta) \\ h(\ell) &= \frac{1}{4}\left(\frac{2a}{\ell}\right)^{\frac{1}{2}} \sin\theta \cos\frac{\theta}{2} + \sin\theta\cos\theta \\ k(\ell) &= -\frac{1}{\ell}\cos 2\theta . \end{aligned} \tag{4.16}$$

Further assuming that $\sigma \ll Y$ and substituting Equation (4.16) into Equations (4.14) and (4.15) gives the following relation for the superdislocation position:

$$\frac{\ell}{a} = \frac{1}{24}\left\{3\sin\theta\cos\frac{\theta}{2} - \frac{1}{\sin\theta\cos\frac{\theta}{2}}\right\}^2 \left(\frac{\sigma}{Y}\right)^2 . \tag{4.17}$$

In this work, the particular angle θ selected will be that which maximizes the extent of yielding (equivalently, the plane of maximum shear. From Equation (4.17) this is

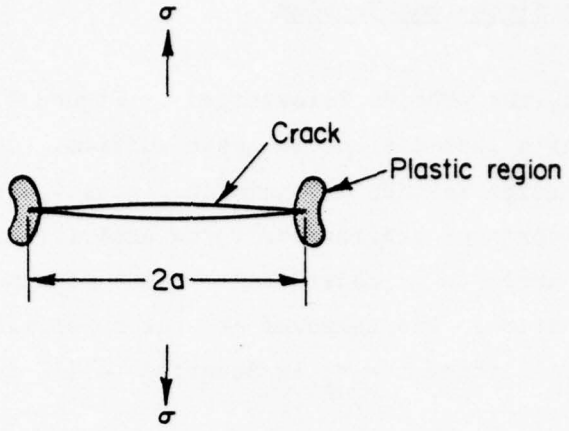

(a) Inclined Strip-Yield-Zone-Superdislocation Model for Small-Scale Yielding (Symmetric Tensile Loading)

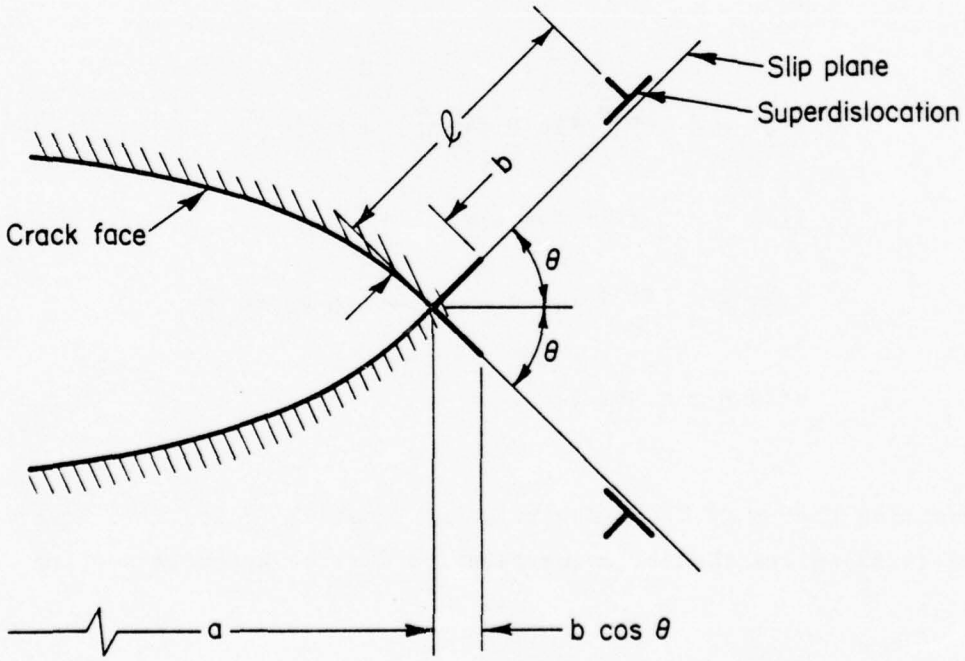

(b) Detail of Crack-Tip Deformation

FIGURE 4.4. APPLICATION OF SUPERDISLOCATION MODEL TO SMALL-SCALE YIELDING UNDER CONSTANT-APPLIED STRESS

$$\frac{d}{d\theta}\left\{ \sin\theta \cos\frac{\theta}{2} \right\} = 0 \ , \tag{4.18}$$

which turns out to be

$$\theta = \cos^{-1}\ (1/3) = 70.53^{\circ} \ . \tag{4.19}$$

This is the value used in this work.

The superdislocation cannot be expected to give precise information about the size and shape of the plastic zone per se. However, this will be unimportant if it does reflect with reasonable accuracy the effect of the plastic deformation at the crack tip. Consider the prediction of δ, the crack-tip-opening displacement in plane strain under fixed load for small-scale yielding conditions. This can be written as

$$\delta = 2b \sin\theta \ .$$

Upon solving for b and substituting into the above, it is found that

$$\delta = \frac{2}{3\sqrt{3}} \frac{1-\nu^2}{\cos\theta/2} \left\{ 3 \sin\theta \cos\frac{\theta}{2} - \frac{1}{\sin\theta \cos\frac{\theta}{2}} \right\} \frac{K^2}{EY} \ , \tag{4.20}$$

where $K = \sigma\sqrt{\pi a}$.

Hence,

$$\delta = \alpha \frac{K^2}{EY} \ , \tag{4.21}$$

where $\alpha = 0.433$ for $\theta = 70.53^{\circ}$.

A comparison between the results obtained from a variety of both approximate and highly rigorous calculations of the crack-opening displacement are given in Table 4.1. It can be seen that the simple superdislocation model compares very favorably with the more precise results.

Relation Between the Singularity-Canceling Equation and Crack Closure

Using the same mathematical procedures that led to the singularity-canceling equation, an expression can be devised for the combined strength of the singular term. Because, in general, the relation between the strain-energy-release rate, $\mathcal{J}$, and K, the stress-intensity factor is given for plane strain by

TABLE 4.1. RELATION BETWEEN STRESS INTENSITY-FACTOR AND CRACK-OPENING DISPLACEMENT FOR SMALL-SCALE YIELDING CONDITIONS

$$\delta = \frac{K^2}{EY}$$

Investigators	Technique	α
Wells	Linear Elasticity	1.159
Goodier and Field	Dugdale Model	0.910
Rice	Deformation Plasticity (J Integral)	0.613
Rice and Johnson	Deformation Plasticity (J Integral)	0.717
Levy, Marcal, Ostegren, and Rice	Incremental Plasticity (Finite-element method)	0.425
Rice	Bilby-Swinden Model (Approximate)	0.440
Rice and Tracey	Incremental Plasticity (Singular Finite Element)	0.493
This report	Inclined Strip Yield (Superdislocation Model)	0.433

$$K^2 = \frac{E}{1-\nu^2} ,$$

it is found that

$$\mathcal{J} = \frac{1-\nu^2}{E} \pi a \left[\sigma - \frac{G}{\pi(\kappa+1)a} \sum_{j=1} b_j f_j \right]^2 . \qquad (4.22)$$

Comparison of Equation (4.22) with Equation (4.12) shows that the bracketed term is just equal to the combined coefficient of the singular term and, hence, is set equal to zero to abolish the crack-tip singularity.

In fracture mechanics, $\mathcal{J}$ has the physical interpretation of being the driving force for crack advance. Consequently, allowing crack growth to occur with $\mathcal{J}$ equal to zero (as would be the case if Equation (4.12) is imposed during the maximum load in fatigue) is inconsistent with the basic notions of fracture mechanics. A more appropriate role for the singularity-canceling equation may be in connection with crack closure under a nonzero load in a cyclic loading sequence. This can be seen in connection with the crack face displacements, Equation (4.10).

Consider small-scale yielding conditions and confine attention to a point on the crack face in the near neighborhood of the crack tip. Let the distance from the crack tip be given by $r = a - x$. Then, introducing the conditions $r \ll a$ and $\ell \ll a$ in Equation (4.10), it is found that

$$\Delta v(r) = r^{\frac{1}{2}} \left\{ \frac{\sigma(\kappa+1)}{G} \left(\frac{a}{2}\right)^{\frac{1}{2}} - \frac{2}{\pi} \sin\theta \cos\frac{\theta}{2} \sum_{j=1}^{M} b_j D_j \right\} , \qquad (4.23)$$

where $D_j = \dfrac{\ell_j + r}{\ell_j^2 + 2r\ell_j \cos\theta + r^2} + \dfrac{2(\ell_j - r)}{\ell_j^2 - 2r\ell_j \cos\theta + r^2}$.

Now, if the right-hand side of Equation (4.23) is expanded in powers of r, the result can be shown to be

$$\Delta v\ (r) = r^{\frac{1}{2}} \left\{ \frac{\sigma(\kappa+1)}{G} \left(\frac{a}{2}\right)^{\frac{1}{2}} - \frac{6}{\pi} \sin\theta \cos\frac{\theta}{2} \sum_{j=1}^{M} \frac{b_j}{\ell^{\frac{1}{2}}} \right\} + \theta\ (r^{\frac{3}{2}}) . \qquad (4.24)$$

Under small-scale yielding conditions, the coefficient of the $r^{\frac{1}{2}}$ term is just the singularity-canceling equation*. Consequently, by removing the crack-tip

---

* To see this, substitute the first of Equations (4.16) into Equation (4.6).

singularity, the crack-face displacements will be of the order $r^{\frac{3}{2}}$. This means that the slope of the displacements will be of order $r^{\frac{1}{2}}$. At the crack tip, $r = 0$. Hence, satisfying the singularity-canceling equation forces the crack faces to close smoothly at the crack tip with no interpenetration.

This is obviously a necessary condition for crack closure (although not sufficient) and, therefore, it is appropriate to impose it at the minimum load in a cyclic loading sequence. Conversely, it is inappropriate to impose the singularity-canceling equation at the maximum load as has been done routinely in all previous work. To do so is inconsistent with all observations on fatigue-crack growth (which reveals that the crack blunts on the increasing load part of the cycle) and with the idea that crack growth can take place with zero δ. This condition should be imposed only at the minimum load, therefore.

The Crack-Growth Criterion and the Solution Procedure

As already noted, the mathematical simplicity of the superdislocation representation of crack-tip plasticity combined with an accurate prediction of the state of deformation at the crack tip gives this approach a strong appeal for use in a fatigue-crack-propagation model. In addition, the displacement field associated with the superdislocations distorts the crack-opening displacement (COD) in the proximity of the crack tip, allowing the possibility of crack closure under positive load. At the same time, an intrusion into the unbroken material at the crack tip is predicted. This can be taken as a measure of the crack advance increment in the load cycle. The latter effect arises from the displacement discontinuity (which is associated with any dislocation) intersecting the crack at its tip, giving a "sliding off" region there.

Because the magnitude of the displacement discontinuity is just equal to the superdislocation strength, the crack-growth rate is simply related to the strength of the most recently emitted superdislocation. Hence, the crack growth at the N^{th} cycle of loading is

$$\left(\frac{da}{dN}\right)_N = b_N \cos\theta \ , \tag{4.25}$$

where θ is the angle between the superdislocation slip plane and the crack plane. Taking the slip plane to be the plane of maximum shear gives $\theta = \cos^{-1}$ $\cos^{-1}(1/3) = 70.3^{\circ}$ as determined in Equation (4.19).

The solution procedure involves an iterative technique to determine the superdislocation strengths and positions in each load cycle. This is done by solving the system of nonlinear algebraic equations given by Equations (4.5) and (4.6). A Runge-Kutta method is currently used. Having the solution, the crack-growth increment is obtained from Equation (4.25). It can, therefore, be recognized that no arbitrary disposable parameters are introduced in order to determine the crack-growth rates. The only parameters that enter the computation are the ordinary mechanical properties of the material being considered and, of course, the cyclic load history.

The iterative procedure used to determine the equilibrium dislocation positions considers that the internal fraction stress, τ_i, acts along the slip plane to always oppose dislocation motion. Therefore, the net stress, F_n, acting to move the n^{th} dislocation along the slip plane is (NB, positive force acts away from the crack plane, negative force acts towards the crack plane)

$$F_n = \begin{cases} 0 , & |\tau_n| \leq \tau_i \\ \tau_n - \text{sgn}(\tau_n)\,\tau_i , & |\tau_n| \leq \tau_i \end{cases} .$$

where, as above, τ_i is taken to be a material constant related to the yield stress (i.e., $\tau_i = Y/3$) and $\text{sgn}(x) = x/|x|$. Note that the friction force resisting movement back towards the crack tip need not (and probably is not) equal to that resisting motion outwards.

In detail, the procedure used in determining fatigue-crack-growth rates under arbitrary cycle-to-cycle loading starting from an undeformed (no previous loads) crack tip is described next. It is understood that the material's elastic modulus, Poisson's ratio, and yield stress, together with an initial crack length, have all been specified in addition to the loading history to be followed. For definiteness, it will be considered that the latter quantities have been given in terms of K_{max} and K_{min} values for each load cycle. Then, the computational procedure is as follows (subscripts denote cycle numbers):

(1) Determine the position along the slip plane occupied by the first dislocation, ℓ_1, from Equation (4.17) using $\sigma = (K_{max})_1 / (\pi a_o)^{\frac{1}{2}}$. (Note that although this is an approximate linearized version of the complete equation, it will give an accurate enough result so that no further iteration is necessary.)

(2) Keeping the applied stress the same, compute the superdislocation strength, b_1, from a linearized version of the singularity-canceling equation, Equation (4.6). Then, from Equation (4.25), calculate the crack-growth increment $(\Delta a)_1$ from the relation $(\Delta a)_1 = b_1 \cos \theta$.

(3) Let the crack extend such that its half length a is

$$a = a_o + (\Delta a)_1$$

where a_o is the initial crack length.

(4) Reduce the applied load to $\sigma = (K_{min})_1 / (\pi a)^{\frac{1}{2}}$ and allow a second superdislocation of strength $b_1' < 0$ to appear on the slip plane. Find an equilibrium solution with the crack-closure condition satisfied. Then assume that as the load is once again increased, the inner dislocation combines with the outer to give a superdislocation of strength $b_1 + b_1'$ at the position ℓ_1. Note that this strength remains fixed for the remainder of the computation.

From this point on, the computational procedure is the same regardless of the number of superdislocations and load cycles performed. So, consider that M - 1 superdislocation pairs have been generated in M - 1 load cycles where M > 1. The computation for the M^{th} load cycle then proceeds as follows.

(5) Increase the applied load to $\sigma = (K_{max})_M / (\pi a)^{\frac{1}{2}}$ and consider that a nascent dislocation exists at the crack tip. Assume that all dislocations move along the slip plane at a speed that is proportional to the net force acting on them; i.e.,

$$\frac{d\ell_j}{dt} = F_j \quad , \quad j = 1, 2, \ldots , M \ .$$

Use the Runge-Kutta method to allow the superdislocation to move towards their equilibrium positions. The strength of the nascent superdislocation, b_M, will be determined by satisfying the singularity-canceling equation.

(6) Continue the iterative solution procedure until equilibrium has been achieved. Then, calculate the crack-growth increment

$$(\Delta a)_M = b_M \cos \theta \ ,$$

and increase the crack length to

$$a = a_o + \sum_{j=1}^{M} (\Delta a)_j \ .$$

(7) Reduce the applied load to $\sigma = (K_{min})_M/(\pi a)^{\frac{1}{2}}$, allow the secondary superdislocation $b^1 < 0$ to appear, determine an equilibrium solution that satisfies the crack-closure condition, then replace b_M by $b_M + b_M^1$ at ℓ_M. This completes the load cycle.

Steps 5 through 7 are repeated for each load cycle after the first.

Table 4.2 shows the results taken from a typical computation. In this example, a uniform load history given by K_{max} = 18 ksi $in^{\frac{1}{2}}$, K_{min} = 9 ksi $in^{\frac{1}{2}}$ was applied to a plate with a_o = 1 inch. The material being simulated is aluminum.

Super-Superdislocation Model for Steady-State Fatigue-Crack Growth Under Uniform Cyclic Loading

In a development similar to that given in a preceding section, a linearized version of the model will be used to consider the case of steady-state fatigue-crack growth under uniform cyclic loading. Specifically, it will be considered here that the applied loads will be adjusted for the increase in crack length such that K_{max} and K_{min} will be the same for each load cycle. As in the above, the "damage" accumulated in the form of plastic deformation during a period of loading will be represented by a single lumped dislocation. The differences are now that (1) it will be assumed that the lumped dislocation moves with the crack tip in a steady-state fashion and (2) it represents the accumulation over a large number of load cycles rather than just one. Consequently, while it was appropriate to refer to the lumped dislocation in the single fixed-load situation as a superdislocation, in the present problem, it must be called a super-superdislocation.

The primary virtue of the super-superdislocation approach is that the number of variables in the problem is considerably reduced. Very economical solutions are therefore possible. But, there is also a price to be paid to achieve this simplicity. One such disadvantageous feature is that the close connection between the crack-tip-opening displacement (CTOD) and the strength of the superdislocation emanating from the crack tip is lost. Hence, the crack-growth criterion based directly on the CTOD cannot now be used. Instead, it will be assumed that the crack-advance increment is proportional to the strength of the super-superdislocation with the constant of proportionality being inferred from results of the cycle-by-cycle computation.

TABLE 4.2. EXAMPLE COMPUTATIONAL RESULT FOR FATIGUE-CRACK GROWTH UNDER UNIFORM CYCLIC LOADING IN ALUMINUM

K_{max} = 18 ksi in.$^{\frac{1}{2}}$
K_{min} = 9 ksi in.$^{\frac{1}{2}}$

Equilibrium Superdislocation Position (10^{-3} inches)

Load Cycle	ℓ_1	ℓ_2	ℓ_3	ℓ_4	ℓ_5	ℓ_6	ℓ_7	ℓ_8	ℓ_9	ℓ_{10}
1	1.98									
2	10.91	1.21								
3	12.32	5.67	0.97							
4	12.32	5.67	3.38	0.32						
5	12.40	5.70	3.38	1.69	0.25					
6	12.44	5.72	3.38	1.74	1.24	0.21				
7	12.49	5.75	3.38	1.81	1.35	1.08	0.19			
8	12.51	5.76	3.38	1.84	1.39	1.14	0.97	0.19		
9	12.54	5.78	3.38	1.87	1.42	1.18	1.03	0.91	0.18	
10	12.56	5.79	3.38	1.89	1.44	1.21	1.06	0.95	0.87	0.18

Superdislocation Strengths and Crack-Growth Increment

Load Cycle	$b_M \times 10^5$	$(\Delta a)_M \times 10^5$	$(b_M + b_M^1) \times 10^5$
1	15.31	5.10	6.97
2	9.64	3.21	3.68
3	7.23	2.41	1.90
4	3.58	1.19	0.51
5	2.95	0.98	0.26
6	2.62	0.87	0.14
7	2.48	0.83	0.09
8	2.39	0.80	0.05
9	2.34	0.78	0.04
10	2.31	0.77	0.03

Linearized versions of the dislocation interaction terms can be deduced by assuming that both dislocations are on the same slip plane and that they occupy positions such that $a \gg \ell_1 \gg \ell_2$. Hence,

$$g_{12} + k_{12} = -\frac{2}{\ell_1}(1 - \cos 4\theta) - \frac{3}{2}\frac{1}{(\ell_1 \ell_2)^{\frac{1}{2}}}(1 + \cos\theta)\sin^2\theta$$

and

$$g_{21} + k_{21} = \frac{3}{2}\frac{\ell_2^{\frac{1}{2}}}{\ell_1^{\frac{3}{2}}}(1 + \cos\theta)\sin^2\theta + 2\frac{\ell_2}{\ell_1^2}(1 - \cos 4\theta) \quad .$$

For convenience in the following, the specific values for all the linearized functions for $\theta = \cos^{-1}(1/3)$ can be written out. These are

$$f_1 = 6.532\,(a/\ell_1)^{\frac{1}{2}} \qquad f_2 = 6.532\,(a/\ell_2)^{\frac{1}{2}}$$

$$g_{11} + k_{11} = 1/\ell_1 \qquad g_{22} + k_{22} = -1/\ell_2$$

$$h_{11} = 0.2722\,(a/\ell_1)^{\frac{1}{2}} + 0.314 \qquad h_2 = 0.2722\,(a/\ell_2)^{\frac{1}{2}} + 0.314$$

$$g_{12} + b_{12} = -\frac{16}{9}\frac{1}{(\ell_1 \ell_2)^{\frac{1}{2}}} - \frac{128}{81}\frac{1}{\ell_1}$$

$$g_{21} + k_{21} = \frac{16}{9}\frac{(\ell_1 \ell_2)^{\frac{1}{2}}}{\ell_1^2} + \frac{128}{81}\frac{\ell_2}{\ell_1^2} \, .$$

A comparison showing the accuracy of the latter two functions is shown in Table 4.3.

The basic premise of the steady-state growth model is that the strength and position of the super-superdislocation are completely determined by the conditions of force equilibrium at maximum and minimum load in the cycle. It is assumed that the resistance to outward motion just balances the stress acting to push the superdislocation out at maximum load. At the minimum load, the resistance just balances the inward driving stress. The appropriate relations therefore are

$$\begin{aligned} \tau_i &= \sigma_{max}\, h + \frac{G}{\pi(\kappa+1)}\, b\,\{g+k\} \\ -\tau_i &= \sigma_{min}\, h + \frac{G}{\pi(\kappa+1)}\, b\,\{g+k\} \quad . \end{aligned} \tag{4.26}$$

TABLE 4-3. COMPARISON OF EXACT AND APPROXIMATE FUNCTIONS

		Exact		Approximate	
ℓ_1	ℓ_2	$g_{12} + k_{12}$	$g_{21} + k_{21}$	$g_{12} + k_{12}$	$g_{21} + k_{21}$
10^{-3}	10^{-6}	-57799	57.79	-57798	57.80
10^{-3}	10^{-5}	-19374	193.71	-19358	193.58
10^{-3}	10^{-4}	- 7386	738.48	- 7202	720.21
10^{-2}	10^{-6}	-17950	1.79	17936	1.79
10^{-2}	10^{-5}	- 5784	5.77	- 5780	5.78
10^{-2}	10^{-4}	- 1939	19.36	- 1936	19.36
10^{-1}	10^{-6}	- 5684	.056	- 5638	.056
10^{-1}	10^{-5}	- 1808	.178	- 1794	.179
10^{-1}	10^{-4}	- 582.6	.573	- 578.0	.578

Using the linearized version of the functions appearing in these equations and taking the case $\theta = \cos^{-1}(1/3)$, then gives

$$\tau_i = \sigma_{max}\left\{\left(\frac{2}{27}\right)^{\frac{1}{2}}\left(\frac{a}{\ell}\right)^{\frac{1}{2}} + \frac{8^{\frac{1}{2}}}{9}\right\} - \frac{G}{\pi(\kappa+1)}\frac{b}{\ell}$$

$$-\tau_i = \sigma_{min}\left\{\left(\frac{2}{27}\right)^{\frac{1}{2}}\left(\frac{a}{\ell}\right)^{\frac{1}{2}} + \frac{8^{\frac{1}{2}}}{9}\right\} - \frac{G}{\pi(\kappa+1)}\frac{b}{\ell} \quad . \tag{4.27}$$

Equations (4.27) can be readily solved to obtain b and ℓ. The results are

$$\ell = \left[\frac{a}{54}\,\frac{\tau_i}{\sigma_{max} - \sigma_{min}} - \frac{2^{\frac{1}{2}}}{9}\right]^{-2} \quad , \tag{4.28}$$

where ℓ is assumed to be positive and

$$b = \frac{\pi(\kappa+1)\ell}{G}\left\{\sigma_{max}\left[\left(\frac{2}{27}\right)^{\frac{1}{2}}\left(\frac{a}{\ell}\right)^{\frac{1}{2}} + \frac{8^{\frac{1}{2}}}{9}\right] - \tau_i\right\} . \tag{4.29}$$

Equivalently, using $K_{max} = \sigma_{max}\sqrt{\pi a}$ and $K_{min} = \sigma_{min}\sqrt{\pi a}$ and taking $\tau_i = Y/\sqrt{3}$, Equation (4.28) can be written

$$\ell = \frac{1}{18\pi}\left(\frac{K_{max} - K_{min}}{Y}\right)^2 \left\{1 - \left(\frac{2}{27}\right)^{\frac{1}{2}}\left|\frac{\sigma_{max} - \sigma_{min}}{Y}\right|\right\}^{-2} \quad , \tag{4.30}$$

whereupon Equation (4.29) becomes

$$b = \frac{\sqrt{3}}{27}\,\frac{\kappa+1}{YG}\,\Delta K\left\{K_{max} - \frac{\Delta K}{2}\left[\frac{1 - \left(\frac{8}{27}\right)^{\frac{1}{2}}\frac{\sigma_{max}}{Y}}{1 - \left(\frac{2}{27}\right)^{\frac{1}{2}}\frac{\Delta\sigma}{Y}}\right]\right\} \cdot \left[1 - \left(\frac{2}{27}\right)\frac{\Delta\sigma}{Y}\right]^{-1} \quad , \tag{4.31}$$

where $\Delta\sigma \equiv \sigma_{max} - \sigma_{min}$, and $\Delta K \equiv K_{max} - K_{min}$.

Now, assuming the crack-growth rate to be as discussed above, then it follows that

$$\frac{da}{dN} = \frac{4}{27\sqrt{3}} \zeta \, b \cos \theta \, . \tag{4.32}$$

where ζ is a (dimensionless) number to be determined empirically as follows.

Consider plane-strain conditions where $\kappa + 1 = 4(1 - \nu)$ and, for simplicity, assume that $\sigma_{max} \ll Y$. Then, substituting Equation (4.31) into Equation (4.32) gives

$$\frac{da}{dN} = \frac{4}{27\sqrt{3}} \zeta \left(\frac{1 - \nu}{YG}\right) \left\{K_{max} \Delta K - \frac{1}{2} (\Delta K)^2\right\} \, . \tag{4.33}$$

Note that the material's properties enter this relation only through the parameter $(1 - \nu)/YG$. Typical values are given in Table 4.4.

TABLE 4.4. VALUES OF THE MECHANICAL PROPERTIES USED IN THE COMPUTATIONS OF FATIGUE-CRACK-GROWTH RATES

Material	G (ksi)	ν	Y (ksi)	$\frac{1 - \nu}{GY}$
Ti-6Al-4V	6000	0.33	120	0.931×10^{-8}
2024-T3Al	3750	0.34	52.5	3.35×10^{-8}

The empirical parameter ζ can be estimated by the results obtained using the complete cycle-by-cycle computational model. The basis for this estimate is given in the following section of this report. The result is

$$\zeta = 0.200 \text{ (dimensionless)} \, . \tag{4.34}$$

Hence, the approximate version of the steady-state crack-growth relation that is the objective of this section can be written

$$\frac{da}{dN} = .018 \left(\frac{1 - \nu}{YG}\right) \left\{K_{max} \Delta K - \frac{1}{2} (\Delta K)^2\right\}, \tag{4.35}$$

where, for definiteness, the parameters appearing in this relation can be defined explicitly as follows:

G = shear modulus (ksi or MN/m^2)

Y = tensile yield stress (ksi or MN/m^2)

ν = Poisson's ratio (dimensionless)

K_{max} = stress-intensity factor at maximum load (ksi $in.^{\frac{1}{2}}$ or $MNm^{-\frac{3}{2}}$)

K_{min} = stress-intensity factor at minimum load (ksi $in.^{\frac{1}{2}}$ or $MNm^{-\frac{3}{2}}$)

$\Delta K = K_{max} - K_{min}$.

Using numerical values in the English system of units in Equation (4.35) will give crack-growth rates in units of in./cycle, the metric units noted will give growth rates in M/cycle.

An alternative way of writing Equation (4.35) is by introducing the stress ratio parameter, R. This is

$$R = \frac{K_{min}}{K_{max}} \quad . \tag{4.36}$$

This parameter can be used to replace K_{max} since from Equation (4.36), $K_{max} = \Delta K/(1 - R)$. Equation (4.35) can then be written as a function of R and ΔK as

$$\frac{da}{dN} = .009 \left(\frac{1 - \nu}{YG}\right) \left(\frac{1 + R}{1 - R}\right) (\Delta K)^2 \quad . \tag{4.37}$$

This alternative form of the steady-state fatigue-crack-propagation-rate relation arising from the super-superdislocation approach is more useful for the cases where R is a constant.

Discussion of the Steady-State Crack-Growth-Rate Model Obtained With the Super-Superdislocation Approach

It may be useful to consider briefly some qualitative features of Equation (4.35). The first point is in regard to the form of the equation. It can be seen that the ΔK dependence corresponds to a "power-law" growth rate with the power 2. It is worth remarking that, at this stage of the development of the model, this result could be expected with absolute certainty purely from dimensional analysis. That is, there are only two length parameters that have been allowed in the linearized version of the problem: K^2 and b. Hence, the resulting expression for da/dN must involve K^2 only.

Most empirically derived steady-state fatigue-crack-growth relations incorporate an exponent in a power-law type of relation that is more nearly equal to 3 than to 2. For example, the extensive results on 2024-T3 aluminum reported by von Euw, et al [7], are very well represented by the simple relation (English units)

$$\frac{da}{dN} = 4.32 \times 10^{-9} \frac{(\Delta K)^3}{1 - R} \quad . \tag{4.38}$$

This indicates that at least one additional parameter with a length dimension must somehow enter the problem. Anticipating that this parameter could be connected with the microstructure of the material, a survey of the literature on the micromechanical aspects of fatigue-crack growth was performed as part of this project. The preliminary results of this study are given in Appendix C of this report.

The second point is connected with the empirical parameter ζ introduced in Equation (4.32) to account for the fact that only a small part of the residual plasticity represented by the super-superdislocation is associated within the crack tip itself. That is, ζ represents the "sliding off" of the dislocations on slip planes emanating from the crack tip that can be identified with the forward thrust of the crack during a given load cycle. As discussed above, this length is exactly equal to the strength of the superdislocation. Hence, the forward component of crack growth is simply $b \cos \theta$. In the super-superdislocation model, the parameter ζ can be given the physical interpretation of being the ratio of the strength of the superdislocation on the crack tip slip plane to the total strength of the super-superdislocation.

A rough estimate of the magnitude of ζ can be made by examining the results of the cycle-by-cycle computational model. Assuming for simplicity that the strength of the nascent superdislocation is the same as for those created in each previous load cycle, the number of load cycles that contribute to the steady-state process is ζ^{-1}. Consequently, ζ^{-1} load cycles should be necessary to establish the steady state. Now, as exemplified by the results shown in Figure 5.3 (see following section), a steady-state growth rate was in fact achieved in about five cycles of loading. This was true for a range of K_{max} and K_{min} values. Hence, ζ can be estimated to be 0.2.

To be sure, this comparison is very approximate. Nevertheless, it does provide some reassurance that the good agreement with experiment described in

the following is not contrived but has, instead, a fundamentally sould basis. It also suggests that a direct computation of ζ can be made from the complete cycle-to-cycle model.

The third point is in the appearance of purely well-known mechanical properties of the material in Equation (4.35). Aside from the possible slight dependence of ζ on the material, this means that the growth rate "law" derived from the super-superdislocation approach can be easily applied to any material without the necessity of performing special tests to determine material-dependent empirical parameters required in the relation. While exhaustive comparisons with experiments have not been performed in this work, some verification is offered in the next section where it is shown that the model works equally well for both 2024-T3 aluminum and Ti-6Al-4V titanium alloy.

Finally, while not in precise agreement with all fatigue-crack-growth data, Equation (4.35) does reflect a number of experimental observations. In particular, for the most common experimental conditions, ΔK = constant, Equation (4.35) would predict with reasonable accuracy a linear dependence of the growth rate on K_{max}. Of most importance in regard to the eventual use of the superdislocation concept in a complete fatigue-crack-growth model is that no arbitrary disposable parameters need to be introduced into the model to obtain a prediction of $\frac{da}{dN}$. As exemplified by Equation (4.35), the only parameters that enter into the analysis are the basic mechanical properties G, Y, and ν. This feature, together with the ability of the model to admit arbitrary variations in the load level from cycle to cycle, make this approach unique.

5. COMPARISONS BETWEEN ANALYSIS AND EXPERIMENT

Comparison With Alternative Analyses

Two features that likely control the rate of fatigue-crack growth are (1) the size of the intensely deformed plastic region surrounding the crack tip that is created in each load cycle and (2) the extent to which the plastically deformed regions created in different load cycles interact with each other. The first of these can be associated with the CTOD calculated with a strip-yield model. It might be noted that strip-yield models of the Dugdale type also offer predictions of the COD. However, in the Dugdale model,

plastic zone interactions do not take place in a realistic way. At the other extreme, a finite element or other two-dimensional elastic-plastic computational scheme applied to fatigue-crack growth requires so much computer time as to be completely impractical for more than a few load cycles. Thus, the analytical approach taken in this work is the simplest that takes direct account of the essential features of fatigue-crack growth and, at the same time, permits a large number of arbitrary load cycles to be studied.

The analytical approach taken in this work rests on two fundamental assumptions. The first is that the CTOD arising from the intense plastic deformation attending the crack tip is the parameter that governs crack growth. The second is that the essential interaction between the plastic deformation created in different load cycles can be represented by an inclined strip-yield superdislocation model. The approach taken here uses what is perhaps the simplest mathematical model in which those considerations (i.e., CTOD and distinguishable plastic zones in each load cycle) can be taken into account in a rigorous fashion.

In the superdislocation approach as applied to a fatigue situation, the plastically deformed regions surrounding the crack tip are represented by single pairs of dislocations. These are considered to "slide off" from the crack tip on slip planes inclined at a fixed angle, θ, from the crack plane. This is shown in Figure 5.1. It can be seen that the plastic deformation resulting from a series of cyclic load applications is discrete, giving a "jogged" appearance to the crack surfaces. The "sliding off" at the crack tip gives rise to a CTOD, δ, and suggests a value for the increment of crack advance per load cycle, Δa. It is worth reemphasizing that crack closure, if it is to occur, will occur naturally in this model and need not be imposed arbitrarily. Conceptually, the analytical approach taken here stands somewhere between the approximate semiempirical treatments of Wheeler [8] and of Willenborg, et al [9], and the more precise, but cumbersome, finite-element elastic-plastic computation being developed by Newman [10]. To put the model into better perspective, a brief description of these competing approaches to fatigue-crack propagation under variable-amplitude cyclic loading may be in order. As background, the four principal models of crack-tip plasticity are shown in Figure 5.2. These are listed in order of both increasing complexity and accuracy. (It may be worth noticing that only the strip-yield models, (b) and (c), give an unambiguous prediction of the CTOD.) Four classes of

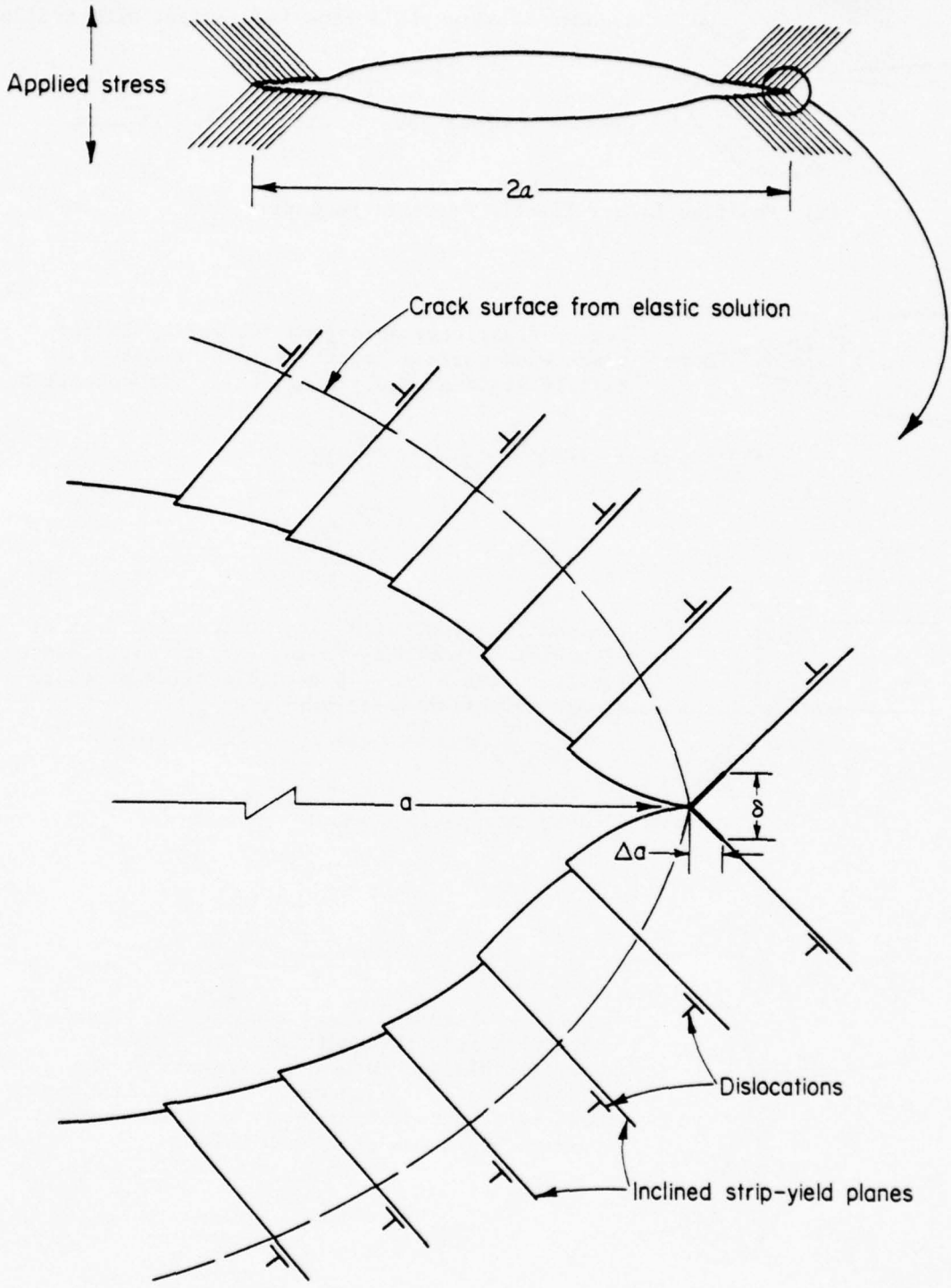

FIGURE 5.1. PLASTIC DEFORMATION ASSOCIATED WITH FATGIUE-CRACK PROPAGATION AS CALCULATED WITH THE INCLINED-STRIP DISLOCATION MODEL

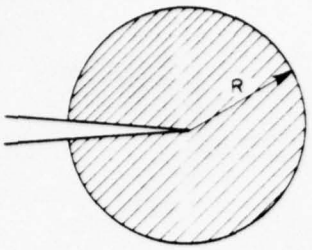

Assumed plastic yield zone is circular with radius

$$R = \frac{1}{2\pi}\left(\frac{K}{Y}\right)^2$$

crack-tip crack-opening displacement is zero.

(a) Modified Linear Elastic-Fracture Mechanics

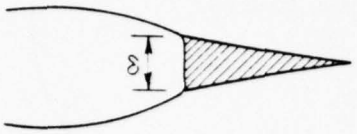

Linear elasticity solutions for partly loaded crack with surface tractions taken equal to tensile yield stress – singularity is cancelled.

(b) Dugdale (BCS) Strip-Yield Model

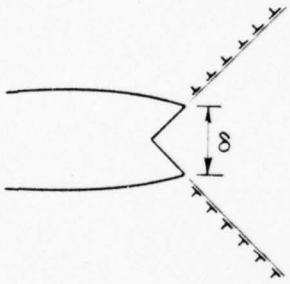

Dislocation model with slip confined to pair of slip planes emanating from the crack tip. Singularity is cancelled. Superdislocation model is simple variation of this.

(c) Bilby-Swinden Strip-Yield Model

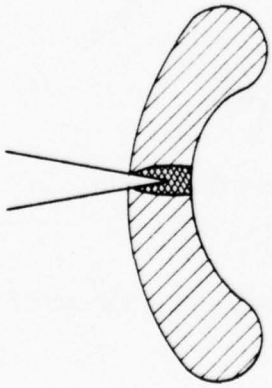

Typical "butterfly" yield zone at tip of crack under plane-strain conditions for elastic/perfectly plastic material. Singularity not cancelled in linear theory. Large strain theory shows existence of "intensely strained region" at crack tip where strains $\simeq$ unity.

(d) Plane Strain Elastic-Plastic Model

FIGURE 5.2. COMPARISON OF CRACK-TIP PLASTICITY MODELS USED IN FATIGUE AND FRACTURE

techniques for fatigue-crack-growth prediction can be identified on the basis of the categorization given in Figure 5.2. These are listed and described in Table 5.1. Note that these can similarly be numbered in order of increasing accuracy and complexity.

Other models which might be mentioned are those of Yokobori and Yoshida [15] and of Neumann [16]. While these have some resemblance to the present work, they have not exploited the potential of this approach to nearly the extent given in this report.

Comparison With Experimental Results

Qualitative results that can be compared with experimental results and with analytical results obtained from more precise approaches (e.g., finite-element methods) have been obtained in two areas

(1) Equilibrium under a single load cycle

(2) Crack growth under constant ΔK cycling.

Using the notation developed in the preceding section, the pertinent results for "small-scale yielding" are found to be

$$\ell = .01354 \frac{K^2}{Y^2} , \tag{5.1}$$

and

$$\delta = 0.4763 \frac{1 - \nu^2}{E} \frac{K^2}{Y} , \tag{5.2}$$

where θ has been selected as the angle of maximum shear stress to maximize the extent of yielding (i.e., $\theta = \cos^{-1} (1/3) = 70.3^{\circ}$) and the internal friction stress has been taken in $Y/\sqrt{3}$. Now, while these results are not important in themselves, they provide a check on the fidelity of the model. In particular, many different analytical approaches have been employed to investigate the small-scale yielding regime and all are in qualitative agreement with Equation (5.2). Quantitatively, as the comparison given in Table 4.1 clearly shows, the models also give quite acceptable results. Again, these findings do not have any direct bearing on the application of the model to fatigue-crack growth except as a necessary basic check.

The extension of the model to multicycle loading has been described in the preceding section of this report. It need only be pointed out here that to

TABLE 5·1. ANALYTICAL PROCEDURES FOR THE PREDICTIONS OF FATIGUE-CRACK GROWTH UNDER SPECTRUM LOADING

Technique	Investigators	Strong Points	Weak Points
Semiempirical extensions of linear elastic fracture mechanics	Wheeler[8], Willenborg, Engle and Wood[9], Elber[11]	Gives simple relations that are easy to apply – offers insight into controlling mechanisms	Lack of firm fundamental basis – difficulty in treating complicated histories – cannot easily be generalized
Dugdale strip yield model with cumulative COD criterion	Rice[12], Weertman[13], Bilby and Heald[14]	Gives closed form result for steady state growth rate	Cannot distinguish load history effects – crack closure does not occur
Inclined strip yield superdislocation model with critical COD criterion	Battelle	Plastic deformation in different load cycles is distinguishable – closure effects handled directly – can be generalized to treat wide range of situations	Computations for complicated load histories may require lengthy computation
Elastic-plastic finite-element analysis	Newman[10]	Highly accurate – can be used to treat wide variety of situations – useful for examining details of crack-growth process	Very time consuming computations so only a few load cycles can be treated – crack extension criterion must be arbitrary.

Accuracy/Convenience ↑

perform a fatigue-crack-growth propagation, all that is needed is a specific cyclic loading sequence and three material parameters: the shear modulus, G; Poisson's ratio, ν; and the tensile yield stress, Y. Computations have been performed for both an aluminum and a titanium alloy using the property values given in Table 5.2. It is believed that the differences between these two sets of values are large enough to test the ability of the model to distinguish between the two materials.

TABLE 5.2. MATERIAL PROPERTIES USED IN COMPUTATION OF FATIGUE-CRACK PROPAGATION

Material	G (ksi)	ν	Y (ksi)
2024-T3 Aluminum	3750	0.34	52.5
Ti-6Al-4V Titanium	6000	0.33	120

Example results are shown in Figure 5.3 for the titanium alloy. Plotted in Figure 5.3 are the crack-growth increments for each load application for three different values of $\Delta K = K_{max} - K_{min}$ for the special case where $R = K_{min}/K_{max} = 0.5$. The most important features of the results shown in Figure 5.3 are, first, that an "accelerated" growth is evident in the first few load cycles and, second, that the growth rate levels off to a constant rate characteristic of the ΔK value applied. These two features are in good qualitative agreement with observations of fatigue-crack growth. A quantitative comparison based on the steady-state growth rates for both the titanium alloy and the aluminum alloy are shown in Figures 5.4 and 5.5, respectively. On the basis of the agreement evident in these two figures, it is believed that the model has proven to be more than adequate, particularly in view of the fact that no arbitrary factors have been introduced to adjust these results.

With regard to the crack-closure phenomenon, attention can be given to the calculated crack-face displacements. Example results are shown for titanium in Figure 5.6 and for aluminum in Figure 5.7. Here, the crack-opening displacements are shown at maximum and minimum load in the twelfth load cycle. The interval shown is that through which the crack has grown since the initiation of growth at the first load cycle. It can be seen that the crack faces are in fact closing upon each other during the minimum load.

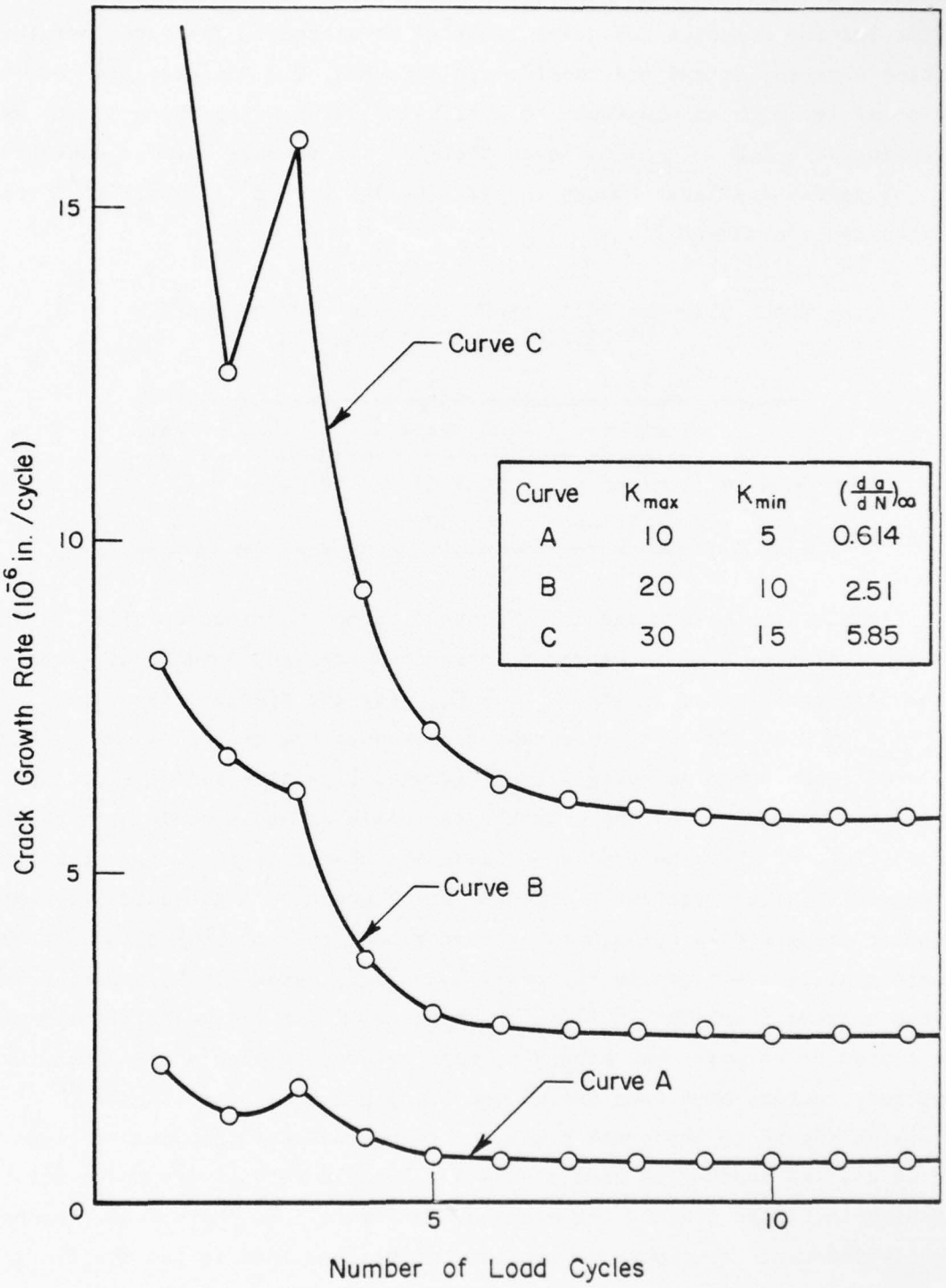

FIGURE 5.3. COMPUTATIONAL RESULTS FOR FATIGUE-CRACK GROWTH IN TITANIUM USING INCLINED STRIP-DISLOCATION MODEL FOR R = 0.5

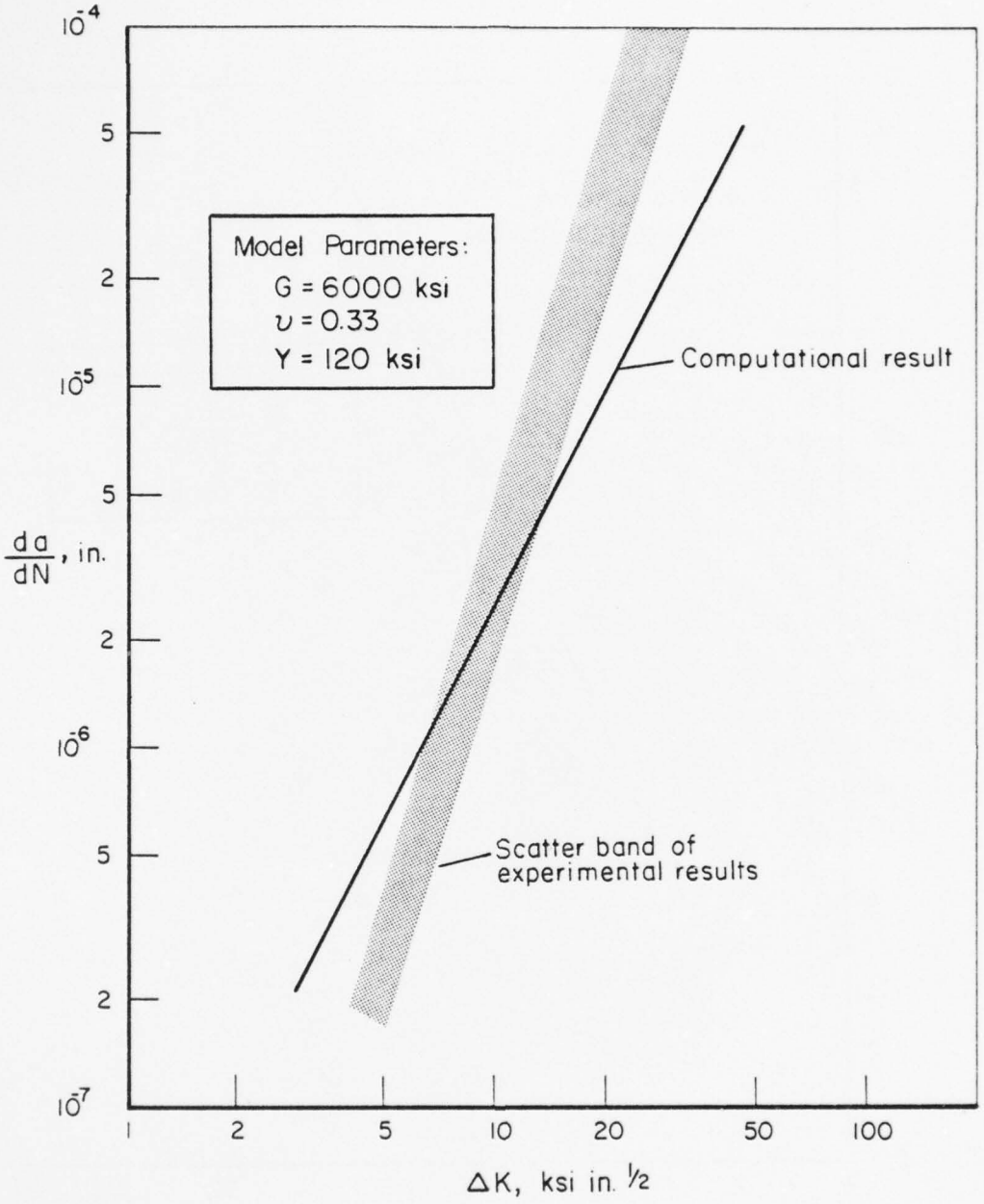

FIGURE 5.4. COMPARISON OF COMPUTATIONAL AND EXPERIMENTAL RESULTS IN Ti-6Al-4V TITANIUM FOR STEADY=STATE CONDITIONS WITH R = 0.5

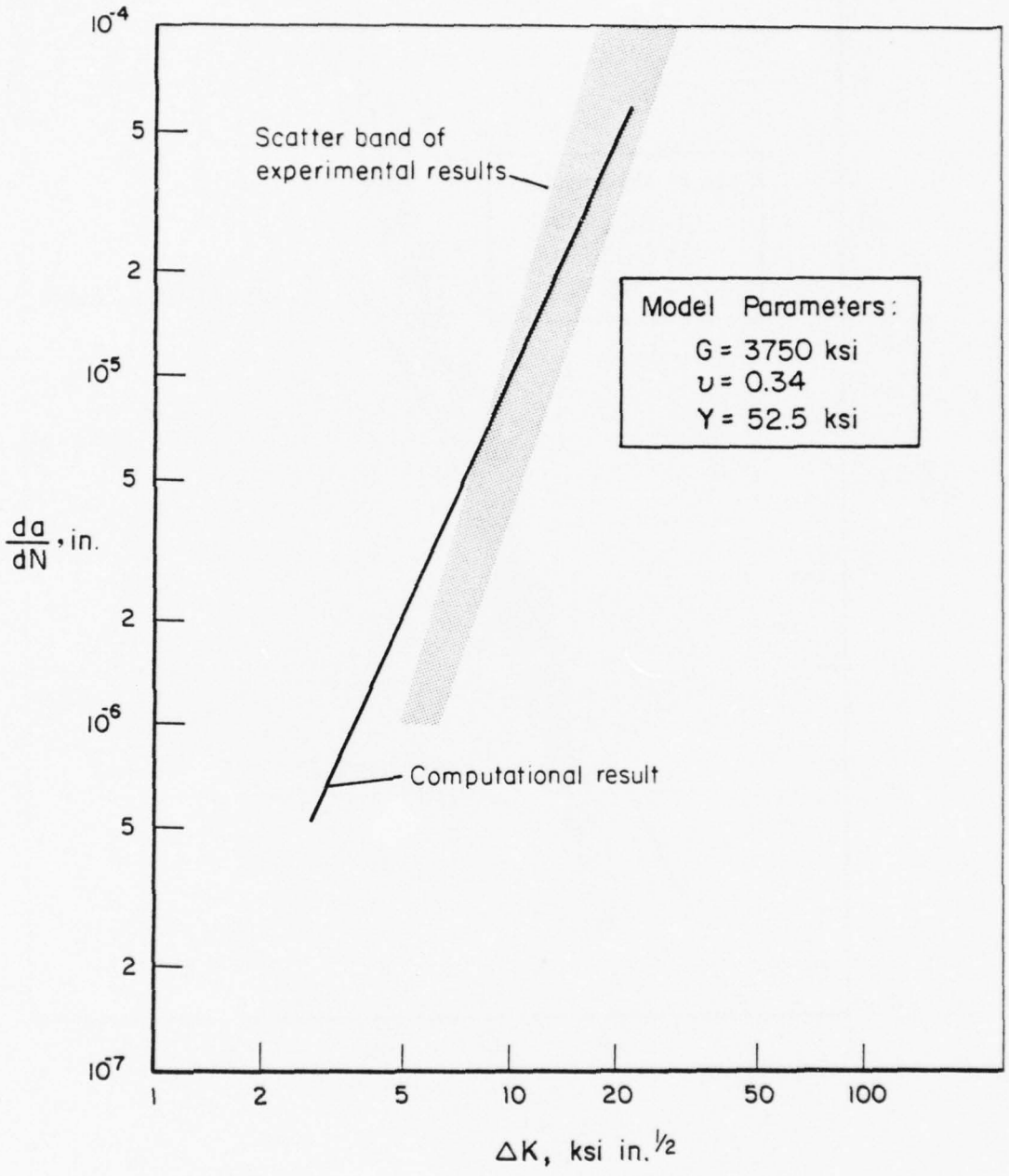

FIGURE 5.5. COMPARISON OF COMPUTATIONAL AND EXPERIMENTAL RESULTS IN 2024-T3 ALUMINUM FOR STEADY-STATE CONDITIONS WITH R = 0.5

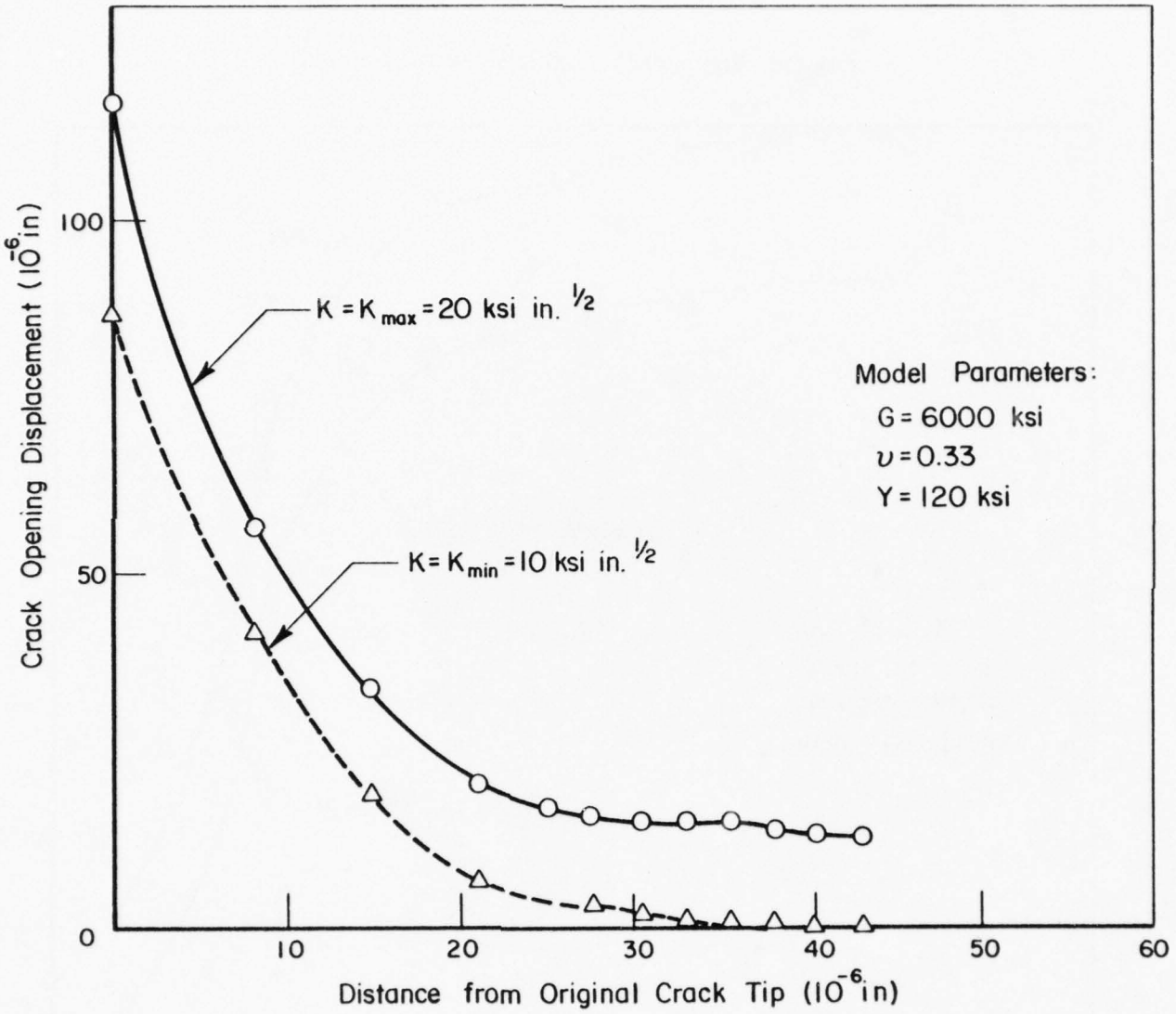

FIGURE 5.6. COMPUTED CRACK-OPENING DISPLACEMENTS IN THE 12TH LOAD CYCLE IN TITANIUM

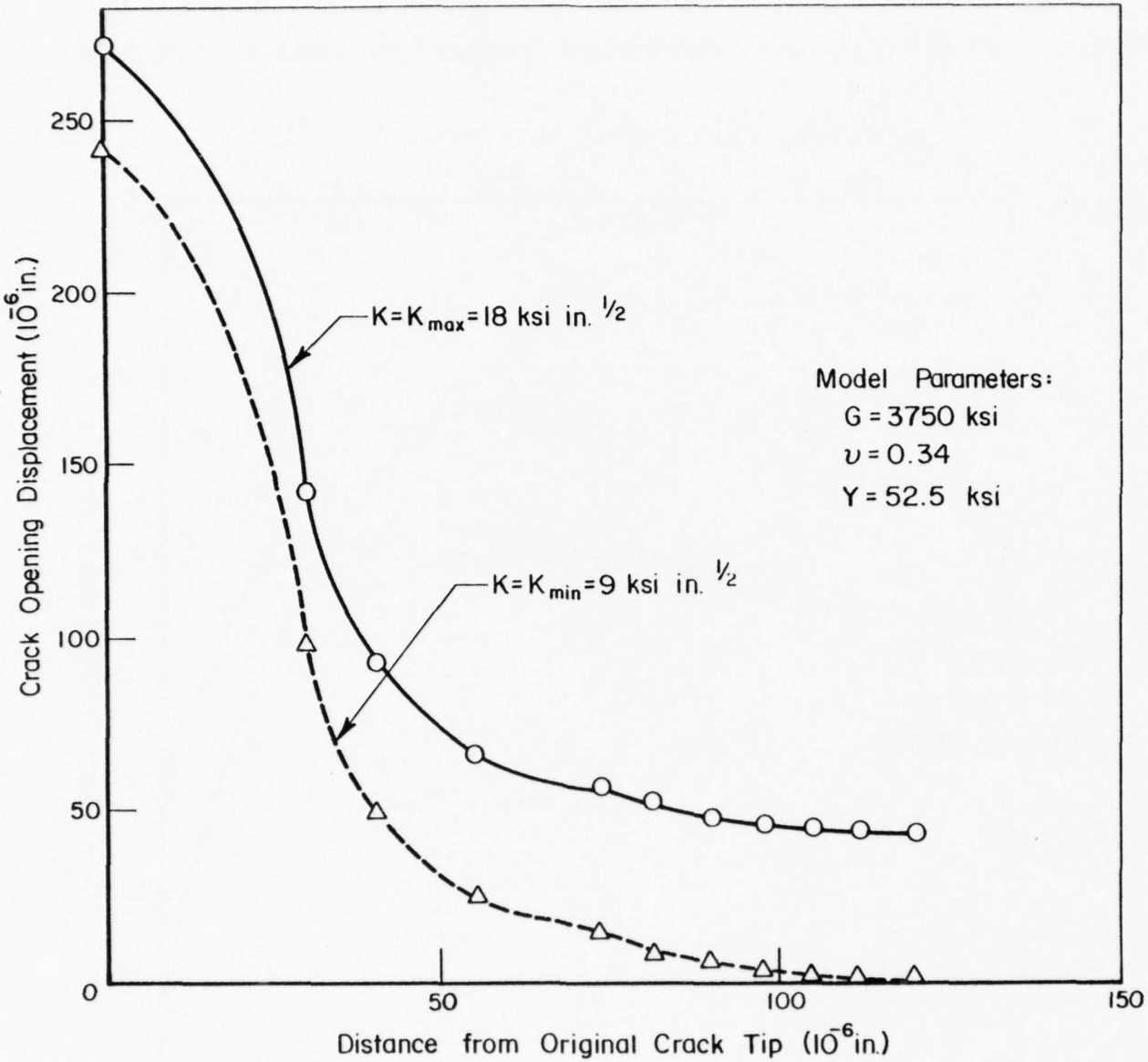

FIGURE 5.7. COMPUTED CRACK-OPENING DISPLACEMENTS IN THE 12TH LOAD CYCLE IN ALUMINUM

On the negative side, there are certain predictions of the present model that are not in such good agreement with experiment. For example, while the model predicts an "R-effect", it is contradicted by the data. That is, while the growth rates for uniform cyclic loading with ΔK = constant tend to increase with $R = K_{min}/K_{max}$, the model predicts a decrease. This is shown in Figure 5.8 for aluminum.

The trend for the $K_{min} = 0$ calculations to overestimate the growth rate, seen in Figure 5.8, is also shown in Figure 5.9. In the latter figure, the measured crack-growth rates for aluminum as a function of K_{max} for $K_{min} = 0$ can be seen to be considerably under the predicted values. However, the correct general trend does seem to be given by the model. Subsequent work is to improve upon the deficiencies in the predictions of the current model.

The Effect of Mechanical Properties

As has been emphasized throughout this report, the computational model depends only on the ordinary mechanical properties of the material being simulated: G, Y, and ν. It is of interest to determine the relative importance of each of these on the fatigue-crack-growth rates. From consideration of the basic equations of the model, Poisson's ratio can be seen to have little effect. So, only G and Y need to be varied. This has been done by taking the particular values used for the aluminum and titanium simulations and interchanging them. The results are as shown in Table 5.3.

TABLE 5.3. COMPARISON OF STEADY-STATE CRACK-GROWTH RATES SHOWING THE EFFECT OF THE MECHANICAL PROPERTIES OF THE MATERIAL

$K_{max} = 20$, $K_{min} = 10$

$\nu = 0.335$

$\left(\frac{da}{dN}\right)$ units of 10^{-6} in./cycle

	Y = 52.5 ksi	Y = 120.0 ksi
G = 3750 ksi	9.61	4.10
G = 6000 ksi	5.91	2.48

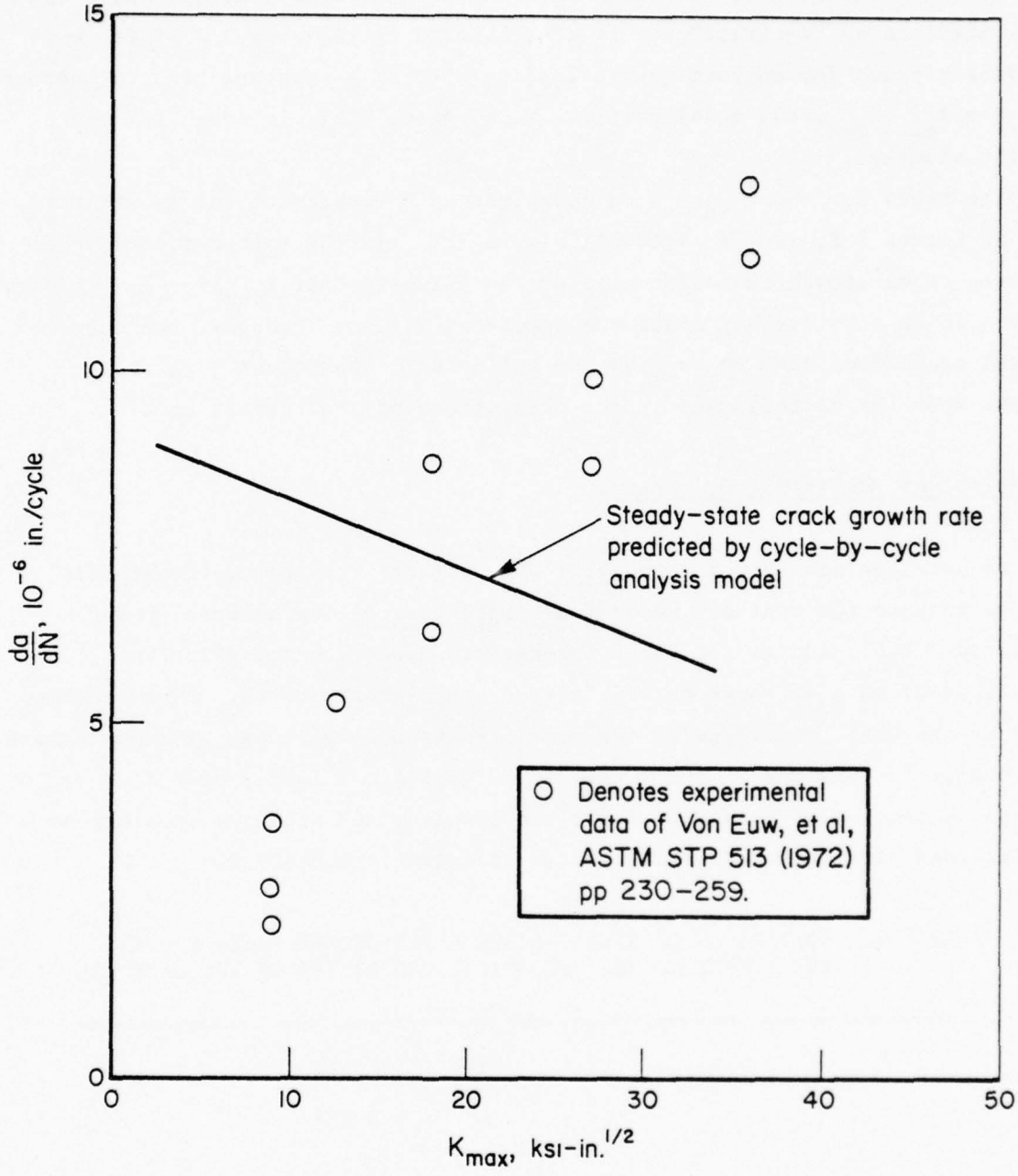

FIGURE 5.8. COMPARISON OF PREDICTED AND OBSERVED FATIGUE-CRACK-PROPAGATION RATES IN 2024-T3 ALUMINUM FOR ΔK = 9 KSI-IN.$^{\frac{1}{2}}$

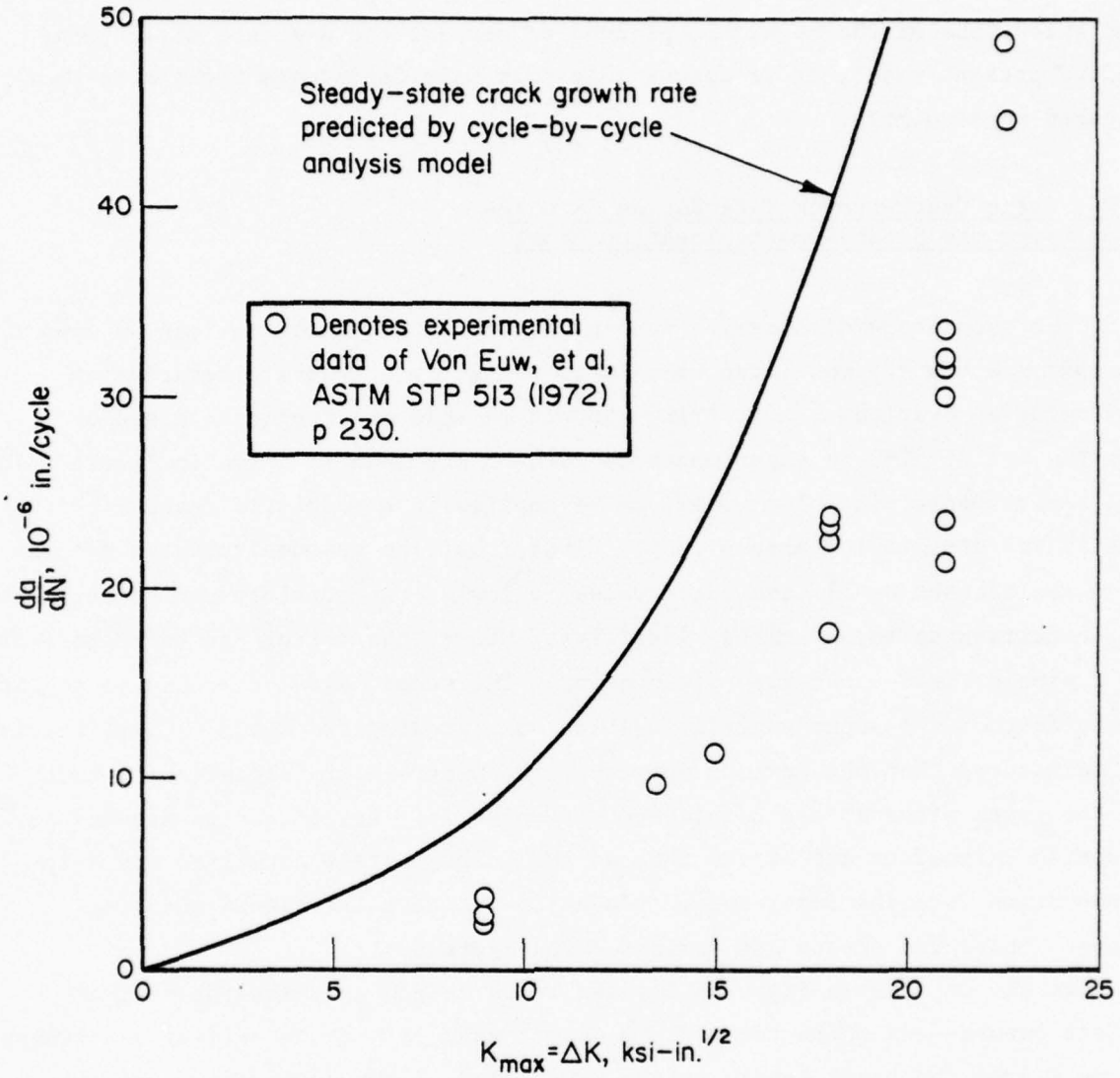

FIGURE 5.9. COMPARISON OF PREDICTED AND OBSERVED FATIGUE-CRACK-PROPAGATION RATES IN 2024-T3 ALUMINUM FOR $K_{min} = 0$

The results in Table 5.3 demonstrate a $(GY)^{-1}$ dependence of the fatigue-crack-growth rates in the cycle-by-cycle computations. This was, of course, already seen in the closed-form expressions found using the super-superdislocation model in the preceding section. However, because further modifications and extensions of the model are planned to correct the R-effect discrepancy in the present model, it is conceivable that this dependence might also be altered subsequently.

A Heuristic Crack-Growth Retardation Calculation Using the Super-Superdislocation Model

The super-superdislocation concept introduced in Section 4 can be used to demonstrate how the model can be made to reflect crack-growth retardation following an overload. A striking example of this phenomenon obtained by von Euw, et al [7], in experiments on 2024-T3 aluminum is shown in Figure 5.10. The super-superdislocation model can be applied in a heuristic fashion by making two simplifying assumptions. First, that the residual plastic deformation contributed by all the load cycles following the overload can be neglected in comparison to the overload plasticity. Hence, the latter can be represented by a single fixed super-superdislocation. The second assumption has to do with the effect of the super-superdislocation on a growing crack tip. Specifically, it is assumed that the maximum effect of the super-superdislocation is felt on the crack plane at the point directly under it. Its effect is assumed to diminish thereafter and become zero at the point where a normal to the slip plane drawn from the super-superdislocation position intersects the crack plane. These two points are indicated in Figure 5.11.

As can be seen in Figure 5.11, the crack length at which the maximum effect occurs--and where the minimum growth rate is expected--is at a distance $\ell \cos\theta$ from the crack length at the imposition of the overload. Similarly, the original growth rate should be reached after a growth increase of $\ell/\cos\theta$. Now, taking the linearized equations for the single dislocation pair and solving for the position gives

$$\frac{\ell}{a_o} = \frac{1}{72}\left(\frac{\sigma}{\tau_i}\right)^2 \left[3\sin\theta\cos\frac{\theta}{2} - \frac{1}{\sin\theta\cos\frac{\theta}{2}}\right]^2 \left[1 - \sin\theta\cos\theta\,\frac{\sigma}{\tau_i}\right]^{-2} . \qquad (5.3)$$

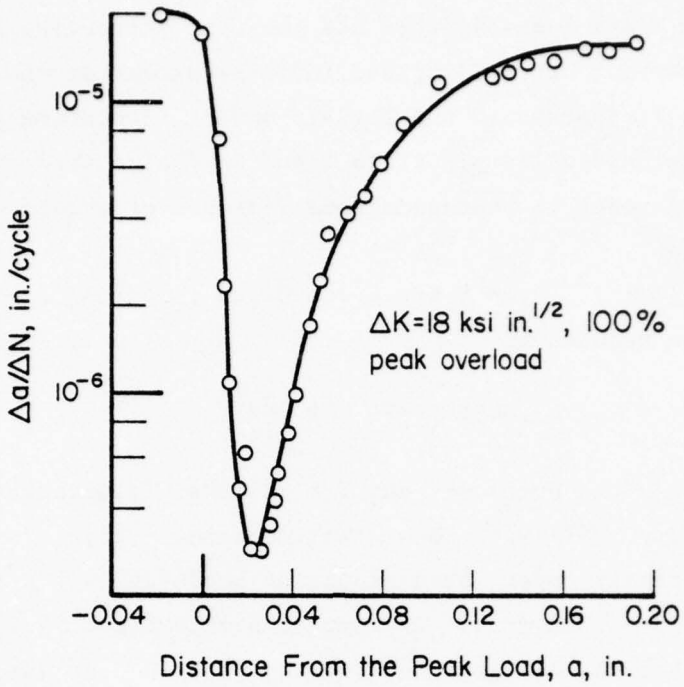

FIGURE 5.10. RETARDED FATIGUE-CRACK-GROWTH RATE IN 2024-T3 ALUMINUM ALLOY FOLLOWING THE APPLICATION OF A SINGLE OVERLOAD[7]

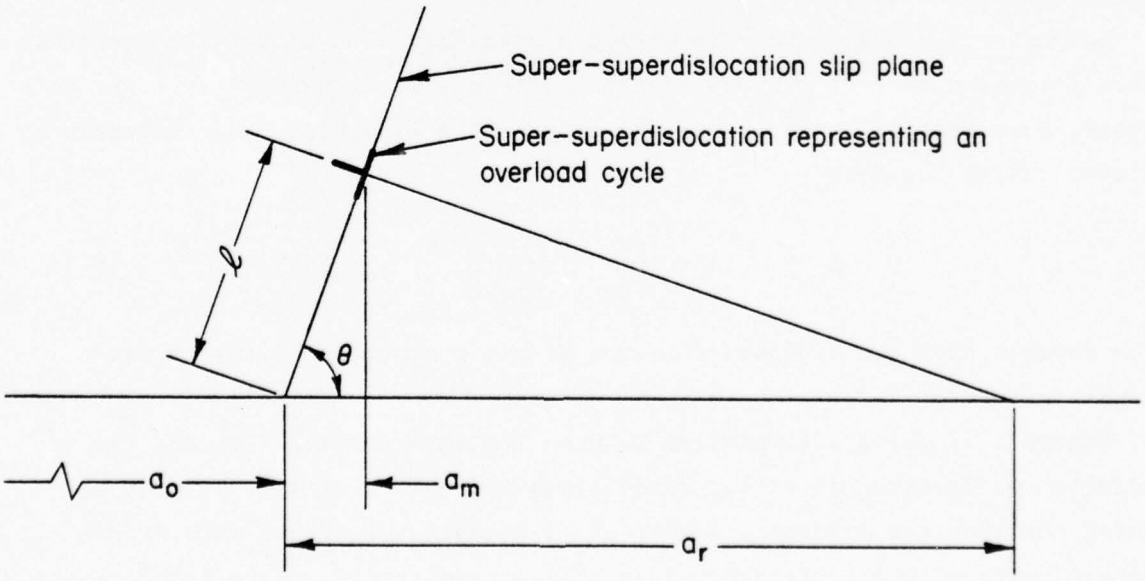

FIGURE 5.11. GEOMETRIC BASIS FOR HEURISTIC CRACK-GROWTH-RETARDATION CALCULATION

Notice that if $\tau_i = Y \sin\theta \cos\theta$, this has the very attractive feature of giving an infinite extent of yielding and infinite extent of yielding and infinite COD at $\sigma = Y$, just as in the Dugdale model. Accepting this for the moment as being more physically plausible than the choice used previously, the potential of the model to reproduce some features of growth-rate retardation can be examined.

Taking $\sigma = K_{oL}/(\pi a_o)^{\frac{1}{2}}$, $\tau_i = Y \sin\theta \cos\theta$ and inserting $\theta = \cos^{-1}(1/3)$, the above expression reduces to

$$\ell = .0457 \left(\frac{K_{oL}}{Y}\right)^2 \left(1 - \frac{\sigma}{Y}\right)^{-2} .$$

For $K_{oL} = 36$ ksi in.$^{\frac{1}{2}}$ (the overload) and $Y = 52.5$ ksi (aluminum) and taking $a_o = 1$ inch, this gives $\ell = .057$ inch. Now, the increase in crack length such that the crack tip is directly under the dislocation produced in the overload cycle is $\Delta a = \ell \cos\theta = \ell/3 = .019$ inch. In comparing with Figure 5.10, it can be seen to be about equal to the distance from the peak load at which the minimum growth rate occurs. The increase in crack length such that the center line of the dislocation intersects the crack tip is $\Delta a = \ell/\cos\theta = 3\ell$, or 0.172 inch. Again referring to Figure 5.10, this is just about the distance from the peak load at which the influence of the peak load vanishes and the steady-state growth rate is recovered.

Comparisons can also be made with the data discussed in Section 3 of this report for the effect of peak overloads in Ti-6Al-4V titanium alloy. For this purpose, Equation (5.3) can be used to express the length of crack affected by the overload in the form

$$a_r = 0.1371 \left\{\frac{Y}{K_{oL}} - \frac{1}{(\pi a_o)^{\frac{1}{2}}}\right\}^{-2} , \qquad (5.4)$$

which reveals that the dependence is not simply a function of the stress-intensity factor.

Figure 5.12 shows a comparison between the experimental data and the prediction of Equation (5.4) for various assumed values of a_o. It must be pointed out that the agreement is deceptive because the actual data were generated with generally larger values of a_o. Admittedly, there is considerable scatter evident; however, the comparison being sought is a qualitative correlation. The actual a_o values used were on the order of 1 inch and larger

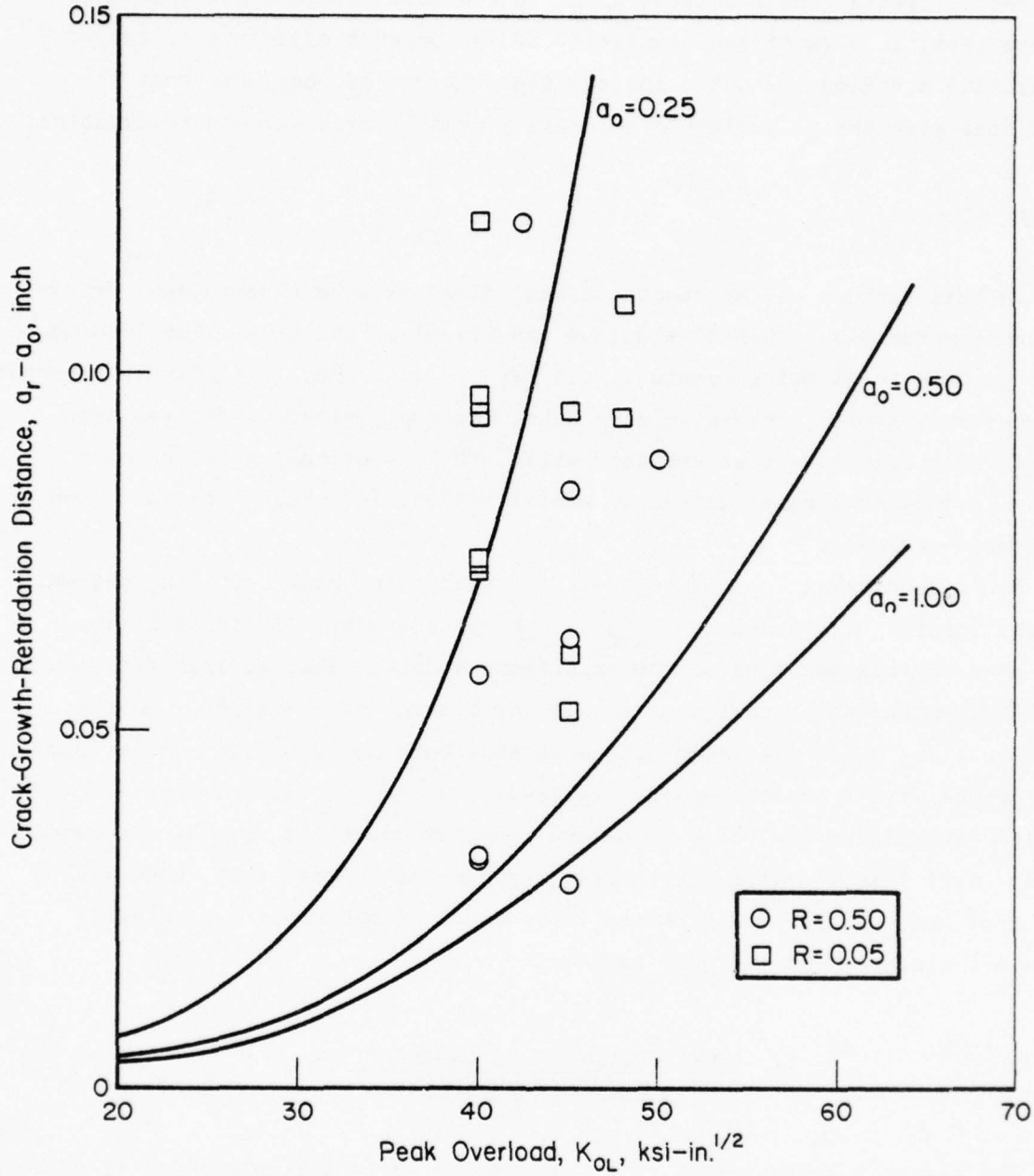

FIGURE 5.12. DISTANCE OF CRACK PROPAGATION FOLLOWING AN OVERLOAD BEFORE STEADY-STATE GROWTH RATE IS RECOVERED IN Ti-6Al-4V

for experimental sensitivity. The lower values shown on the computed lines are used to display the predicted trend in the more design-sensitive range. Nevertheless, in view of the simplicity of the present calculation, the qualitative agreement is quite instructive. It can be concluded that the model does have the potential to accurately predict crack-growth retardation.

Closure

In this section of the report, computations have been performed for two different materials: 2024-T3 aluminum and Ti-6Al-4V titanium. For loading corresponding to ΔK being constant, the results show that a relatively constant fatigue-crack-growth rate is quickly achieved; e.g., within about ten load cycles. Although some discrepancies exist, the comparisons between these steady-state growth rates and experimental results for these materials show quite good agreement.

For reasons that are not entirely clear at this point, computations made for the special case where $R = K_{min}/K_{max} = 0.5$ are virtually right in the middle of the scatter band of the experimental data. This is true for both the aluminum and the titanium materials for a range of ΔK values. On the negative side, while the calculations do show both an "R effect" and a load interaction effect in nonconstant amplitude cycling, in neither case are the results satisfactory as yet. These are probably connected so that the remedy for one will likely make a substantial improvement in the other, however. A number of options are open in which improvement of the model can be made. These are discussed in the next section.

6. CONCLUSIONS AND RECOMMENDATIONS FOR FURTHER RESEARCH

The specific objective of this work was to apply a simple model of plastic relaxation at a crack tip to the fatigue problem. The model allows an estimate of the plastic flow at each stage in a reasonably simple way using the "super-dislocation" idea which further allows a look at cycle-by-cycle growth with residual plasticity left from previous cycles still playing a role. Thus, a sequential calculation is made in a logically self-consistent manner with

due attention being paid to the equilibrium of each of the superdislocations. Perhaps the main criticism that could be leveled at this approach is that the superdislocation is an oversimplification of the plastic field which may limit the chances of the present model exhibiting the trends usually observed in experiments on fatigue. In fact, as pointed out earlier in this report, the present results do not in all respects duplicate those to be obtained by experiment. However, this is due to the details contained in the present model rather than to the overall philosophy. In this section, some of the main consequences of the results are discussed and recommendations for further work to overcome the objectionable features are given.

In the first place, with the complete model, a strictly logical evaluation is conducted with the results being a direct consequence of the growth criterion and the variety of stress interactions occurring between the dislocations and the crack. As one highly significant result, the cycle-by-cycle calculations do predict a steady-state growth rate. Before discussing possible changes that could be made in the growth conditions, consider the computational results in terms of a simplified view of the steady-state situation as applied to the complete model. The way that the growth is specified on the crack at the σ_{min} load, the crack closes at the crack tip after advance ($\delta = 0$) and the dislocation on the current slip band changes its strength and/or position to accommodate the condition as well as being in equilibrium. The net effect is that when σ_{max} is applied again, it is acting on a residual stress due to the dislocations left behind. These residual stresses just balanced σ_{min}. Hence, on the current crack, an effective stress of $(\sigma_{max} - \sigma_{min})$ is acting. It is then expected from the linearized results that $\delta = 0.44\ K^2/EY$. This result for crack advance is proportional to $\Delta K = K_{max} - K_{min} = \sqrt{\pi a}\ (\sigma_{max} - \sigma_{min})$. This neglects, of course, any effect that neighboring dislocations have on the current one being emitted from the crack tip; therefore, the result can only be approximate. The actual computational results are quite close to the results suggested by the above argument. Hence, the numerical results for the complete model demonstrate that the progressive development and dispersion dislocations will in fact lead to a steady-state growth rate which is approximately proportional to $(\Delta K)^2$ even when all the dislocation stress fields are correctly taken into account.

Previous models appearing in the literature have never shown this with a self consistent logical scheme in which the process of producing dislocations,

etc., is followed through in a sequential way. It might be noted that the model does demonstrate a deviation from the $(\Delta K)^2$ law which depends precisely on the dislocation interactions (our model of the plastic field). However, the precise form of the complete numerical results do not show the desired experimental trend. So, some modifications are obviously in order.

As discussed in the preceding section of this report, there are many aspects of the present model which can certainly be improved upon. By exploring the options that are open to improve the present shortcomings and incorporating the satisfactory candidates to build upon the presently successful features, it is believed that these can be overcome. Consequently, the model can be used as the basis of the computational approach that is the objective of this work. Some of the possibilities are as follows:

(1) The singularity-canceling equation is currently imposed at the maximum as well as at the minimum load level in each load cycle. In addition to being physically unreasonable, this unduly constrains the crack-tip deformation and, hence, leads to incorrect growth-rate predictions. As one example, a threshold ΔK level is precluded. What is essentially needed is a mathematical relation that can be used to replace the singularity-canceling equation at maximum load. Such a condition, possibly one involving the amount of opening at the crack tip, must therefore, be sought.

(2) At the minimum load level in a load cycle, the nascent superdislocation is decomposed into two superdislocations to represent the loss of plasticity involved in unloading. The criterion for the decomposition is currently one that maximizes their strengths. This is somewhat arbitrary and certainly other plausible choices exist that could be used. The computed growth rates are sensitive to the exact choice, however, particularly when $K_{min} = 0$. Thus, a more rigorous procedure is needed.

(3) The super-superdislocation concept, in which the superdislocations generated in several different load cycles are lumped together, offers both significant computational efficiency in the complete cycle-by-cycle model and a simple testing

ground for new ideas. Further development of this concept for these dual purposes is therefore warranted.

To take the model as it presently exists to the point where the objectives of the work can be accomplished will require improvements in the manner in which the computations are performed as outlined above. Measures leading to improved qualitative agreement with the observed R effect and crack-growth retardation must also be incorporated into the model. Comparison with alternative approaches and with crack growth and other experimental data (e.g., crack-closure measurements) can then be made.

To improve the computational efficiency of the model, a scheme for determining when and how the superdislocations representing the residual plasticity from previous load cycles can be lumped together in one or more super-superdislocations should be pursued. The point at which an optimum balance between accuracy and computational time requirements should be determined (NB, while this point could depend on the load spectrum under consideration, the computed growth rates must be independent of the manner in which the super-superdislocations are introduced.) Linearization of the governing equations to achieve more economical computations might also be investigated.

Finally, it must be emphasized that, while the work performed so far in developing the model is quite promising, there can be no assurance that the approach described above will ever produce a useful tool for practical applications. It is possible that the goal of a fundamentally valid model that can be used in an economical manner simply cannot be attained. If the inclined-strip yield-superdislocation model cannot be constructed to meet the goal of an accurate and efficient fatigue crack-growth predictive technique, then such a goal is probably not within the current state of the art.

7. REFERENCES

1. Bilby, B. A., and Swinden, K. H., "Representation of Plasticity at Notches by Linear Dislocation Arrays", Proc. Roy. Soc., Vol A285, No. 22, 1965.

2. Atkinson, C., "The Interaction Between a Dislocation and a Crack", Int. J. Fracture Mech., Vol 2, No. 567, 1966.

3. Atkinson, C., and Kay, T. R., "A Simple Model of Relaxation at a Crack Tip", Acta Met., Vol 19, No. 679, 1971.

4. Atkinson, C., and Clements, D. L., "The Influence of Anisotropy and Crystalline Slip on Relaxation at a Crack Tip", Acta Met., Vol 21, No. 55, 1973.

5. Feddersen, C. E., and Hyler, W. S., "Fracture and Fatigue-Crack-Propagation Characteristics of ½-Inch Mill-Annealed Ti-6Al-4V Titanium Alloy Plate", Final Report to Naval Air Development Center from Battelle's Columbus Laboratories, Contract No. N00156-70-C-1336, November 1, 1971.

6. Feddersen, C. E., Porfilio, T. L., Rice, R. C., and Hyler, W. S., "Part-Through Crack Behavior in Three Thicknesses of Mill-Annealed Ti-6Al-4V Plate", Final Report to Naval Air Development Center from Battelle's Columbus Laboratories, Contract No. N62269-73-C-0036, December 31, 1972.

7. von Euw, E.F.J., Hertzberg, R. W., and Roberts, R., "Delay Effects in Fatigue-Crack Propagation", Stress Analysis and Growth of Cracks, ASTM STP 513, American Society for Testing and Materials, 1972, p 230.

8. Wheeler, O. E., "Spectrum Loading and Crack Growth", J. Basic Eng., 1972.

9. Willenborg, J., Engle, R. M., Jr., and Wood, H. A., "A Crack-Growth-Retardation Model Using an Effective Stress Concept", AFFDL-TM-71-1-FBR, 1971.

10. Newman, J. C., Jr., "Finite-Element Analysis of Fatigue-Crack Propagation Including the Effects of Crack Closure", Ph.D. Dissertation in Engineering Mechanics, Virginia Polytechnic Institute and State University, Blacksburg, Virginia, May 1974.

11. Elber, W., "Fatigue-Crack Closure Under Cyclic Tension", Eng. Fracture Mech., Vol 2, No. 37, 1970.

12. Rice, J. R., "Mechanics of Crack-Tip Deformation and Extension by Fatigue", Fatigue-Crack Propagation, ASTM STP 415, American Society for Testing and Materials, 1967, p 247.

13. Weertman, H., "Theory of Rate of Growth of Fatigue Crack Under Combined Static and Cyclic Stresses", Int. J. Fracture Mech., Vol 5, No. 13, 1969.

14. Bilby, B. A., and Heald, P. T., "Crack Growth in Notch Fatigue", Proc. Roy. Soc., Vol A305, No. 429, 1968.

15. Yokobari, T., and Yoshida, M., "Kinetic Theory Approach to Fatigue-Crack Propagation in Terms of Dislocation Dynamics", Int. J. Fracture, Vol 10, No. 467, 1974.

16. Neumann, P., "The Geometry of Slip Processes at a Propagating Fatigue Crack", Acta Met., Vol 22, No. 1167, 1974.

APPENDIX A

DERIVATION OF THE BASIC EQUATIONS FOR THE CYCLE-BY-CYCLE ANALYSIS MODEL FOR FATIGUE-CRACK GROWTH UNDER ARBITRARY SPECTRUM LOADING

General Analytical Approach

The analytical approach taken in this work rests on two fundamental assumptions: (1) the crack-tip crack-opening displacement (CTCOD) arising from the intense plastic deformation attending the crack tip is the parameter that governs crack growth and (2) the essential feature of fatigue-crack growth is the interaction between the plastic deformation created in different load cycles. By basing the work upon an inclined strip-yield model, the approach taken here uses what is perhaps the simplest mathematical model in which those considerations (i.e., CTCOD and distinguishable plastic zones in each load cycle) can be taken into account in a rigorous fashion.

Because experimental results on fatigue-crack propagation are almost always reported in terms of a linear-elastic stress-intensity-factor parameter, it may be useful to show the connection between this parameter and the crack-opening displacement (COD) parameter to be used in the model. Obtained from the Dugdale strip-yielding crack model [1]*, the commonly used expression [2] for the latter quantity

$$\delta = \frac{8}{\pi} \frac{Y\alpha}{E} \log \sec \frac{\pi}{2} \frac{\sigma}{Y} \quad , \tag{A-1}$$

where δ = COD at the crack tip

2α = crack length

σ = applied tensile stress

Y = yield stress

E = elastic modulus.

For the case where σ is small in comparison to Y, the above expression can be linearized to get

$$\delta = \frac{\sigma^2 \pi \alpha}{EY} + \ldots \quad .$$

---

* References for this appendix are given on page 78.

Now, the stress-intensity factor for this situation is simply $K = \sigma\sqrt{\pi a}$. Hence, for $\sigma/Y \ll 1$, it can easily be seen that

$$\delta = \frac{K^2}{EY} \quad . \tag{A-2}$$

This means that for the load levels ordinarily used in fatigue-crack-growth experiments, treating K as the driving force for crack extension is equivalent to using δ for this purpose. Note that an alternative point of view is to use the Griffith theory to express the strain-energy-release rate as $\mathcal{G} = \delta Y$. Then, from the equivalence between the strain-energy-release rate and stress-intensity factor given by $K^2 = E\mathcal{G}$, the result given as Equation (A-2) is obtained.

The general idea upon which the present analysis is based--the representation of a crack and its attendant zones of plastic deformation by dislocation arrays--evolved from the work of Head and Loust [3] and Bilby, et al [4]. When both approaches are tractable, it can be shown that the dislocation array approach leads to solutions that are identical to those obtained through continuum elasticity, e.g., the Dugdale problem. The virtue of this dislocation approach is that it is often tractable when continuum theory is not. This is true in particular for the inclined strip-yield zone solution given by Bilby and Swinden [5], which is the basis of the development pursued in this report. A drawback of the dislocation models is that a singular integral equation must be solved. This would make the Bilby-Swinden model per se exceedingly cumbersome for use in representing fatigue-crack growth despite its advantageous features. Consequently, the simplification afforded by Atkinson's superdislocation concept [6-8] has been introduced to enable a large number of load cycles to be examined.

The notation used in the following generally corresponds to that used by Rice [9]. Results not specifically referenced elsewhere can be found in Reference 9.

Mathematical Development

It will be considered in this report that crack growth occurs in an isotropic linear elastic body under plane strain (or generalized plane stress) conditions. Crack-tip plasticity will be represented by discrete dislocations, finite in number, that are confined to specified slip planes. Because discrete

dislocations can be treated within the theory of elasticity, it is appropriate to adopt the complex variable approach developed by Muskhelishvili. In this approach, the stresses and displacements for elastic deformation in the xy plane are expressed in terms of two arbitrary functions of the complex variable $z = x + iy$ by the relations

$$\sigma_{11} + \sigma_{22} = 4 \text{ Re } \{\phi'(z)\} \quad , \tag{A-3}$$

$$\frac{1}{2} (\sigma_{22} - \sigma_{11}) + i\sigma_{12} = \bar{z}\phi''(z) + \psi'(z) \quad , \tag{A-4}$$

and

$$2G (u_1 + iu_2) = \kappa\phi(z) - \overline{z\phi'(z)} - \overline{\psi(z)} \quad . \tag{A-5}$$

Here, G is the shear modulus and

$$\kappa = \begin{cases} 3 - 4\nu \text{ , plane strain} \\ \dfrac{3 - \nu}{1 + \nu} \text{ , plane stress} \end{cases} \quad , \tag{A-6}$$

where ν is Poisson's ratio. Note that in Equations (A-3) through (A-5) and in the following, the prime notation indicates differentiation with respect to z, the bar notation is used to denote the complex conjugate, and the convention $\overline{F(z)} = \bar{F}(\bar{z})$ is used throughout. Also note that + and - signs used as subscripts denote limits of the function as the x-axis is approached from the regions $y > 0$ and $y < 0$, respectively.

The basic relations needed are those for the interaction between a dislocation and a crack in an infinite body under remotely applied loading. It is considered that the crack lies along the x-axis with the tips of the crack being at the position (a,0) and (-a,0). The dislocation is located at the position $Z = \xi + i\eta$ and has a Burger's vector $B = b_1 + ib_2$. Although we will confine our attention to tensile loading in treating crack growth, at this point in the development of the model a more general applied loading of biaxial tension plus shear is considered; i.e., as $\sqrt{x^2 + y^2} \to \infty$ $\sigma_{11} = T_1$, $\sigma_{22} = T_2$, and $\sigma_{12} = S$ (see Figure A-1).

A solution for the stress and displacement fields for the problem shown in Figure A-1 can be obtained by linear superposition after first determining the complex potentials for two subproblems. These subproblems correspond to an isolated dislocation and an isolated crack.

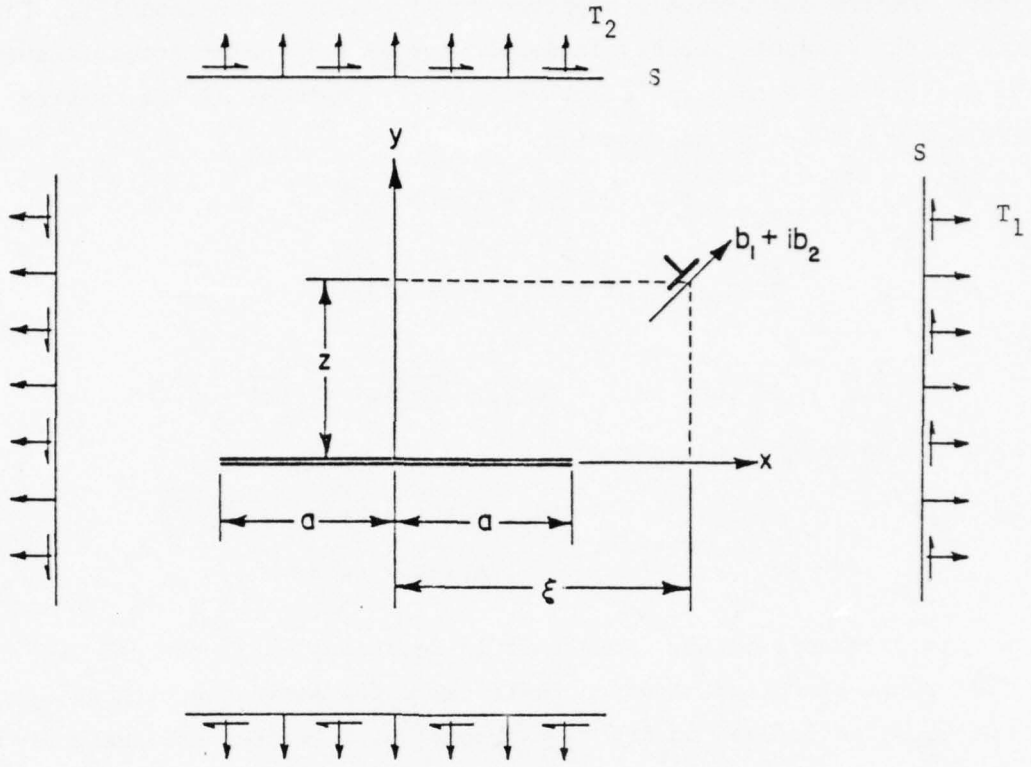

FIGURE A-1. LOADING CONFIGURATION

The Isolated Dislocation

The complex potentials for a dislocation with Burger's vector $b_1 + ib_2$ at the generic position $Z = \xi + i\eta$ are given by

$$\phi'(z) = \frac{G(b_1 + ib_2)}{i\pi(\kappa + 1)} \frac{1}{z - Z} , \tag{A-7}$$

and

$$\Omega'(z) = -\frac{G(b_1 - ib_2)}{i\pi(\kappa + 1)} \frac{1}{z - Z} - \frac{G(b_1 + ib_2)(Z - \bar{Z})}{i\pi(\kappa + 1)(z - Z)^2} , \tag{A-8}$$

where

$$\Omega(z) = z\phi'(z) + \psi(z) . \tag{A-9}$$

Combining Equations (A-3) through (A-5) with (A-9) gives

$$\sigma_{11} + \sigma_{22} = 4 \text{ Re } \{\phi' (z)\} ,$$

$$\tfrac{1}{2} (\sigma_{22} - \sigma_{11}) + i\sigma_{12} = (\bar{z} - z) \phi'' (z) - \phi' (z) + \Omega' (z) ,$$

and

$$2G (u_1 + iu_2) = \kappa\phi (z) - \overline{\Omega(z)} + (\bar{z} - z) \overline{\phi' (z)} .$$

Or, by substituting Equations (A-7) and (A-8) into the above, we have

$$\tfrac{1}{2} (\sigma_{11} + \sigma_{22}) = \frac{2}{\pi} \frac{G}{\kappa + 1} \text{ Im} \left\{ \frac{b_1 + ib_2}{z - Z} \right\} , \tag{A-10}$$

$$\tfrac{1}{2} (\sigma_{22} - \sigma_{11}) + i\sigma_{12} = \frac{G}{i\pi (\kappa + 1)} \left\{ \frac{(b_1 + ib_2) (z - \bar{z} + \bar{Z} - Z)}{(z - Z)^2} - \frac{2b_1}{z - Z} \right\} , \tag{A-11}$$

and

$$u_1 + iu_2 = \frac{1}{2\pi i (\kappa + 1)} \left\{ \kappa (b_1 + ib_2) \log (z - Z) - (b_1 + ib_2) \log (\bar{z} - \bar{Z}) + \frac{(b_1 - ib_2) (z - \bar{z} + \bar{Z} - Z)}{\bar{z} - \bar{Z}} \right\} , \tag{A-12}$$

for the dislocation.

It is important to recognize that here and throughout this work, care must be taken with the branches of the log function in the expression for the displacements. It is this function, of course, that gives the discontinuity in displacement characteristic of the dislocation. Relations such as Equation (A-12), it might be noted, can be used in incorporating the crack-closure effect [10-12].

The Isolated Crack

For the crack problem, it can be shown that for the stresses to vanish at infinity, we must have

$$\psi (z) = \overline{\phi} (z) - z\phi' (z) .$$

Equations (A-3) through (A-5) can then be written in terms of a single potential function as follows:

$$\sigma_{11} + \sigma_{22} = 4 \text{ Re } \{\phi'(z)\} , \tag{A-13}$$

$$\tfrac{1}{2} (\sigma_{22} - \sigma_{11}) + i\sigma_{12} = \bar{\phi}'(z) - \phi'(z) - (z - \bar{z}) \phi''(z) , \tag{A-14}$$

and

$$2G (u_1 + iu_2) = K\phi(z) - \phi(\bar{z}) + (\bar{z} - z) \overline{\phi'(z)} . \tag{A-15}$$

For these conditions, Rice shows that the potential function is given by the relation

$$\phi'(z) = - \frac{1}{2\pi} (z^2 - a^2)^{-\frac{1}{2}} \int_{-a}^{a} [p_2(t) - ip_1(t)] \frac{(a^2 - t^2)^{\frac{1}{2}}}{(t - z)} dt . \tag{A-16}$$

The simplest situation is where the surface tractions are constant. This arises, in particular, when the solution for a crack in a body acted upon by uniform remote tension and shear is to be obtained by superposition. Referring to Figure A-1, the applied load exerts a stress field on the x-axis that is

$$\sigma_{22} - i\sigma_{12} = T_2 - iS .$$

Hence, we have $p_1 = - S_2$ and $p_2 = T_2$. Substituting these into Equation (A-16) then gives

$$\phi'(z) = - \frac{1}{2\pi} \frac{T_2 - iS}{(z^2 - a^2)^{\frac{1}{2}}} \int_{-a}^{a} \frac{(a^2 - t^2)^{\frac{1}{2}}}{t - z} dt ,$$

so that

$$\phi'(z) = - \tfrac{1}{2} (T_2 - iS) \left[1 - \frac{z}{(z^2 - a^2)^{\frac{1}{2}}} \right] . \tag{A-17}$$

It is easily found that

$$\phi''(z) = - \tfrac{1}{2} (T_2 - iS) \frac{a^2}{(z^2 - a^2)^{\frac{3}{2}}} , \tag{A-18}$$

and, by integrating Equation (A-17),

$$\phi(z) = - \tfrac{1}{2} (T_2 - iS) [z - (z^2 - a^2)^{\frac{1}{2}}] . \tag{A-19}$$

The constant of integration corresponds to rigid body translation and has been omitted from Equation (A-19).

Because $(z^2 - a^2)^{\frac{1}{2}} = i (a^2 - z^2)^{\frac{1}{2}}$ and taking the positive value of $(a^2 - z^2)^{\frac{1}{2}}$ on the upper side of the branch cut, it is found that when $y \to 0$,

$$\phi_+ - \phi_- = (iT_2 + S)\ (a^2 - x^2)^{\frac{1}{2}} \quad ,$$

on the interval $|x| < a$ and zero outside the interval. Hence, from Equation (A-15), the discontinuity in the displacements on the crack faces due to the applied stress can be obtained from

$$[u_1 + iu_2]_+ - [u_1 + iu_2]_- = \frac{(\kappa + 1)}{2G}\ (iT_2 + S)\ (a^2 - x^2)^{\frac{1}{2}} \ .$$

Hence, the crack-opening displacement is given more explicitly by

$$\Delta u_1 + i\Delta u_2 = \frac{\kappa + 1}{2G}\ (S + iT_2)\ (a^2 - x^2)^{\frac{1}{2}} \quad |x| \leq a \ . \qquad \text{(A-20)}$$

To obtain the displacement elsewhere in the body, the uniform field due to stresses $\sigma_{11} = T_1$, $\sigma_{22} = T_2$ and $\sigma_{12} = S$ must be superposed. Using Equations (A-3) through (A-5), this is easily found to give

$$u_1 + iu_2 = \frac{1}{2G}\left[\frac{\kappa - 1}{4}\ (T_1 + T_2)\ z + \tfrac{1}{2}\ (T_1 - T_2 + 2iS)\ \bar{z}\right] .$$

But, because this expression gives zero contribution to the COD under tensile loading alone, it will not be used in the following.

Dislocation and Crack Together

To obtain a solution for a dislocation located near a crack, we first determine the stresses exerted by an isolated dislocation on the line segment where the crack is to be located. For the dislocation positioned as shown in Figure A-1, Equations (A-10) and (A-11) should be combined to get an expression for the normal and shear stress exerted on the x-axis. This is

$$\sigma_{22} + i\sigma_{12} = 2\mathrm{Re}\left\{\frac{G\,(b_1 + b_2)}{i\pi\ (\kappa + 1)\ (x - Z)}\right\} - \frac{G}{i\pi\ (\kappa + 1)}\left\{\frac{2b_1}{x - Z} + \frac{(b_1 + ib_2)\ (Z - \bar{Z})}{(x - Z)^2}\right\} \qquad \text{(A-21)}$$

The next step is to determine the potential function for a crack with stresses acting on its surfaces which will wipe out the dislocation stresses on the crack. This is accomplished by substituting Equation (A-21) into Equation (A-16). To integrate the result, we need the following general result which can be obtained by contour integration:

$$\int_{-a}^{a} \frac{(a^2 - t^2)^{\frac{1}{2}}}{(t - z)\ (t - Z)}\ dt = \pi \left\{ \frac{(z^2 - a^2)^{\frac{1}{2}} - (Z^2 - a^2)^{\frac{1}{2}}}{z - Z} - 1 \right\} . \tag{A-22}$$

As above, the branch of the complex square root is defined such that $(a^2 - z^2)^{\frac{1}{2}}$ is the branch cut along $(-a, a)$ taking the positive value on the $y > 0$ side. Also, note that for large z, $(a^2 - z^2)^{\frac{1}{2}} \rightarrow -iz + 0(1)$ so that $(z^2 - a^2)^{\frac{1}{2}} = i\ (a^2 - z^2)^{\frac{1}{2}}$. With these results we obtain

$$\begin{aligned} \phi'(z) = {} & \frac{G}{2\pi i\ (K+1)} \frac{(b_1 - ib_2)}{} \left\{ 2 + \frac{(Z^2 - a^2)^{\frac{1}{2}} - (z^2 - a^2)^{\frac{1}{2}}}{z - Z} \right. \\ & \left. + \frac{(\overline{Z}^2 - a^2)^{\frac{1}{2}} - (z^2 - a^2)^{\frac{1}{2}}}{z - \overline{Z}} \right\} \\ & - \frac{G}{2\pi i\ (K+1)} \frac{(b_1 - ib_2)\ (\overline{Z} - Z)}{(z^2 - a^2)^{\frac{1}{2}}} \left\{ \frac{(z^2 - a^2)^{\frac{1}{2}}\ (\overline{Z}^2 - a^2) + a^2 - \overline{Z}z}{(\overline{Z}^2 - a^2)^{\frac{1}{2}}\ (\overline{Z} - z)^2} \right\} \end{aligned} \tag{A-23}$$

It will be necessary in the following to have an explicit expression for $\phi''(z)$ as well as $\phi'(z)$. This is obtained by differentiating Equation (A-23). The result is

$$\begin{aligned} \phi''(z) = {} & \frac{G}{2\pi i\ (K+1)} (b_1 + ib_2) \left\{ \frac{-z}{(z^2 - a^2)^{\frac{3}{2}}} \left[2 + \frac{(Z^2 - a^2)^{\frac{1}{2}}}{z - Z} + \frac{(\overline{Z}^2 - a^2)^{\frac{1}{2}}}{z - \overline{Z}} \right] \right. \\ & \left. + \frac{1}{(z^2 - a^2)^{\frac{1}{2}}} \left[\frac{(z^2 - a^2)^{\frac{1}{2}} - (Z^2 - a^2)^{\frac{1}{2}}}{(z - Z)^2} + \frac{(z^2 - a^2)^{\frac{1}{2}} - (\overline{Z}^2 - a^2)^{\frac{1}{2}}}{(z - \overline{Z})^2} \right] \right\} \\ & - \frac{G}{2\pi i\ (K+1)} (b_1 - ib_2) \frac{(\overline{Z} - Z)}{(z^2 - a^2)^{\frac{1}{2}}\ (\overline{Z} - a^2)^{\frac{1}{2}}\ (\overline{Z} - z)^2} \left\{ \frac{a^2\ (\overline{Z} - z)}{z^2 - a^2} \right. \\ & \left. + \frac{2\ (z^2 - a^2)^{\frac{1}{2}}\ (\overline{Z}^2 - a^2)^{\frac{1}{2}} + 2a^2 - 2\overline{Z}z}{\overline{Z} - z} \right\} \end{aligned} \tag{A-24}$$

This completes the derivation of the basic equations. We now turn to the inclined strip-yield model itself.

The Inclined Strip-Yield Crack Model

Basis for the Model

The equations developed in the preceding section describe the interaction between a crack and a dislocation in an infinite isotropic body with remotely

applied loads under plane-strain conditions. These are the fundamental elements to be used in formulating the solution for a crack with crack-tip plasticity represented by strip-yield zones. As shown in Figure A-2, we intend to characterize the extent of yielding by the position and strength of a single superdislocation on each slip plane. Note that the angle between the slip plane and the crack plane is not to be associated with a particular crystallographic direction. Instead, the intent is to characterize plastic deformation over, perhaps, several grains. This means that the angle should be at least 45 degrees to be in general accord with the shape of macroscopic plastic-yield zones observed around crack tips; see, for example, the experimental evidence presented by Hahn, et al [13].

In this section, the development is confined to a single set of slip planes as would occur in one-half cycle of loading. It is intended that the deformation be symmetric with respect to the origin of coordinates. Consequently, it will suffice to describe the location and strength of the dislocation in the first quadrant (i.e., position 1 in Figure A-2). As shown in Figure A-3, we will let $2a$ be the crack length, ℓ be the distance from the crack tip to the dislocation, θ be the angle between the crack plane and the slip plane, and b be the strength of the dislocation.

If B_j denotes the Burger's vector of the dislocation at position Z_j, it will be convenient to let

$$B_j = b\mu_j \quad , \quad j = 1, 2, 3, 4 \quad , \tag{A-25}$$

where the μ_j's are dimensionless quantities which depend only on θ. We further note that the positions of all of the dislocations can be expressed relative to the position

$$Z_1 = a + \ell e^{i\theta} \quad . \tag{A-26}$$

For references purposes in the following discussion, it is convenient to summarize the locations and strengths of the dislocations as in Table A-1.

TABLE A-1. LOCATIONS AND STRENGTHS OF DISLOCATIONS

j	Z_j	μ_j
1	Z_1	$e^{i\theta}$
2	$\overline{Z}_1$	$-e^{-i\theta}$
3	$-Z_1$	$-e^{i\theta}$
4	$-\overline{Z}_1$	$e^{-i\theta}$

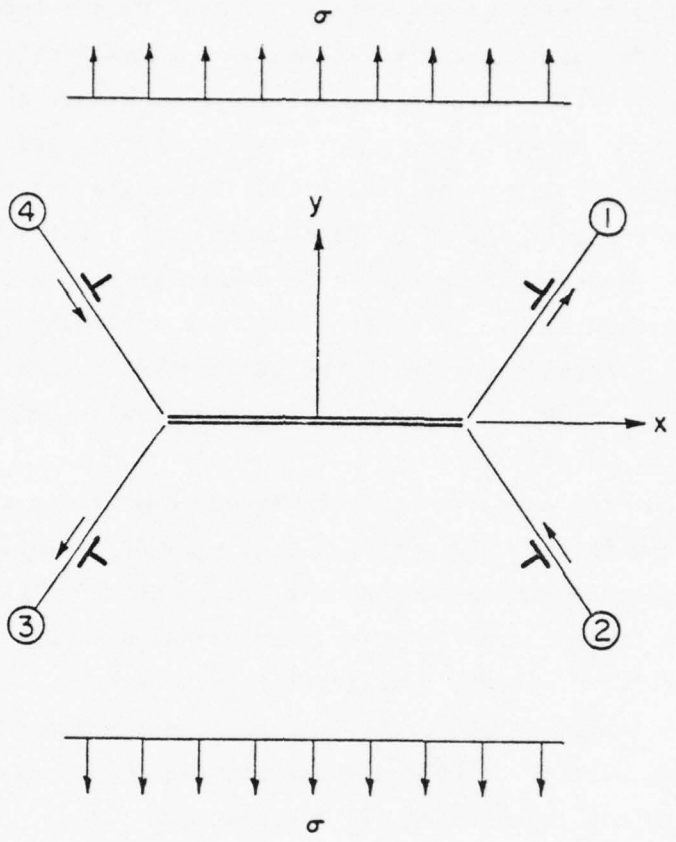

FIGURE A-2. INCLINED STRIP-YIELD ZONE MODEL

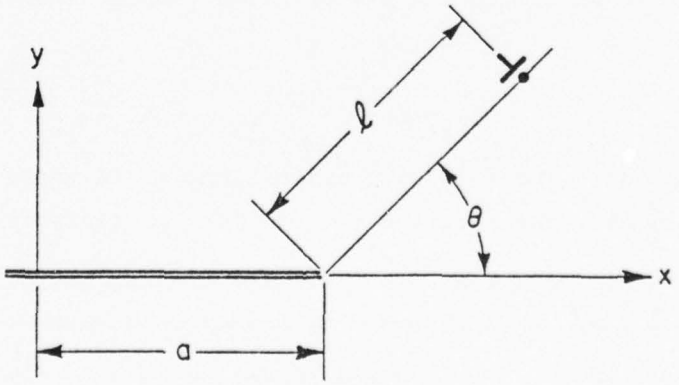

FIGURE A-3. COORDINATE SYSTEM

The stress and displacement fields for the inclined strip-yield problem are obtained by superposition using the solutions for the following subproblems:

- Four symmetrically placed isolated superdislocations
- A crack with nonuniform surface tractions equal and opposite to the dislocation stresses
- Remotely applied tension
- Crack with uniform traction equal and opposite to the applied stress.

In each of the two above crack solutions, there is a singularity at the crack tips. It is taken as axiomatic in this work that the combined singularity must be abolished. This proviso gives one equation which can be used to help determine the two unknowns occurring in the problem. The two unknowns are the strengths and positions of the dislocations; i.e., the quantities b and ℓ. The second equation needed is obtained by assuming that the net resolved shear force acting on a dislocation in the slip plane is balanced by a known retarding or friction force related to the yield stress.

The Singularity-Cancelling Equation

The singularity at the crack tips can be abolished by setting the coefficient of the singular term in the stress field equal to zero. More directly, by combining Equations (A-13) and (A-14), we find that

$$\sigma_{22} - i\sigma_{12} = \phi'(z) + \phi(\bar{z}) + (z - \bar{z})\,\phi''(z) .$$

Consequently, on the x-axis,

$$\sigma_{22} - i\sigma_{12} = \phi_+'(x) + \phi_-'(x) .$$

Or, using Equation (A-17) with $T_2 = \sigma$ and $S = 0$ together with Equation (A-23), we obtain

$$\sigma_{22} - i\sigma_{12} = -\sigma\left\{1 - \frac{|x|}{(x^2 - a^2)^{\frac{1}{2}}}\right\} - \frac{iGb}{\pi(K+1)}\left\{\sum_{j=1}^{4}\frac{\mu_j}{(x^2 - a^2)^{\frac{1}{2}}}\right.$$

$$\cdot\left[2 + \frac{(Z_j^2 - a^2)^{\frac{1}{2}} - (x^2 - a^2)^{\frac{1}{2}}}{x - Z_j} + \frac{(\bar{Z}_j^2 - a^2)^{\frac{1}{2}} - (x^2 - a^2)^{\frac{1}{2}}}{x - \bar{Z}_j}\right]$$

$$\left. - \sum_{j=1}^{4}\frac{\bar{\mu}_j}{(x^2 - a^2)^{\frac{1}{2}}}(\bar{Z}_j - Z_j)\left[\frac{(x^2 - a^2)^{\frac{1}{2}}(\bar{Z}_j^2 - a^2)^{\frac{1}{2}} + a^2 - \bar{Z}_j x}{(\bar{Z}_j - x)^2(\bar{Z}_j^2 - a^2)^{\frac{1}{2}}}\right]\right\} \quad |x| \geq a .$$

The singularity-cancelling equation can be extracted from this expression almost by inspection. It is the coefficient of the term $(x^2 - a^2)^{-\frac{1}{2}}$ evaluated at $x = a$. By setting this to zero, we obtain

$$0 = \sigma a - \frac{iGb}{\pi(\kappa+1)} \left\{ \sum_{j=1}^{4} \mu_j \left[2 + \frac{(Z_j^2 - a^2)^{\frac{1}{2}}}{a - Z_j} + \frac{(\bar{Z}_j^2 - a^2)^{\frac{1}{2}}}{a - \bar{Z}_j} \right] + a \sum_{j=1}^{4} \frac{\bar{\mu}_j (\bar{Z}_j - Z_j)}{(\bar{Z}_j - a)(Z_j^2 - a^2)^{\frac{1}{2}}} \right\} .$$

From the data given in Table A-1, it is evident that

$$\sum_{j=1}^{4} \mu_j = 0 .$$

Consequently, the singularity-cancelling equation reduces to an expression that can be written

$$\sigma a = \frac{Gb}{\pi(\kappa+1)} \operatorname{Im} \left\{ \sum_{j=1}^{4} \mu_j \left[\frac{(Z_j^2 - a^2)^{\frac{1}{2}}}{Z_j - a} + \frac{(\bar{Z}_j^2 - a^2)^{\frac{1}{2}}}{\bar{Z}_j - a} \right] + a \sum_{j=1}^{4} \bar{\mu}_j \frac{(\bar{Z}_j - Z_j)}{(\bar{Z}_j - a)(\bar{Z}_j - a^2)^{\frac{1}{2}}} \right\} . \tag{A-27}$$

Equation (A-27) is the first of the two basic equations needed for determining the two unknowns b and ℓ. Notice that this relation is to be interpreted for given values of the applied stress and crack length, for a single application of the load only.

References

1. Dugdale, D. S., "Yielding of Steel Sheets Containing Slits", J. Mech. Phys. Solids, Vol 8, No. 100, 1960.

2. Goodier, J. N., and Field, F. A., "Plastic Energy Dissipation in Crack Propagation", Fracture of Solids, Gordon and Breach, New York (1963), p 103.

3. Head, A. K., and Louat, N., "The Distribution of Dislocations in Linear Arrays", Australian J. Physics, Vol 8, No. 1, 1955.

4. Bilby, B. A., Cottrell, A. H., and Swinden, K. H., "The Spread of Plastic Yield from a Notch", Proc. Roy. Soc., Vol A272, No. 304, 1963.

5. Bilby, B. A., and Swinden, K. H., "Representation of Plasticity at Notches by Linear Dislocation Arrays", Proc. Roy. Soc., Vol A285, No. 22, 1965.

6. Atkinson, C., "The Interaction Between a Dislocation and a Crack", Int. J. Fracture Mech., Vol 2, No. 567, 1966.

7. Atkinson, C., and Kay, T. R., "A Simple Model of Relaxation at a Crack Tip", Acta Met., Vol 19, No. 679, 1971.

8. Atkinson, C., and Clements, D. L., "The Influence of Anisotropy and Crystalline Slip on Relaxation at a Crack Tip", Acta Met., Vol 21, No. 55, 1973.

9. Treatise on Fracture, Edited by H. Liebowitz, Chapter 3, Academic Press, New York (1969), "Mathematical Analysis in the Mechanics of Fracture" (J. Rice).

10. Elber, W., "Fatigue Crack Closure Under Cyclic Tension", Eng. Fracture Mech., Vol 2, No. 37, 1970.

11. Elber, W., "The Significance of Fatigue Crack Closure", ASTM STP 486, American Society for Testing and Materials, 1971, p 230.

12. Adams, N.J.I., "Fatigue Crack Closure at Positive Stresses", Eng. Fracture Mech., Vol 4, No. 543, 1972.

13. Hahn, G. T., Hoagland, R. G., and Rosenfield, A. R., "Local Yielding Attending Fatigue Crack Growth", Met. Trans., Vol 3, No. 1189, 1972.

APPENDIX B

EXPERIMENTAL MEASUREMENTS OF FATIGUE-CRACK GROWTH AND RETARDATION IN Ti-6Al-4V ALLOY

Introduction

Selected fatigue-crack-propagation experiments were conducted to provide substantiation of the analytical developments of this research program. Included were the generation of fatigue-crack-propagation data under conditions of constant cyclic stress-intensity-factor range (i.e., constant ΔK), the study of the overload effects on crack-growth retardation, the calibration of specimen compliance, and observations of crack-closure effects. This experimental effort was directed toward complementing and refining results obtained on previous NADC-sponsored programs and to establish a firmer experimental basis for the iterative approach to this experimental-analytical development activity.

Experimental Approach

Fatigue-crack-propagation data are usually generated using test specimens which directly simulate cracked structural elements or which satisfy the constraints of fracture-toughness testing. Under constant-amplitude loading, these specimens exhibit increasing crack-growth rates with advancing crack length since the applied stress-intensity factor is also increasing. However, in this program, to achieve a more definitive description of crack behavior, fatigue-crack-propagation data were generated under conditions of constant cyclic stress-intensity-factor range, ΔK. In addition to providing the basic data for quantifying the free parameters of the evolving model, this approach provides a clearer picture of the influence of the dominant mechanical variables for several reasons. First, if the rate, da/dN, is uniquely dependent upon the stress-intensity factor, K, or on its range, ΔK, the crack-growth curve of crack length versus cycle count will be linear. This would permit a direct and convenient means of fitting crack growth which is complexly nonlinear under the more usual conditions of constant-amplitude loading. Second, the dependency of fatigue-crack-propagation rate, da/dN, on K or ΔK can be more clearly

established. Third, a large number of overload combinations can be studied over a range of crack lengths in one specimen.

Although a constant cyclic stress-intensity-factor range, ΔK, also can be achieved through configuration control, as in the tapered double-cantilever beam (DCB) specimen, such geometric constraints are not generally desirable. The tapered DCB specimen, while available to provide a constant ΔK independent of crack length under constant-amplitude loading, does not simulate the broad class of crack configurations encountered in structures nor is there a large body of such fatigue-crack-propagation data for correlation of the evolving model.

Program Details

The basic experimental details of this research program are presented in the following subsections. Descriptions of materials, test specimens, and experimental procedures are included.

Materials

The fatigue-crack-growth and retardation studies were conducted on both mill-annealed and beta-processed Ti-6Al-4V titanium alloy plate. The mill-annealed material (normally ½-inch thick) produced by Reactive Metals, Inc. (RMI), was available at Battelle from a previous NADC-sponsored research program. The beta-processed material (normally 5/16-inch thick) produced by Titanium Metals Corporation of America (TMCA) was provided by NADC from surpluses in the Federal Aviation Administration's Supersonic Transport Program at the Boeing Company.

Chemistry. The average chemistry for these materials is presented in Table B-1. The mill-annealed plate chemistry was certified by RMI for Ingot 295338. The beta-processed plate chemistry was certified by TMCA for Heat No. K2701 and verified by Boeing Company.

TABLE B-1. CHEMICAL COMPOSITION

Material	Weight, percent						
	Al	V	Fe	O	C	N	H
Mill Annealed	6.4	4.2	0.18	0.127	0.022	0.010	0.008
Beta Processed	6.4	4.2	0.07	0.150	0.022	0.028	0.0060

Mechanical Properties. The static-tensile properties of each material are presented in Table B-2. The properties of the mill-annealed plate were determined at BCL; those of the beta-processed material were developed by TMCA and verified by Boeing.

TABLE B-2. MECHANICAL PROPERTIES

Material	Grain Direction	Tensile Ultimate Strength, TUS, ksi	0.2 Percent Offset Tensile Yield Strength, TYS, ksi	in 2-Inch Gage Length, e, percent	Reduction in Area, RA, percent
Mill Annealed	L	137	130	15	35
Beta Processed	L	139	126	17	29
Beta Processed	T	140	126	17	30

Metallography. The metallography of the mill-annealed-plate material has been discussed in the final report of the NADC-sponsored research program. The following discussion describes the metallographic characterization of the beta-processed material.

Sampling of the beta-processed Ti-6Al-4V plate was accomplished to enable examination in three planes--surface, longitudinal thickness (parallel to rolling direction), and transverse thickness (transverse to rolling direction). Standard metallographic techniques were used to grind and polish samples. Krolls' etchant (HF, HNO_3) was used to reveal microstructure. Samples were reetched to show more clearly the grain size variation that exists across the plate thickness. Representative photomicrographs are shown in Figures B-1 and B-2.

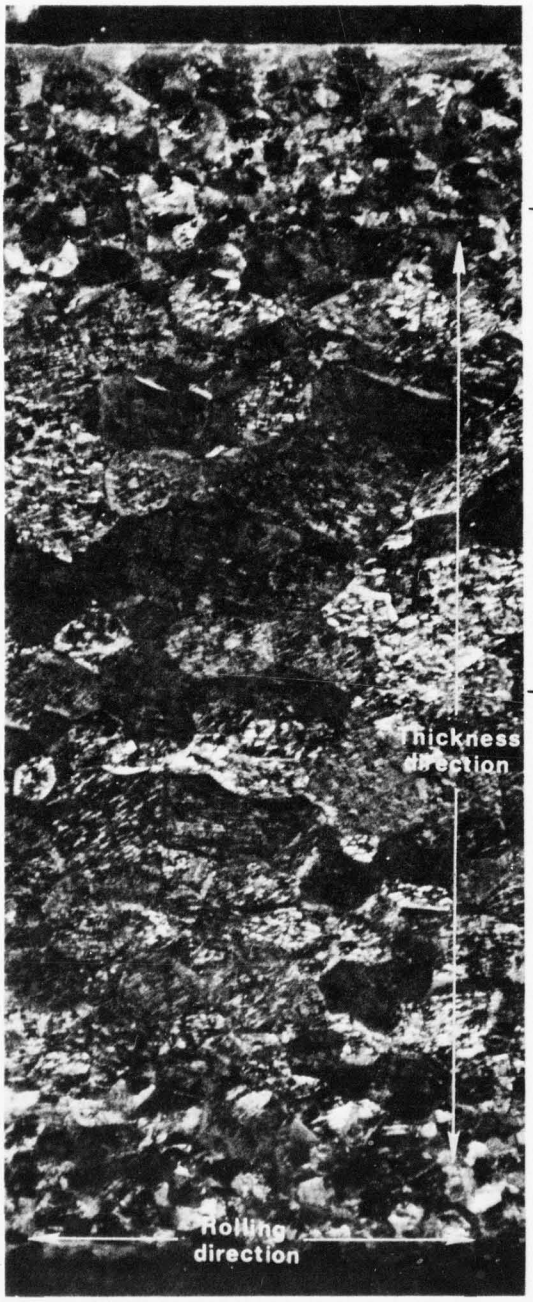

20 X 4H738

(a) Full cross-section.

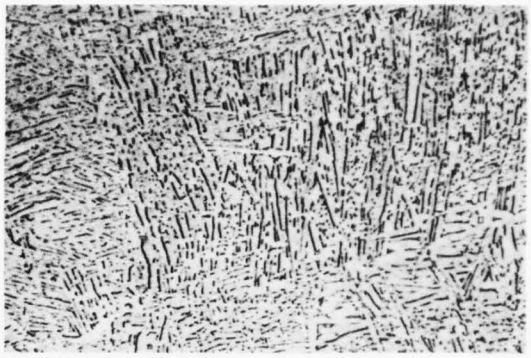

500 X 4H737

(b) Sample near surface.

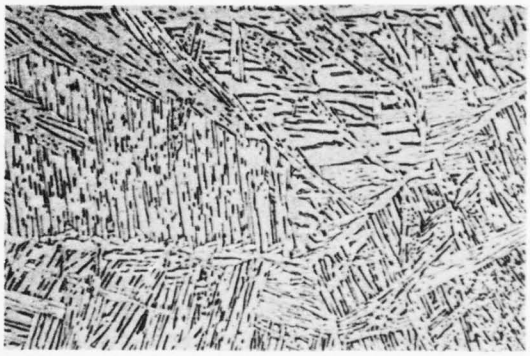

500 X 4H736

(c) Central sample.

FIGURE B-1. THICKNESS CROSS-SECTION OF BETA-PROCESSED TITANIUM PLATE

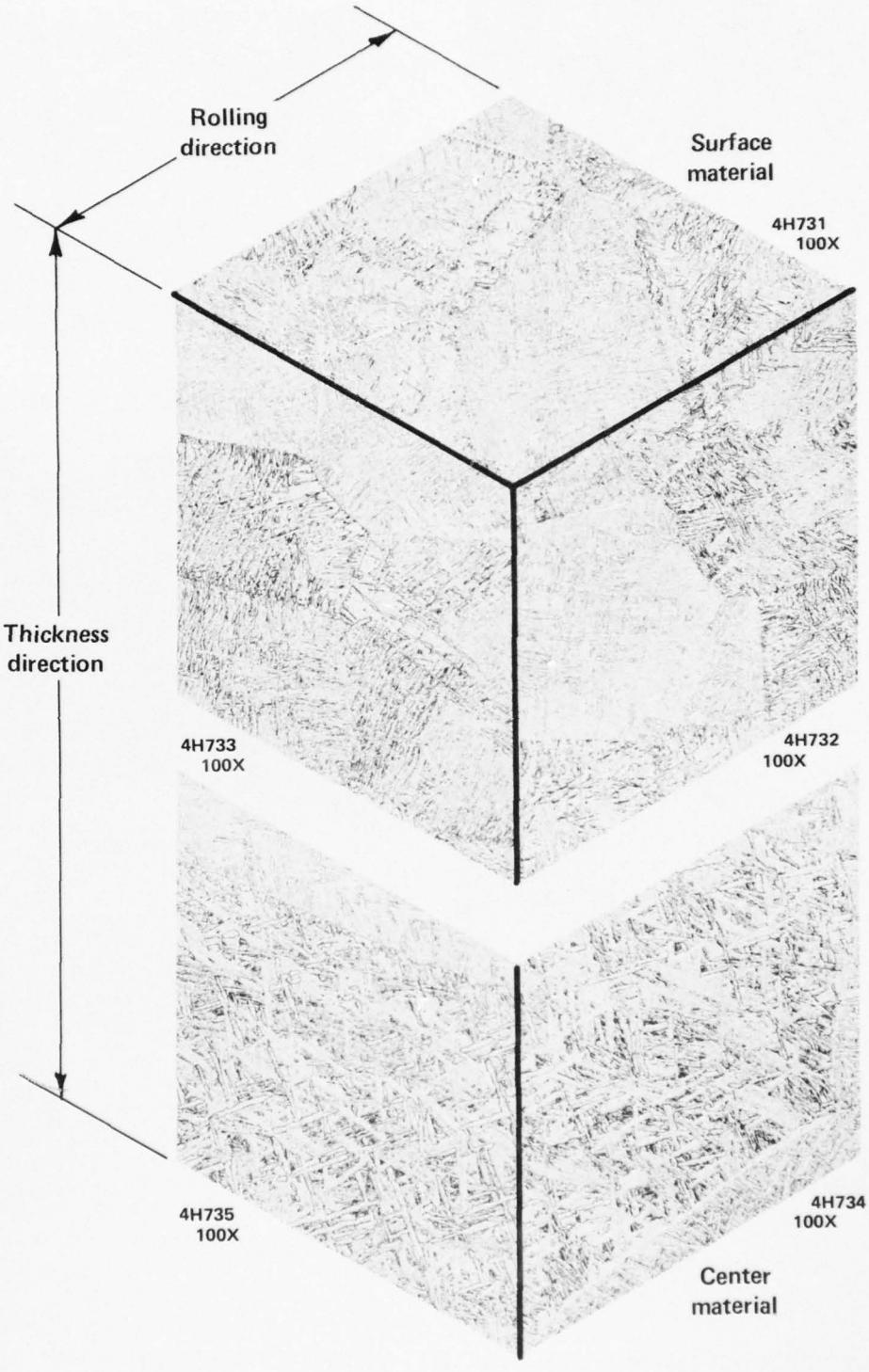

FIGURE B-2. THREE-DIMENSIONAL VIEW OF MICROSTRUCTURE

The large grain size of the prior beta grains in this plate of transformed beta microstructure is a feature almost discernible with the naked eye. As shown in Figure B-1(a), the cross-section photomacrograph reveals another feature--the variation in prior beta grain size that exists between the more heavily worked surface layers and center material. The smaller surface layer grains are about 300 microns across (ASTM Grain Size about 1), while the grains of the center material are three to eight times larger.

Grain size variation across plate thickness is not an unusual feature in titanium alloys but as shown in Figure B-1(a), the structure of this plate is characterized by an unusually abrupt change in grain size between surface layers and center material. As shown in Figure B-1(b) and (c), this is not a large difference between the microstructures of the two different grain size materials. The acicularity of the alpha platelets is a bit more defined in the center material but, basically, the transformation products and form are the same from both small and large grains. A feature of both microstructures is the lack of a pronounced alpha lining at prior beta grain boundaries. Where alpha grain boundary lining is apparent, it is thin, discontinuous, and not well developed, indicating the preferred degree of rapid cooling from the beta temperature.

A pronounced elongation of grains in the rolling direction is not observed in this material although a slight alignment of the prior beta grains is apparent (Figure B-1). This lack of fibering is revealed further in the three-dimensional view of the microstructure as presented in Figure B-2 (100X). Again, the outstanding feature of this transformed beta structure is the prior beta grain size difference between surface and center material. Differences in mechanical properties might be expected between materials (or across thickness sections) with this much difference in grain size.

Test Specimens

The specimen design used in the program is illustrated in Figure B-3. The single large pin hole drilled at each end was used to provide more positive alignment in these relatively low load tests. The actual ¼-inch hole was saw-notched as a crack starter.

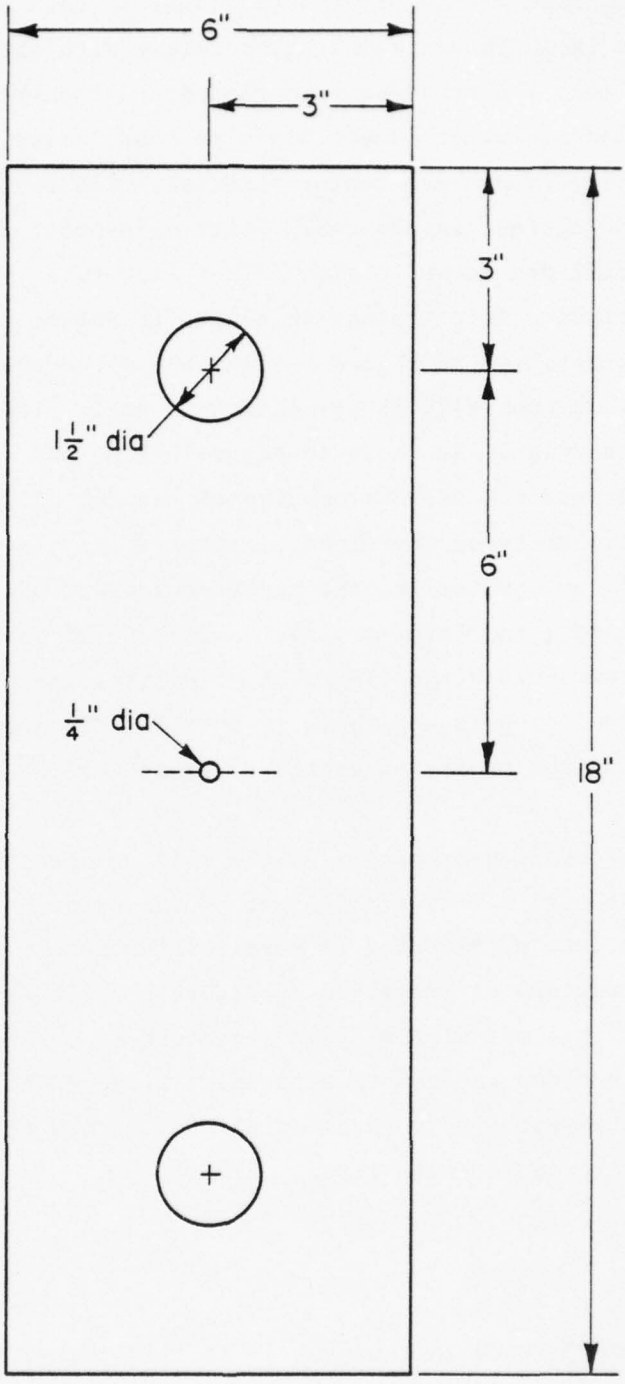

FIGURE B-3. SPECIMEN CONFIGURATION

Experimental Procedures

All tests were conducted in BCL's Structures Laboratory on a 50-kip servo-controlled electrohydraulic testing system.

Fatigue-Crack Propagation. The central hole of each test specimen was notched with a fine saw cut and precracked to an initial crack length of approximately 0.50 inch. Each specimen was then cyclically loaded over a stress range to provide the desired ΔK and R values. Surface crack length was monitored with an optional comparator. Crack length measurements were made at approximately every 0.050 inch at which time the loading was decremented to maintain the desired K_{max} value according to the relation

$$\sigma = K [W \tan \pi a/W]^{-\frac{1}{2}} , \qquad (B\text{-}1)$$

where σ = gross applied stress

K = applied stress-intensity factor

W = panel width

a = half-crack length.

The crack length and associated cycle counts were recorded and plotted to maintain a continual record of crack growth.

In summary, the transformed beta microstructure of this plate appears to be typical of Ti-6Al-4V betatized material. The differences between the prior beta grain sizes of surface and center areas, as well as the abrupt change in grain size between areas, is a noteworthy feature.

Overload Procedures. The overload-crack-retardation experiments were conducted as a simple extension of the procedures described above. Single overloads (or overstresses) were applied periodically during the basic fatigue-crack-propagation tests. A load-compliance record was made for each overload such that increases in crack extension could be related to specimen compliance. A miniaturized clip gage was mounted in the mouth of the EDM notch to monitor specimen compliance during loading.

Matrix of Test Data

Crack propagation in these two materials was evaluated both with and without overloads. The matrix of data generated is indicated as follows:

Maximum Cyclic Stress-Intensity Factor, K_{max}, ksi-in.$^{\frac{1}{2}}$	Stress Ratio, R	Number of Test Specimens			
		Mill Annealed		Beta Annealed	
		Without Overload	With Overload	Without Overload	With Overload
10	0.05	1	1	--	--
20	0.05	2	1	1	1
20	0.05	2	1	1	1

A number of overloads and overload ratios were applied to each of the overload specimens. Retardation was considered to have been overcome when the crack-propagation rate as determined under constant ΔK conditions was reestablished.

Experimental Results

The principal experimental results derived in this research program are summarized in the following sections. While these data provide an initial basis for the analytical-experimental iteration, they will be expanded as this model development is continued.

Constant ΔK Crack-Growth Behavior

A typical crack-growth curve generated under conditions of constant stress-intensity-factor range is shown in Figure B-4. The curve has the expected linearity until the crack length exceeds half the panel width whereat some divergence is noted. At maximum, the curve slope prior to fracture diverged from the initially established curve by a factor of 3.

The cause of this divergence could be attributed either to an inadequacy of the width correction in defining the ΔK level of loading or to other mechanical factors affecting the growth rate. In the light of the extensive mechanics analyses on this specimen configuration, the former case is highly unlikely. Therefore, it is considered that other net section stress influences come into play.

Fatigue-Crack-Propagation Rate

The fatigue-crack-propagation-rate behavior derived from these conducted under conditions of constant cyclic stress-intensity-factor range are summarized

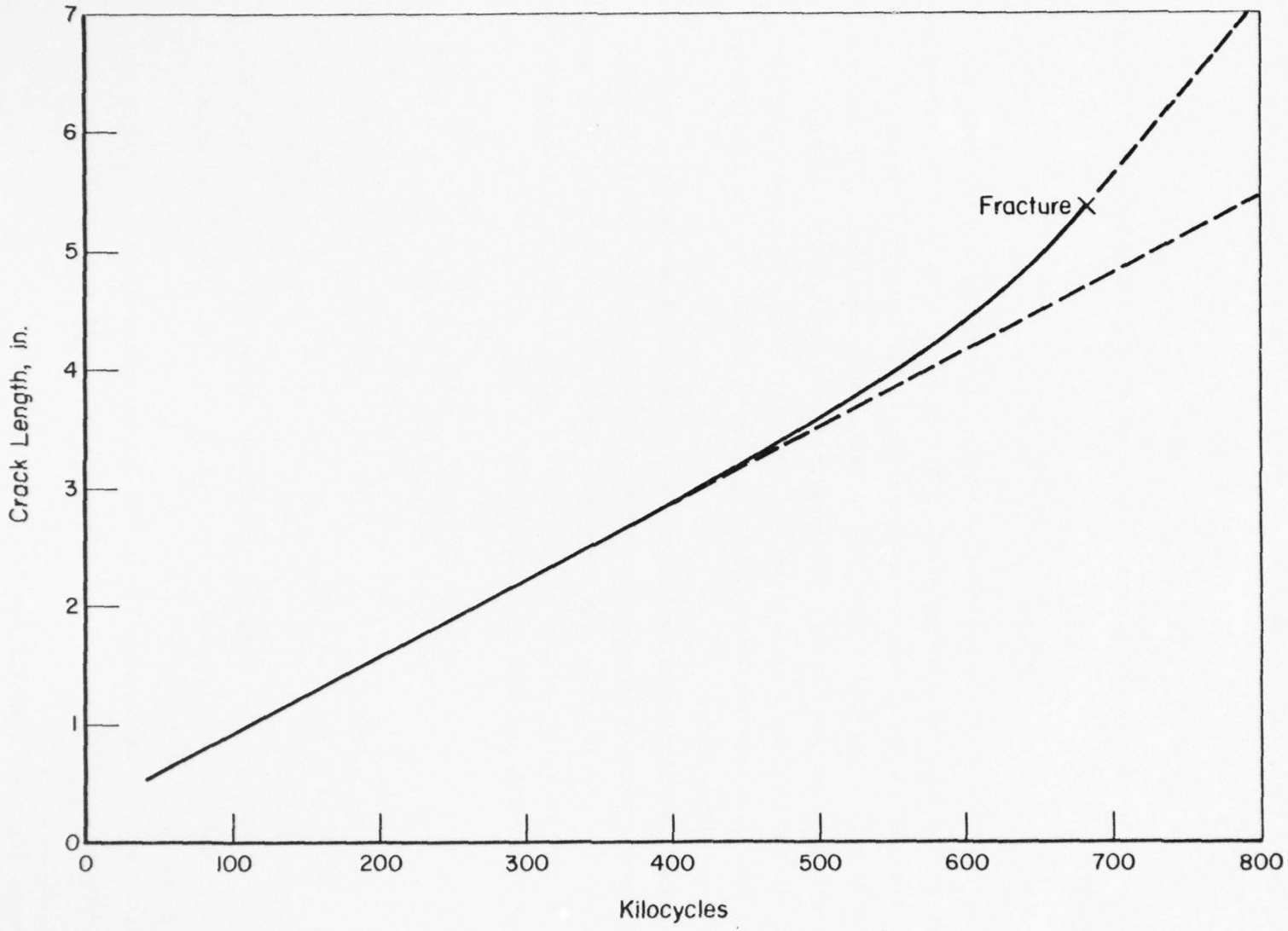

FIGURE B-4. TYPICAL CONSTANT ΔK CRACK-GROWTH CURVE (SPECIMEN 3, K_{max} = 20 KSI-IN.$^{\frac{1}{2}}$, (R = 0.5)

in Figure B-5. The results are presented over dual abscissa formats. On the left, the rates are presented in terms of the actual stress-intensity-factor range,

$$\Delta K = (1 - R)\, K_{max} \quad ; \tag{B-2}$$

on the right, the results are presented in terms of effective stress-intensity-factor range,

$$\Delta K_{eff} = (1 - R)^{m} K_{max} \quad , \tag{B-3}$$

where m is the Walker [1]* exponential parameter derived from a collapse of test data on the mill-annealed material. This display shows both the effect on stress ratio and the difference in behavior of the two materials tested.

It should be noted that these rate results are presented in terms of total crack length, $2a$, for consistency in comparison with previously published results. In the main body of this report, the analytical-experimental comparisons have been presented in terms of the half-crack length, a, for consistency with the generalized model.

A broader perspective of these results may be gained by comparing them with the summary results of a previous NADC-sponsored program [2] as shown in Figure B-6. The shaded areas represent previous test data generated under conditions of constant-amplitude loading. The solid lines represent the average rate results of these data modeled by the formulation

$$\frac{d(2a)}{dN} \approx \frac{C(\Delta K)^{n}}{(1 - R)\, K_{c} - \Delta K} \quad , \tag{B-4}$$

where $C = 0.267$ μin./cycle

$n = 3.30$

$K_{c} = 267$ ksi-in.$^{\frac{1}{2}}$.

The results of this present program, translated directly from Figure B-5, are overlayed on the previous results as individual symbols. The correlation appears to be quite good.

A difference in crack behavior in the two materials was also notable in the macroscopic appearances of their crack surfaces. As shown in Figure B-7,

---

* References for this appendix are listed on page 100.

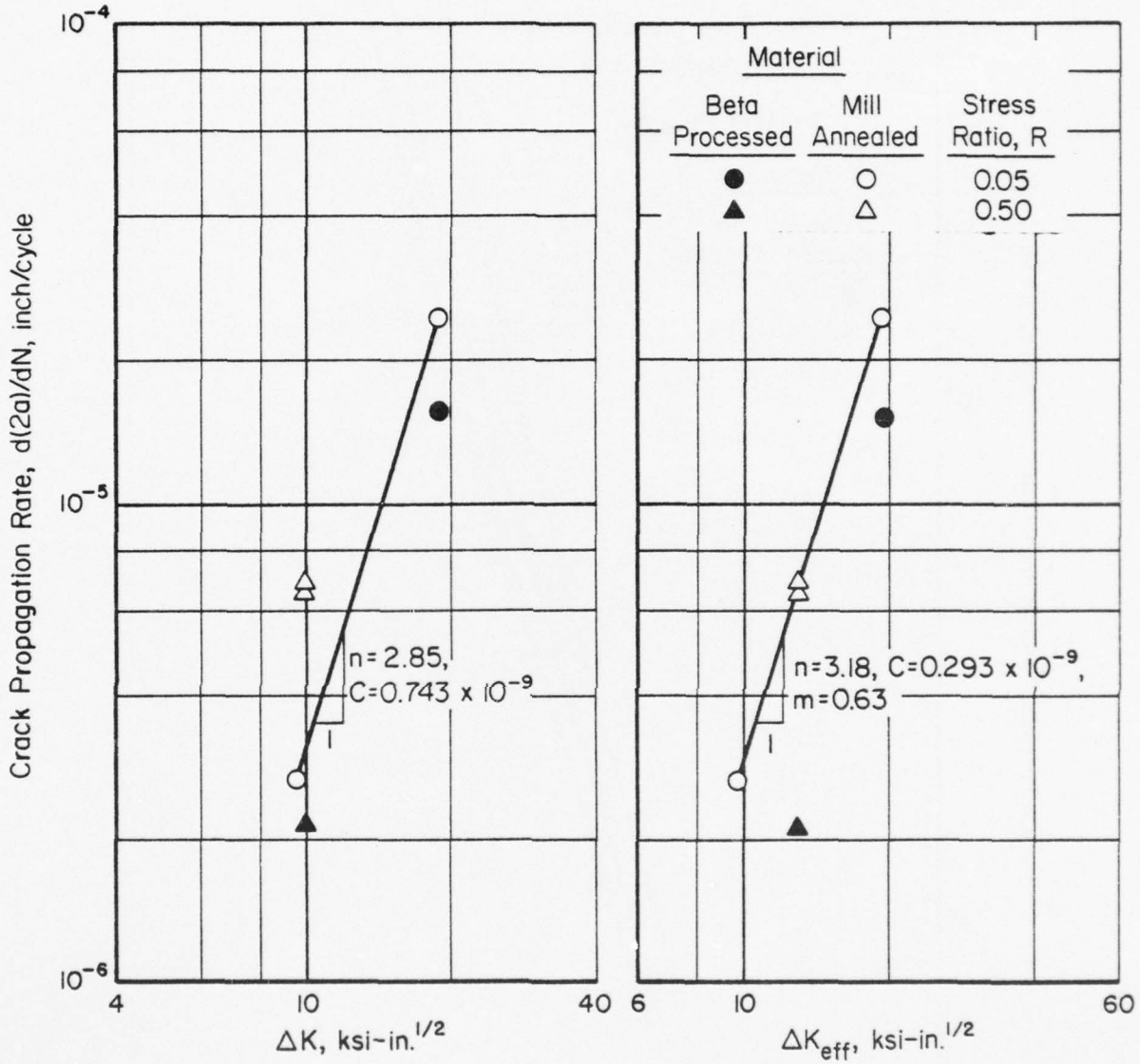

FIGURE B-5. CRACK-GROWTH-RATE BEHAVIOR

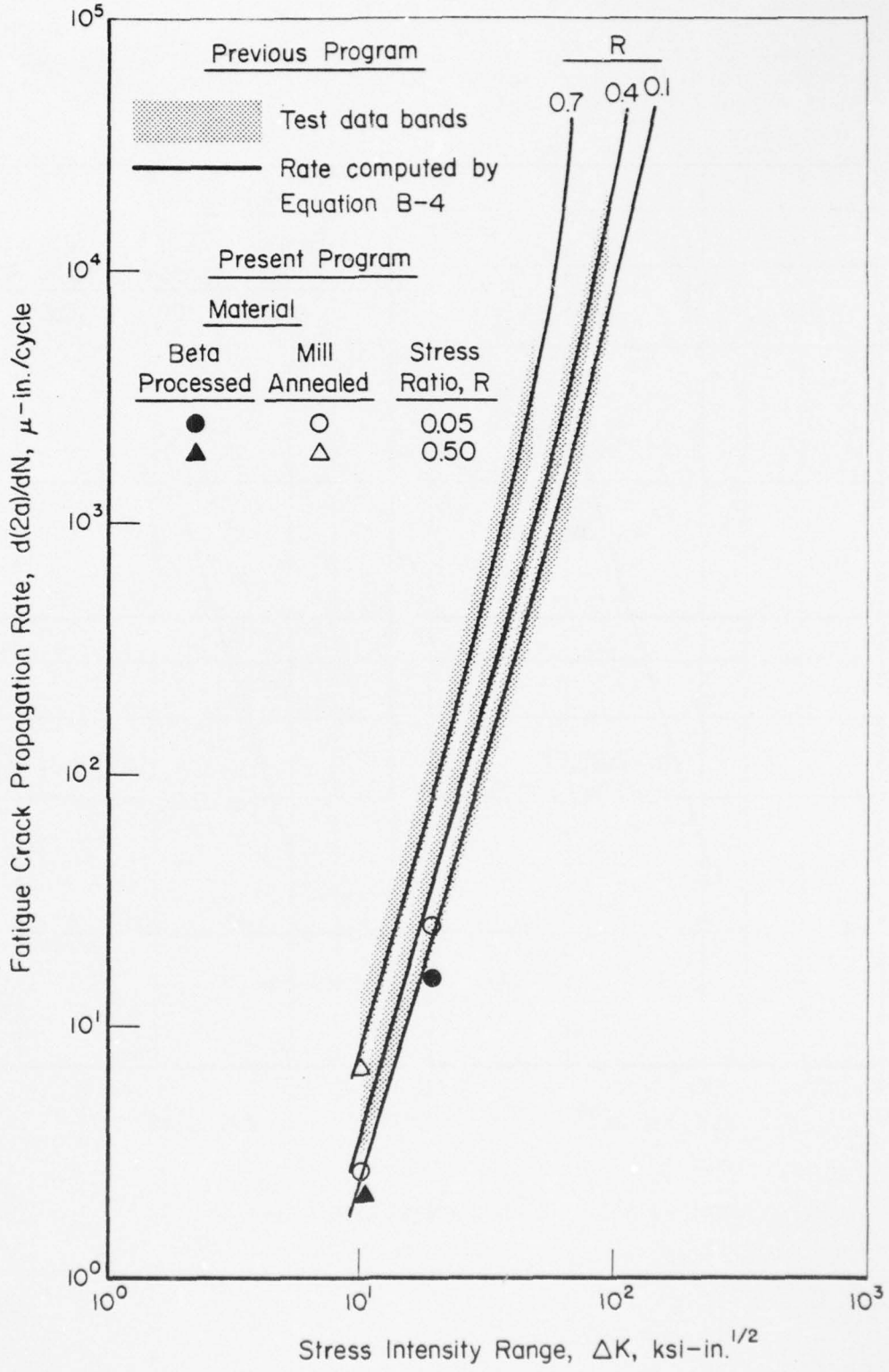

FIGURE B-6. COMPARISON OF PRESENT AND PREVIOUS DATA

AD-A031 071 BATTELLE COLUMBUS LABS OHIO F/G 11/6
INITIAL DEVELOPMENT OF A FATIGUE-CRACK-RETARDATION MODEL.(U)
JAN 76 M F KANNINEN, C E FEDDERSEN N62269-74-C-0618
UNCLASSIFIED BATT-G-2920 NADC-76076-30 NL

2 OF 2
AD
A031071

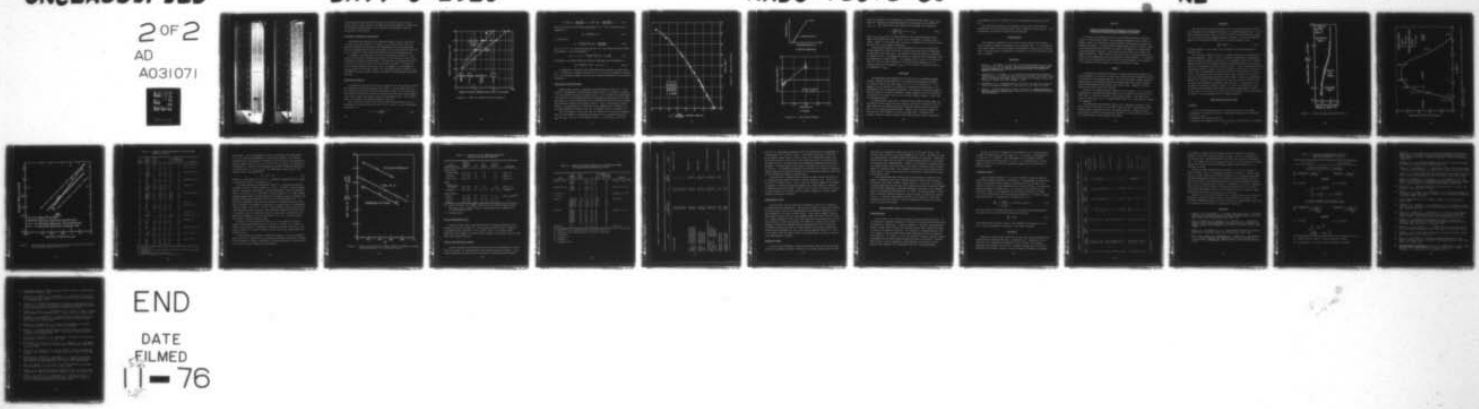

END

DATE
FILMED
11-76

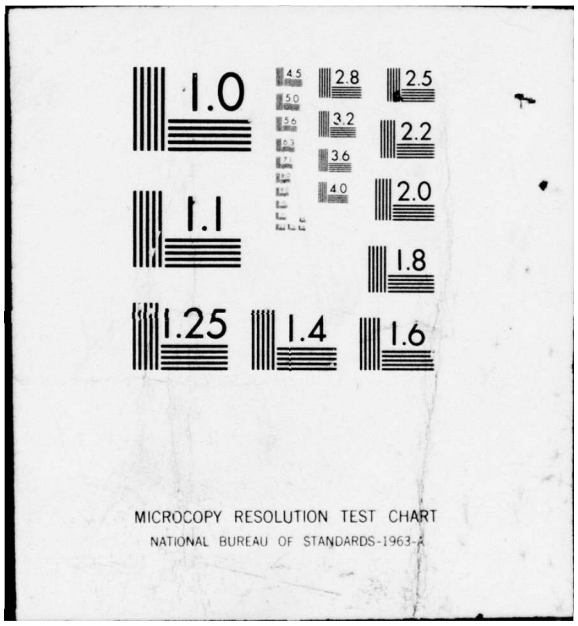
1.0
1.1
1.25
1.4
1.6
1.8
2.0
2.2
2.5
2.8
3.2
3.6
4.0
4.5
5.0
5.6
MICROCOPY RESOLUTION TEST CHART
NATIONAL BUREAU OF STANDARDS-1963-A

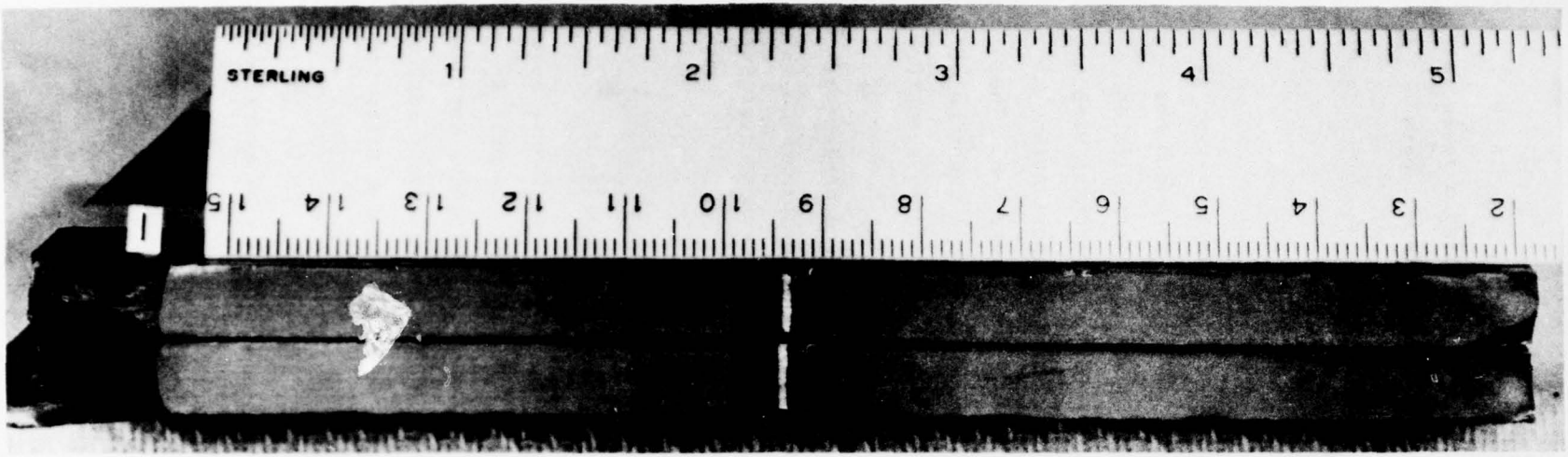

Mill Annealed

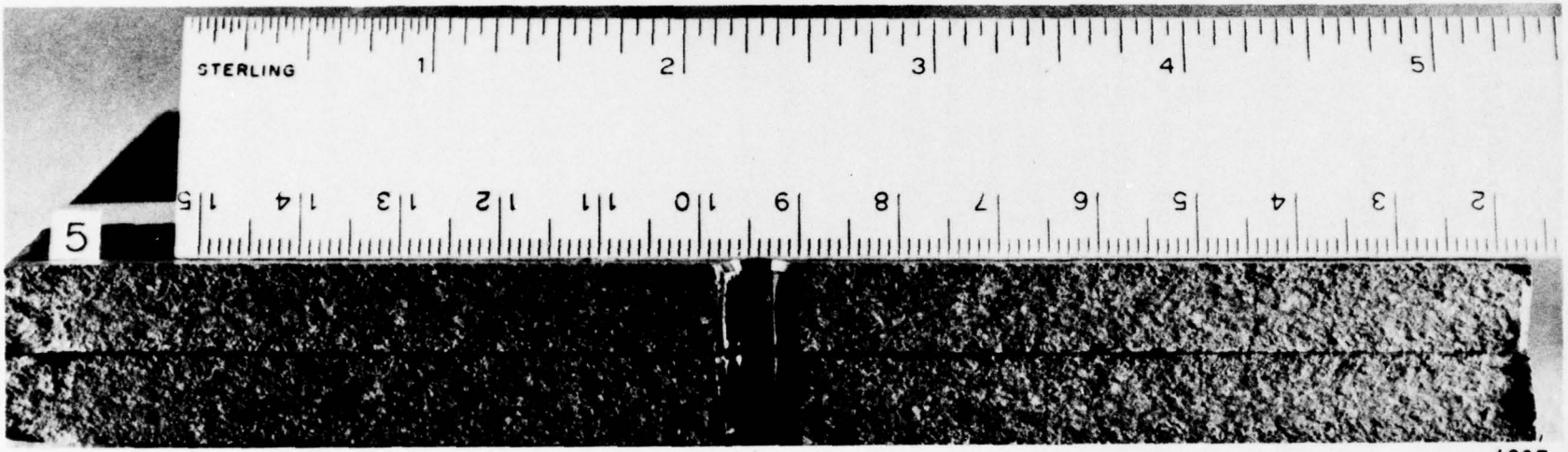

Beta Annealed

FIGURE B-7. CONTRASTING APPRARANCES OF CRACK SURFACES FOR K_{max} = 20 KSI-IN.$^{\frac{1}{2}}$ AND R = 0.05

the BCL material which exhibited the higher rate behavior had a relatively smooth "satiny" finish; whereas, the NADC material which exhibited a lower rate had a coarser textured finish. This difference is attributed to the beta processing of this material.

Influence of Overloads on Retardation

Retardation was measured as the additional number of cycles required for a crack to grow from the point of overload to a recovery point at which the previously monitored uninterrupted crack-propagation rate was reestablished. This is determined from the basic crack-growth curve as the horizontal displacement of tangents of equal slope before and after the overload application.

A summary of the overload test results is presented in Figure B-8. The number of kilocycles of retarded crack growth, N_R, is plotted as a function of the percent of single overload applied. Although there is considerable scatter in the data, a distinct influence of stress ratio is evident. The number of cycles retarded increases with stress ratio, but appears to be independent of the K_{max} value over the range studied. The retardation behavior appears to be equivalent for both materials, although the general crack-propagation rates were different.

Compliance Calibration

To demonstrate and verify the elastic response of the test specimens, specimen compliance was calibrated against crack length. The clip gage located in the central hole was used to monitor displacement adjacent to the crack surface. Load deflection records were made after precracking, during the overload applications, and at other crack lengths during the crack-growth tests. The following analytical formulation of specimen compliance was used.

For a system of colinear cracks under a remote tensile stress field, the Westergaard [3] stress function, Z, and its first integral, $\overline{Z}$, may be expressed, respectively, as

$$Z = \sigma \left[1 - \left(\frac{\pi a / W}{\pi z / W} \right)^2 \right]^{-\frac{1}{2}} , \qquad \text{(B-5)}$$

and

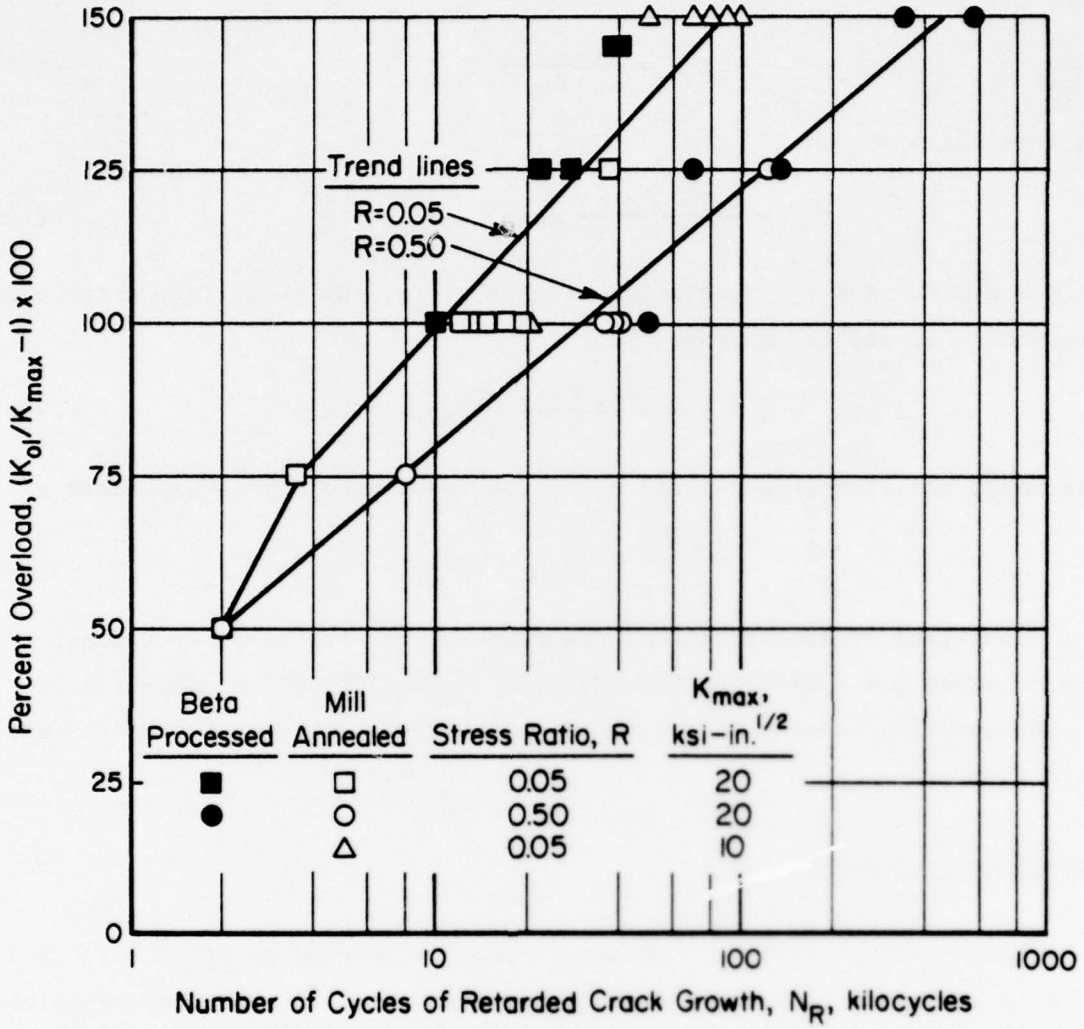

FIGURE B-8. EFFECT OF OVERLOAD ON CRACK RETARDATION

$$\overline{Z} = \frac{\sigma W}{\pi} \cos^{-1} \left(\frac{\cos \pi z/W}{\cos \pi a/W} \right) + C = i \frac{\sigma W}{\pi} \cosh^{-1} \left(\frac{\cos \pi z/W}{\cos \pi a/W} \right) + C \quad . \qquad \text{(B-6)}$$

Since the relative crack-surface displacement, $2\eta_o$, in the y direction may be expressed as

$$2\eta_o = \frac{4(1 - \nu^2)}{E} \text{ Im } \overline{Z} \quad , \qquad \text{(B-7)}$$

it follows that

$$2\eta_o = \frac{4(1 - \nu^2)}{E} \frac{\sigma W}{\pi} \cosh^{-1} \left(\frac{\cos \pi x/W}{\cos \pi a/W} \right) \quad , \qquad \text{(B-8)}$$

for $-a \leq x \leq a$. For the paeticular case of $x = 0$, the centerline crack surface displacement, Δ, may be expressed as

$$2\eta_o, \; x = 0 = \Delta = \frac{4(1 - \nu^2)}{E} \frac{\sigma W}{\pi} \cosh^{-1} \left(\sec \frac{\pi a}{W} \right) \quad . \qquad \text{(B-9)}$$

Accordingly, the stress-normalized effective compliance may be expressed as

$$\frac{\Delta}{\sigma} = \frac{4(1 - \nu^2)}{E} W \cosh^{-1} (\sec \pi a/W) \quad . \qquad \text{(B-10)}$$

A comparison of analytical and experimental results based on a panel width of $W = 6$ inches and a material modulus of $E = 15 \times 10^6$ psi is presented in Figure B-9. The correlation appears very good and confirms the adequacy of the analytical formulation.

Observations on Crack Closure

Fatigue-crack closure, a phenomenon first documented by Elber [4], is the closure or impingement of fatigue-crack surfaces prior to the complete unloading of a test specimen containing a fatigue crack. If one considers the load-deformation record of a test specimen wherein the deformation is monitored in the crack-tip region, an initial nonlinearity will be observed although the overall loading and structural conditions are linearly elastic. This is illustrated in Figure B-10(a). The nonlinearity is attributed to the compression (or relaxation) of the crack surfaces as closure occurs (or is relieved) during the loading cycle.

From this figure it can be seen that the effectivity of closure is dependent upon its relationship to the maximum and minimum cyclic stresses respectively, σ_{max} and σ_{min}. That is, if the opening stress, σ_o, is above σ_{min}, the crack

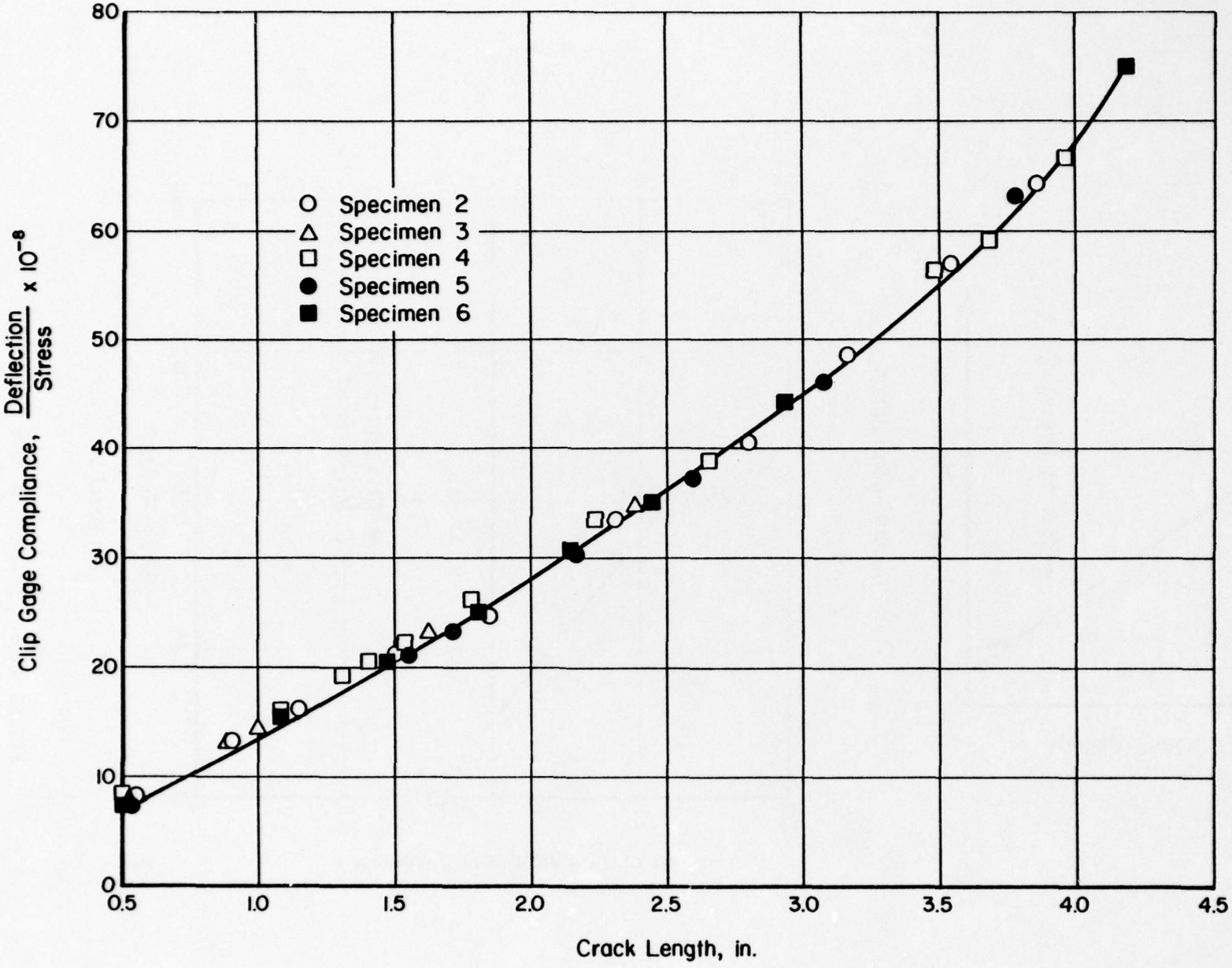

FIGURE B-9. COMPLIANCE CALIBRATION

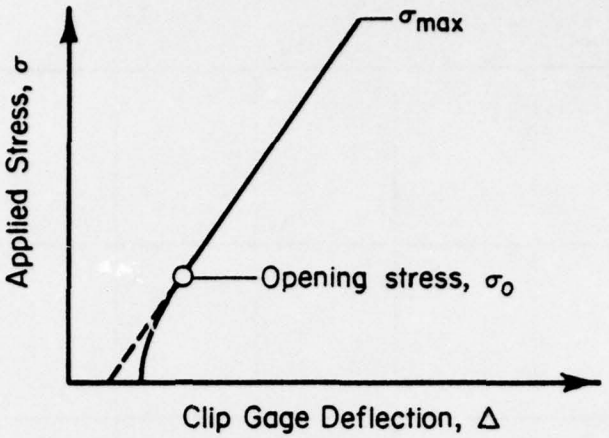

(a) Record Interpretation

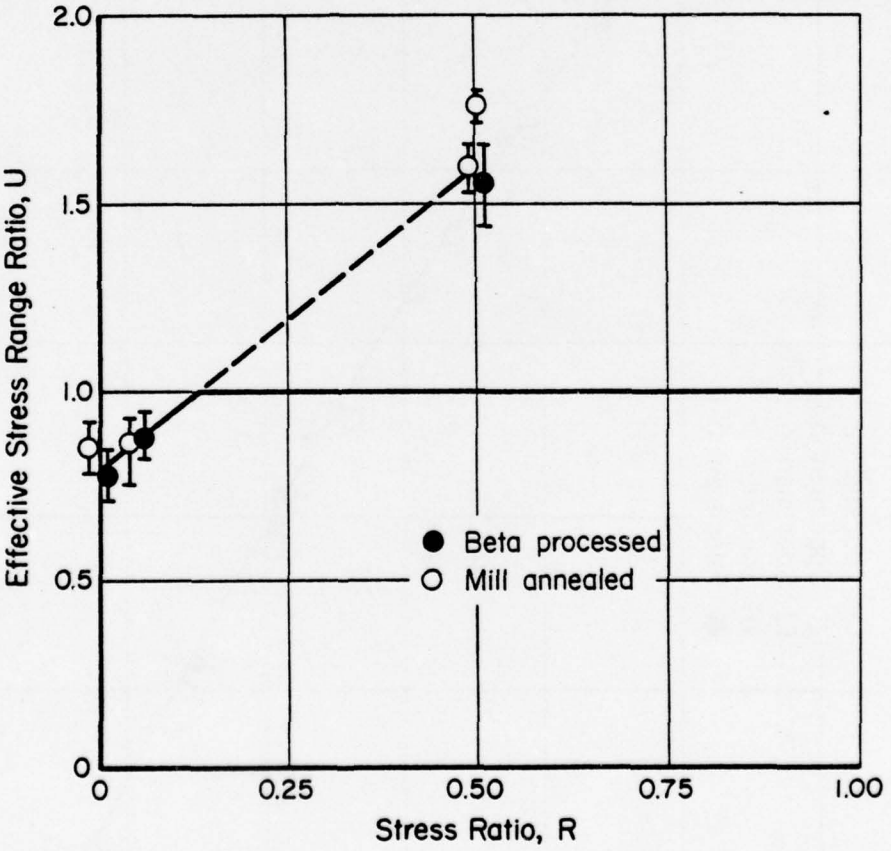

(b) Results

FIGURE B-10. CRACK-CLOSURE BEHAVIOR

will not be opened in full proportion to the applied stress range, $\sigma_{max} - \sigma_{min}$. Rather its opening and associated damage will be attenuated in proportion to $\sigma_{max} - \sigma_o$. This gives rise to the effective stress-range ratio defined as

$$U = \frac{\sigma_{max} - \sigma_o}{\sigma_{max} - \sigma_{min}} \text{ for } \sigma_o > \sigma_{min} \quad , \tag{B-11}$$

where σ_{max} and σ_{min} are the stress extremes of the preceding fatigue cycles. Where U is greater than unity, closure is not considered to influence crack growth. Where U is less than unity, closure is considered to be a direct scalar factor on ΔK in crack-growth calculation.

Crack-opening stresses, σ_o, were determined by the use of an Elber-type closure gage at the crack tip as well as from the records used for calibration on specimens without overloads. The resultant values are generally normalized in Equation (B-11). The average and range of U values for the stress-ratio tests are summarized in Figure B-10(b). It is apparent that closure is not effective above R = 0.15 for these conditions and not particularly dominant at R = 0. Closure effects were determined at K_{max} = 10 and 20 ksi-in.$^{\frac{1}{2}}$ and were found to be independent of K_{max}.

Conclusions

The experimental data generated on this portion of the research program present a refined characterization of the fatigue-crack-propagation behavior of Ti-6Al-4V plate in the lower range of ΔK (i.e., 10 to 20 ksi-in.$^{\frac{1}{2}}$). It is apparent that the behavior is influenced by processing as demonstrated by the differences in the two materials evaluated. The response to overloads, however, does not appear to be greatly different, thereby suggesting that the retardation is affected by the plastic zone size (or related residual stresses) rather than the processing factors.

In testing under conditions of constant stress-intensity-factor range, the crack-growth curves exhibit far more linearity (as would be expected) than tests under conditions of constant-amplitude loading and confirm the basic dominant role of ΔK in determining rate behavior. However, this linearity appears to hold only for crack lengths up to half the panel width. Divergence from linearity behond this point indicates that either the finite-width corrections

are inadequate (which is unlikely) or that other mechanical factors come into play.

The compliance response of the specimen, as well as the crack-closure observations, are quite consistent with current concepts of crack behavior. This substantiates the validity of the analytical approach.

Recommendations

The successful completion of this first stage of analytical and experimental iteration suggests continuation of this research work. It is recommended that higher ranges of ΔK be investigated and additional stress ratios be considered. The metallurgical investigation of differences in the two materials should also be pursued.

References

1. Walker, K., "The Effect of Stress Ratio During Crack Propagation and Fatigue for 2024-T3 and 7075-T6 Aluminum", Effects of Environment and Complex Load History on Fatigue Life, ASTM STP 462, American Society for Testing and Materials, 1970, pp 1-14.

2. Feddersen, C. E., and Hyler, W. S., "Fracture and Fatigue-Crack-Propagation Characteristics of ½-Inch Mill-Annealed Ti-6Al-4V Titanium Alloy Plate", Final Report to Naval Air Development Center from Battelle's Columbus Laboratories, Contract No. N00156-70-C-1336, November 1, 1971.

3. Westergaard, H. M., "Bearing Pressures and Cracks", Transactions of Amercian Society of Mechanical Engineers, J. App. Mech., Vol 61, 1939, pp A49-A53.

4. Elber, W., "The Significance of Fatigue Crack Closure", Damage Tolerance in Aircraft Structures, ASTM STP 406, American Society for Testing and Materials, 1971, pp 230-242.

APPENDIX C

A SURVEY OF MICROSTRUCTURAL INFLUENCES ON FATIGUE-CRACK-GROWTH-RATE DATA WITH SPECIAL REFERENCE TO Ti-6Al-4V

To provide a more general overview of the mechanics-materials interface relevant to fatigue-crack growth, this program was augmented with a brief, but general, survey of relationships observed between microstructural features and fatigue-crack growth. Although special reference was placed on Ti-6Al-4V, other alloys and materials were included to provide a more definitive interpretation of microstructural influences. These results are included in this report for general information. They reflect an initial basis for linking microstructural effects and for generalizing the evolving model to other materials. It should be noted that the International System of Units has been adopted in this appendix to be consistent with the majority of sources which were included.

Summary

A review of the published literature on fatigue-crack growth suggests that power-law growth in Ti-6Al-4V is sensitive to microstructural changes which result in variations in the fatigue mechanism. Microstructures which promote secondary cracking along α/β interfaces display slow growth rates while microstructures which promote dimpled rupture display fast growth rates. Examples of similar effects are found in other alloy systems.

Typically, the power-law growth exponent in this alloy is 3.4. It is also suggested that the power-law regime begins at $\Delta K \simeq 13\ MNm^{-\frac{3}{2}}$, coinciding with the lower limit of striation formation on the fracture surface. The upper limit occurs at about $K_{max} = \frac{1}{2} K_c$. At higher growth rates, the Forman equation appears to be adequate.

The normalized stress-intensity factor, $\Delta K/E$, required to produce a given growth rate in Ti-6Al-4V is on the order of that for other titanium-base alloys, ferritic steels, martensitic steels, and aluminum alloys. Austenitic steels, which deform by planar slip are much more resistant to crack growth over much of the stress-intensity range normally encountered.

Background

The form of the fatigue-crack-growth curve for metals and alloys is quite well established and is typified by Figure C-1 (Crooker and Krause [1]*). In the curve of growth rate per cycle, $\Delta a/\Delta n$, as a function of stress-intensity range, ΔK, the existence of three separate regions is evident. The central power-law region is a well-defined straight line on a double-logarithmic plot,

$$\frac{\Delta a}{\Delta n} = \alpha(\Delta K)^m \quad . \qquad \text{(C-1)}$$

The major emphasis in this report will be placed on the region described by Equation (C-1).

The individual regions of Figure C-1 roughly correlate with differences in fracture appearance. Yuen, et al [2], reported the quantitative fractographic data for Ti-6Al-4V plotted in Figure C-2.** The moderate values of ΔK, corresponding roughly with the region of power-law crack-growth behavior, are associated with a predominately striated fracture surface. These striations are shallow lines whose spacing is close to $\Delta a/\Delta n$ for Ti-6Al-4V (as well as for a number of other alloys) as demonstrated by Bates and Clark [3] and confirmed by Yuen, et al [2]. For example, Bates' and Clark's data, shown in Figure C-3, revealed that the striation spacing was always within a factor of two of the macroscopic growth rate. Figure C-2 also shows that at both the high and low ends of the ΔK range, other microscopic mechanisms come into play. The high values of ΔK (roughly the instability region of Figure C-1) cause the introduction of the dimpled rupture mechanism, characteristic of failure under monotonic loading. At the other end of the scale, the low values of ΔK (roughly the threshold region of Figure C-1) are associated with the cleavage mechanism.

Power-Law Fatigue-Crack Growth

Ti-6Al-4V

Of all the titanium-base alloys, Ti-6Al-4V has been the most widely investigated. The results in Table C-1 are derived from data of 10 different

---

* References are listed on page 116.

** Throughout this appendix, only data for positive stress ratios are considered.

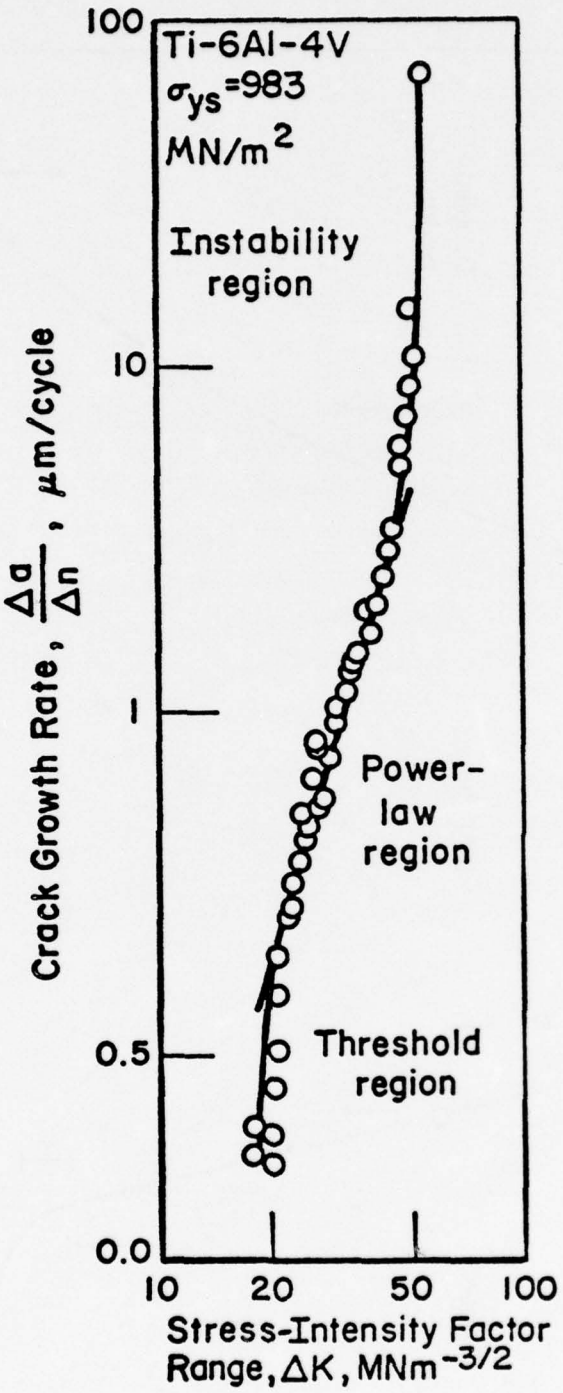

FIGURE C-1. TYPICAL FATIGUE-CRACK-GROWTH CURVE [1]

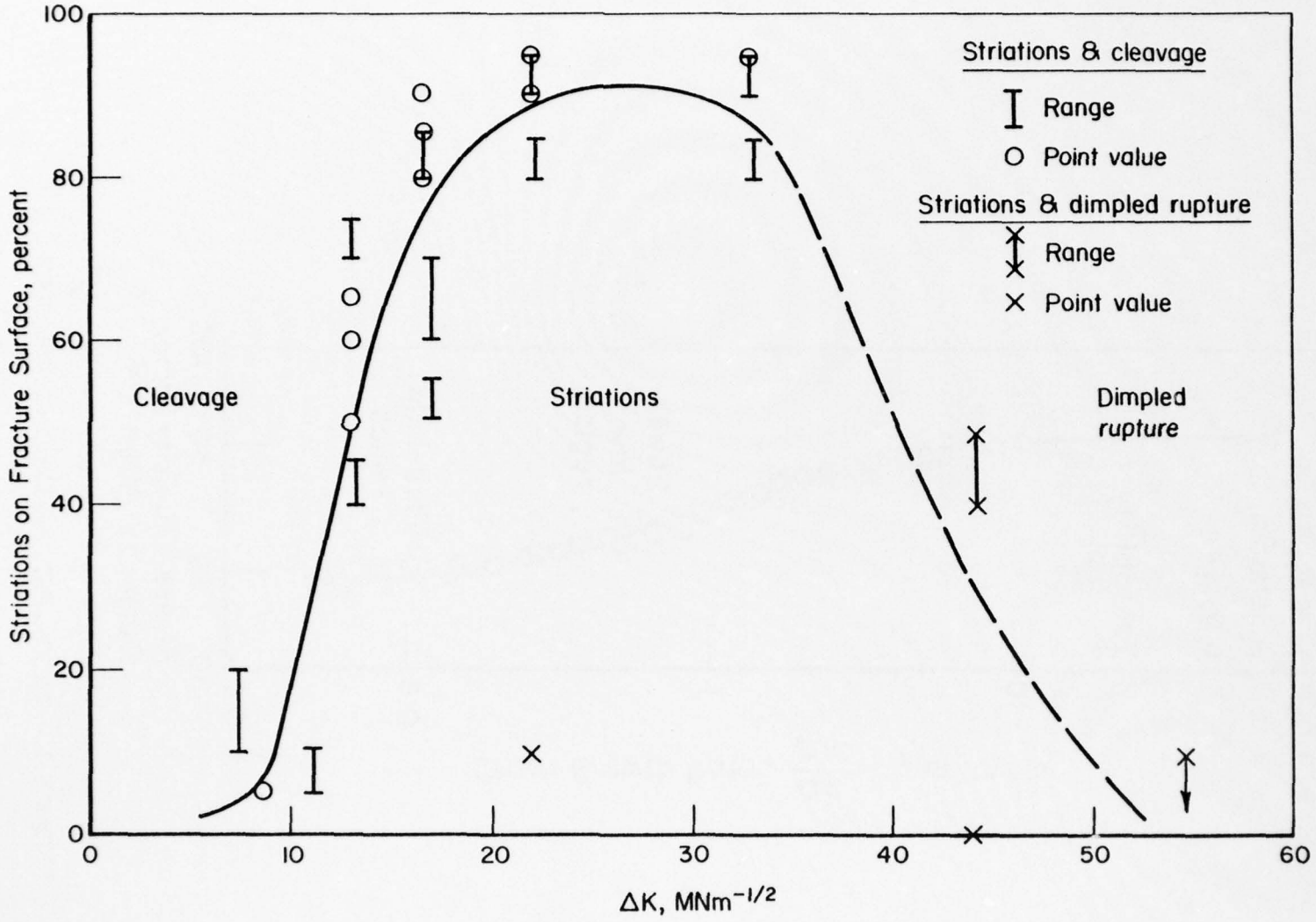

FIGURE C-2. APPEARANCE OF FRACTURE SURFACES OF Ti-6Al-4V AS A FUNCTION OF STRESS-INTENSITY RANGE [2] (Data for R > 0 only.)

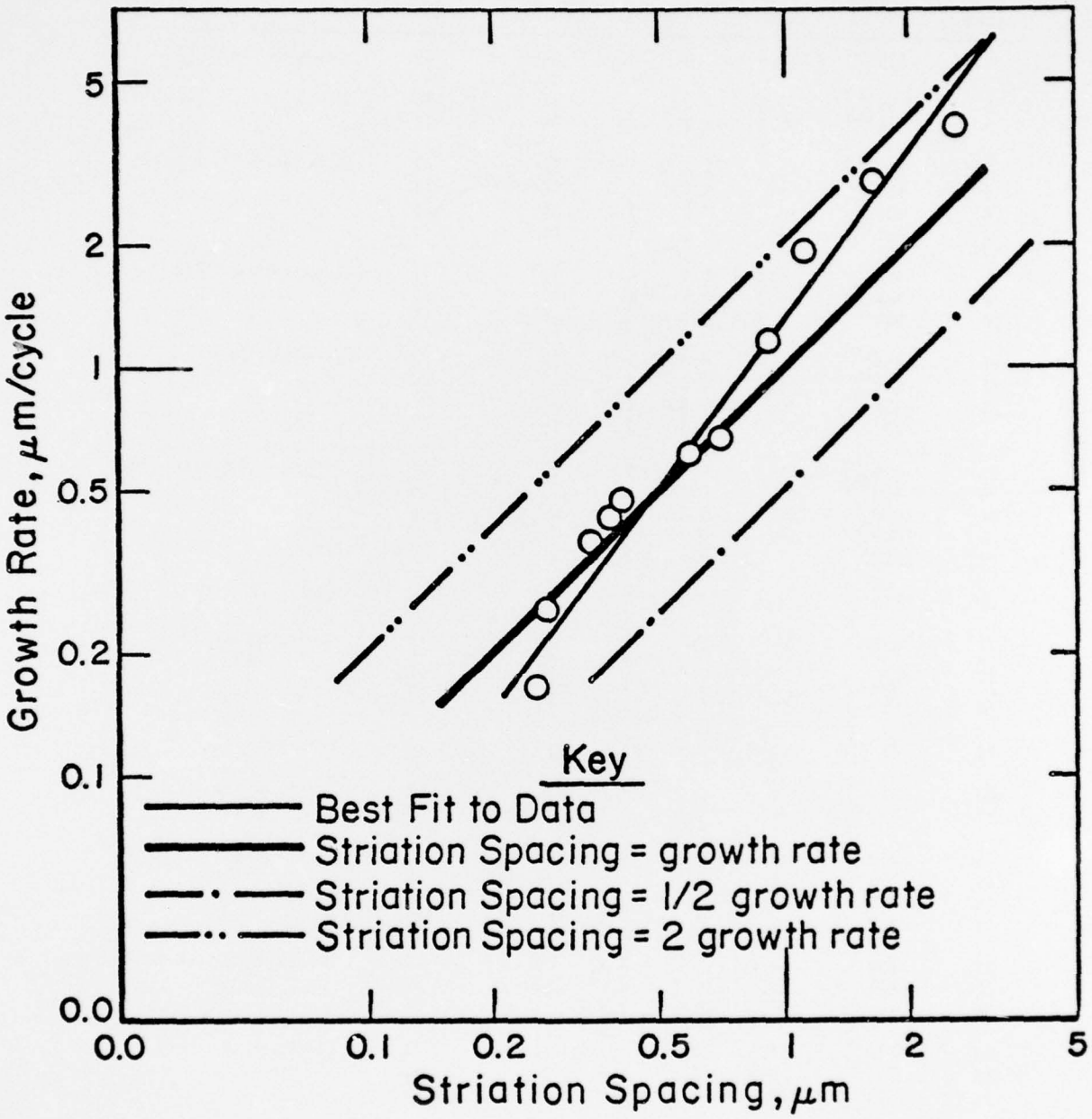

FIGURE C-3. RELATION BETWEEN FATIGUE-CRACK-GROWTH RATE AND SPACING OF STRIATIONS ON THE FRACTURE SURFACE OF Ti-6Al-4V [3]

TABLE C-1. RESULTS OF POWER-LAW ANALYSIS OF FATIGUE-CRACK GROWTH IN Ti-6Al-4V

Curve Number	Yield Strength (MNm^{-2})	Thickness (B, mm)	R	M	ΔK ($MNm^{-\frac{3}{2}}$) Actual	ΔK ($MNm^{-\frac{3}{2}}$) Normalized to R = 0[a]	Reference
1	875	101.6	0.0	3.0	24	24	Bates & Clark [3]
2	799[b]	3.2	0.33	2.9	20	23	Bucci, et al [4]
3	944[b]	0.2	3.7	22	24		
4	792[b]	--	0.0	3.0	31	31	Crooker & Krause [1]
5	820[b]	--	0.0	3.3	32	32	
6	903[b]	--	0.0	3.3	26	26	
7	985[b]	--	0.0	3.3	26	26	
8	944	6.3	0.1	4.4	18	19	Feddersen & Hyler [5]
9	944	6.3	0.4	4.4	16	20	
10	944	6.3	0.7	4.2	13	19	
11	834[b]	25.4	0.08	2.3	22	23	Harrigan [6]
12	841[b]	12.7	0.30	2.1	17	20	
13	834[b]	25.4	0.30	1.6	19	22	
14	1102[b]	12.7	0.30	2.1	14	17	
15	835[b]	10	0.35	3.1	25[c]	28	Irving & Beevers [7]
16	863[b]	10	0.35	3.1	25[c]	28	
17	1000[b]	10	0.12	3.1	27[c]	28	
18	1000[b]	10	0.35	3.1	25[c]	28	
19	1000[b]	10	0.61	3.1	22[c]	27	
20	935	1.6	0.1	2.5	17	18	Jones [8]
21	930	12.6	0.3	3.9	18	21	Paton, et al [9]
22	937	12.6	0.3	4.2	22	25	
23	951	12.6	0.3	5.4	15	18	
24	1040	12.6	0.3	5.4	15	18	
25	974[d]	0.8	0.1	3.8	17	18	Pittinato [10]
26	835[b]	--	0.33	2.7	20[c]	23	Robinson, et al [11]
27	950[b]	--	0.33	2.7	20[c]	23	
28	710	6.4	0.1	3.5	24	23	Thompson [12]
29	772	6.4	0.1	2.7	28	29	
30	861	6.4	0.1	3.5	28	29	
31	903	6.4	0.1	2.4	20	21	
32	930	10.2	0.1	5.2	11	12	Thompson, et al [13]
33	896	10.2	0.1	4.4	13	14	
34	--	10.2	0.1	3.8	15	16	
35	730[e]	25.4	0.1	3.1	21	21	Yoder, et al [14]
36	772[d]	25.4	0.1	4.9	24	25	
37	841	25.4	0.1	4.2	27	28	
38	916	2.0	0.0	3.0	22	22	Yuen, et al [2]
39	916	2.0	0.1	3.5	21	23	
40	916	2.0	0.5	3.2	17	22	
41	916	2.0	0.7	3.2	15	21	
42	916	2.0	0.9	3.2	15	23	

(a) See Figure C-4.
(b) Variations in yield strength produced by variations in chemistry and processing.
(c) Extrapolated.
(d) Extra-low intersitial atom content (ELI).
(e) Ultra-low interstitial content, 0.06 wt. percent oxygen.

laboratories. Only room-temperature tests in relatively inert environments (i.e., air, inert gas atmospheres, or vacuum) are included. The data are characterized by the exponent m of Equation (C-1) and the ΔK value required to produce a growth rate of 0.25 μm/cycle (10×10^{-8} in./cycle); the latter will be denoted $\Delta K'$. Three of the investigations involved systematic variations in the stress ratio, R ($R \equiv K_{min}/K_{max}$). For these data, ΔK was found to vary linearly with R (see Figure C-4),

$$\Delta K' = \Delta K_0 - 9R \quad , \tag{C-2}$$

where ΔK_0 is the value of $\Delta K'$ for R = 0. Subsequent comparisons will be based on ΔK_0 derived from $\Delta K'$ via Equation (C-2).

Two other variables are considered in Table C-1. Processing variations provided a spread of yield strengths of $\sim$ 700 to $\sim$ 1100 MNm^{-2}, while thickness varied by two orders of magnitude. Thickness appeared to have no significant effect on either ΔK_0 or m. The effect of yield strength is not clear, because strength changes result from microstructural changes and there is evidence that fatigue-crack-retarding microstructures can be produced (Barsom [15]). In particular, secondary cracks have been observed to propagate along α/β interfaces inclined to the propagation direction of the main crack in beta-annealed Ti-6Al-4V (Paton, et al [9]). In turn, these interfaces contain a microstructural phase which can be altered by heat treatment (Rhodes and Williams [16]). It is possible that the conflicting reports on the effect of oxygen on crack-growth rate (Thompson, et al [13], and Yoder, et al [14]) actually reflect variations in the grain boundary phase.

Because of the microstructural effect, it is not possible to define a "master" fatigue-crack-growth curve for Ti-6Al-4V. However, it is useful to define typical behavior. Accordingly, average values taken from Table C-1 are listed in Table C-2, along with results for the other alloy classes which are discussed below.

A final variable to consider is fracture toughness. The only systematic data at hand are a comparison of two processing treatments resulting in similar yield strengths but large K_c differences by Crooker and Krause [1] which result in virtually identical power-law growth behavior.

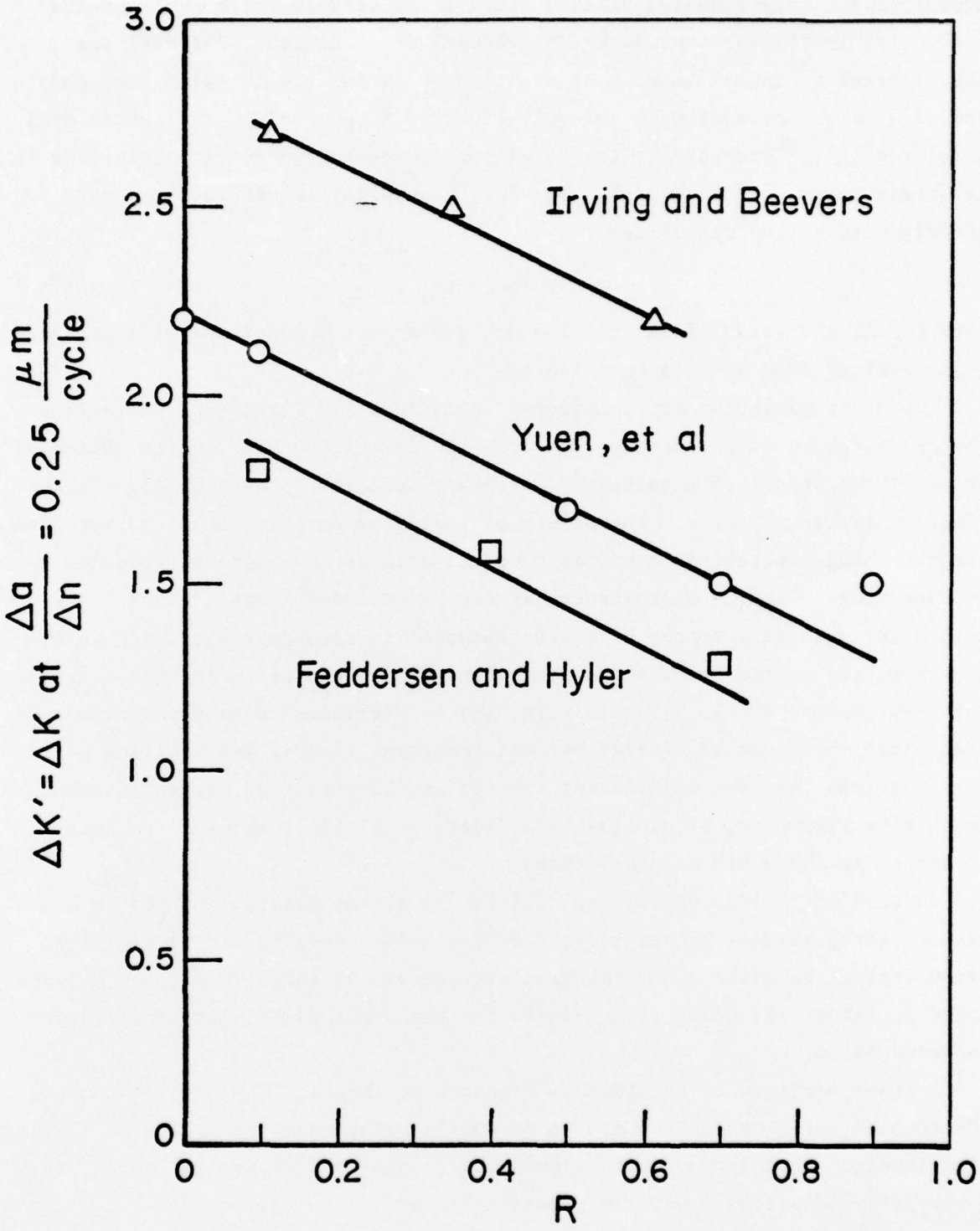

FIGURE C-4. EFFECT OF STRESS RATIO ON STRESS INTENSITY TO PRODUCE A FATIGUE-CRACK-GROWTH RATE OF 0.25 μm/CYCLE IN Ti-6Al-4V

TABLE C-2. EVALUATION OF THE PARAMETERS DESCRIBING POWER-LAW FATIGUE-CRACK GROWTH[a]

Alloy Classification	Elastic Modulus (MNm^{-2})	m[b]	ΔK_o ($MNm^{-\frac{3}{2}}$)	$\Delta K_o/E$ ($10^{-4} m^{\frac{1}{2}}$)	Reference
Titanium Base					
Titanium Metal	110×10^3	3.4	18	1.6	Table C-3
Ti-6Al-4V	110×10^3	3.4	22	2.0	Table C-1
Other Alloys	110×10^3	3.3	27	2.5	Table C-3
Steels					
Ferritic and Martensitic	200×10^3	2.65	35	1.75	Table C-4
Austenitic	200×10^3	6.1	34 - 63	1.70 - 3.15	Thompson[17]
Aluminum Base					
2024-T3	68×10^3	2.6	13 - 20	1.9 - 2.9	Hahn & Simon[18]
7075-T6	68×10^3	2.6	10 - 15	1.5 - 2.2	"
Others	68×10^3	2.7	12 - 16	1.8 - 2.4	"

(a) $\Delta a/\Delta n$ (μm/cycle) = $0.25 \left(\frac{\Delta K}{\Delta K_o}\right)^m$, where ΔK_o is the stress-intensity range for $\Delta a/\Delta n = 0.25$ μm/cycle. Data on titanium-base alloys normalized to R = 0 via Equation (C-2).

(b) Average values.

Other Titanium-Base Alloys

Data for several other titanium-base alloys, including commercially pure titanium, are given in Table C-3. This allows the range of yield strengths to be extended to 200 - 1200 MNm^{-2} (Y/E = 0.0011 - 0.006). In contrast, these additional alloys appear to be more fatigue resistant than Ti-6Al-4V and the base metal less fatigue resistant.

Ferritic and Martensitic Steels

Several significant conclusions have resulted from investigations on steels. The data in Table C-4 provide results from selected systematic studies. In all cases, particular care was taken by the authors to delineate power-law growth.

TABLE C-3. RESULTS OF POWER-LAW ANALYSIS OF FATIGUE-CRACK GROWTH FOR TITANIUM ALLOYS OTHER THAN Ti-6Al-4V

Alloy	Yield Strength (MNm^{-2})	Thickness (B, mm)	R	m	ΔK ($MNm^{-\frac{3}{2}}$) Actual	ΔK ($MNm^{-\frac{3}{2}}$) Normalized to R = 0[d]	Reference
Commercial Purity	247[a]	2	0.35	4.3	16	19	Robinson & Beevers [19]
	250[a]	2	0.35	4.3	16	19	
	390[a]	2	0.35	4.3	16	19	
Commercial Purity	220[a]	--	0.07	2.7	17	18	Robinson, et al [11]
	260[a]	--	0.07	2.7	17	18	
	260[a]	--	0.70	2.7	17	23	
Ti + 0.27% O_2	--	6	0.1	3.1	15	16	Thompson, et al [13]
Ti + 0.5% O_2	--	6	0.1	3.1	12	13	
4Al-3Mo-1V	860[b,e]	1.25	0.05	2.5	28[c]	28	Boeing [20]
	860[b,e]	1.25	0.67	2.0	17[c]	23	
	1000[b,e]	4.0	0.05	4.9	33[c]	33	
	1000[b,e]	4.0	0.67	3.8	19	25	
	1000[b,e]	12.7	0.05	4.9	33[c]	33	
	1000[b,e]	12.7	0.67	6.1	19	25	
6Al-6V-2Sn	1095[b]	(f)	0.1	2.6	19	20	Amateau, et al [21]
	1126[b]	(f)	0.1	2.6	22	23	
	1038[b]	(f)	0.1	2.6	25	24	
	1194[b]	(f)	0.1	2.6	27	28	
	946[b]	(f)	0.1	2.6	30	31	
	1095[b]	(f)	0.3	2.9	16	19	
	1126[b]	(f)	0.3	2.6	21	24	
	1038[b]	(f)	0.3	2.6	25	28	
	1194[b]	(f)	0.3	1.8	28	31	
7Al-2Nb-1Ta	758	--	0.0	5.0	30	30	Crooker [22]

(a) Variations in yield strength produced by variations in grain size.

(b) Variations in yield strength produced by variations in processing.

(c) Extrapolated.

(d) See Figure C-4.

(e) Estimated.

(f) Designated "Plate".

TABLE C-4. EVALUATION OF CONSTANTS IN FATIGUE-GROWTH EQUATION FOR FERRITIC AND MARTENSITIC STEELS

Steel	Yield Strength (MNm^{-2})	m	ΔK_o ($MNm^{-\frac{3}{2}}$)	Author
Fe-0.08C-0.38Mn	115	2.6	--	Birkbeck, et al [23]
	123	2.9	--	
	134	2.8	--	
	134	2.5	--	
	135	2.7	--	
	178	2.8	--	
	178	2.8	--	
A36 (ferrite/pearlite)	248	3.3	37	Barsom [15]
ABS-C (ferrite/pearlite)	269	3.2	34	
A302-B (ferrite/pearlite)	386	3.0	39	
A537-A (ferrite/pearlite)	407	2.8	35	
HY-80 (martensitic)	655	2.4	36	Barsom [15]
HY-130 (martensitic)	965	2.1	30	
10Ni (martensitic)	1254	2.2	35	
12Ni (martensitic)	1268	2.3	33	
A2 Weld Metal (ferrite/pearlite)	345	2.9	30	Richards & Lindley [24]
Ducol W30B (bainite)	366	2.5	35	
1%C Steel (spherodite)	415	2.9	30	
H1 Weld Metal (bainite)	524	2.5	35	
3Cr-Mo (bainite)	710	2.9	33	
Maraging (annealed)	965	2.5	40	Bathias & Pelloux [25]
Maraging (peak aged)	1791	2.5	40	
Maraging (peak aged)	1688	2.9	--	Miller [26]
Maraging (overaged)	1500	2.5	--	

Note that the crack-growth parameters are quite reproducible and independent of yield strength (Y/E = 0.0006 - 0.007). With regard to the mass of data that do not display values close to those of Table C-4, Richards and Lindley [19] and Ritchie and Knott [20] point out that those data tend to low values of ΔK_o and high values of m and arise when the micromechanism departs from striation formation. A similar effect can be noted in the results of Paton, et al [9], on Ti-6Al-4V. The observed high-growth rates reflect the intrusion of monotonic failure modes and the resultant intrusion of the instability region of Figure C-1 and the accompanying change in fracture mode.

A second point to be made from the results on steel is that the effect of R on power-law crack growth is minimal (Ritchie and Knott [27]). This is not the case for titanium alloys. Thus, it does not currently appear to be possible to generate a universal fatigue-crack-growth law, unless separate R variation is defined for each alloy class. Finally, note in Table C-2 that $\Delta K_o/E$ is about 17 percent higher for Ti-6Al-4V than for steels, suggesting a slightly higher inherent crack-growth resistance.

Aluminum-Base Alloys

Hahn and Simon [18] have reported an extensive survey of the literature on high-strength aluminum alloys. The results in Table C-2, which are extracted from their survey, are for dry atmospheres and intermediate frequencies to be most comparable to the data of other systems. These results appear to show a metallurgical effect, with ΔK_o being somewhat higher for 2024-T3 than for 7075-T6. However, Rosenfield, et al [28], have shown that crack-growth rates in 7075 can be reduced to those characteristic of 2024-T3 by a proper choice of heat treatment, avoiding the toughness minimum associated with the T-6 condition. Furthermore, Garrett and Knott [29] have evidence that intrusion of monotonic fracture modes increases both the m value and the apparent effect of R. Thus, it is possible that the "real" behavior of aluminum alloys is closer to that of steel than generally believed.

Austenitic Steels

The only major difference in power-law behavior among the alloys surveyed was found in austenitic steels. Over most of the range, growth rates for these

materials are significantly slower than for all of the other alloys. The results cited in Table C-2 are from Thompson's [17] survey. He points out that the large exponent is observed despite the presence of striations. Bathias and Pelloux [25] report that the curve of stristion spacing versus ΔK is the same for austenitic and maraging steels. However, the striations in maraging steels are aligned normal to the crack front while those in austenitic are at various angles in different grains. They suggest that the crack front advances piecemeal along its length, accounting for the discrepancy in macroscopic and microscopic growth rates.

These observations have implications for development of models of crack growth. Austenitic steels are an extreme example of planar slip materials--dislocation lines tend to remain straight and not to cross slip. In contrast, the other materials surveyed cross slip extensively and form dislocation tangles. This well-known difference in monotonic deformation patterns is also observed after cyclic straining (Abdel-Raouf, et al [30]). The extreme change in microscopic deformation behavior apparently does not affect the microscopic growth rate (i.e., striation configuration) leading to the probability that highly artificial dislocation models of crack-tip deformation patterns may be sufficient to analyze crack growth.

Upper and Lower Limits of the Power-Law Range in Ti-6Al-4V

Threshold Region

As yet, there is not sufficient evidence to define threshold behavior. On the particularly important question of the effect of strength and microstructure, the evidence is conflicting. Irving and Beevers [7] find that microstructural changes strongly affect $\Delta a/\Delta n$ in the threshold region, while Crooker and Krause [1] come to the opposite conclusion. The situation is compounded because this is the region of very low growth rates where experimental errors are expected to be greatest. As a result, it is not yet possible to define a general fatigue-crack-growth law for rates below the power-law region for Ti-6Al-4V. However, Weiss and Lal [31] have suggested a three-parameter curve based on Neuber analysis which appears to be a reasonable basis for further development.

The data in Table C-5 suggest that the transition from threshold behavior to power-law growth occurs in the range 0.01 - 0.4 μm/cycle, corresponding to ΔK values of $\sim$ 8 - 20 $MNm^{-\frac{3}{2}}$. This corresponds to the cleavage-striation mechanism change observed by Yuen, et al [2]. It is suggested that an intermediate value of $\Delta K = 13\ MNm^{-\frac{3}{2}}$ be tentatively adopted as the lower limit of power-law growth.

Instability Region

As with threshold behavior, it is not yet possible to make any definite conclusions regarding the onset of instability. The appearance of dimpled rupture on the fracture surface suggests a connection with K_c and there is an indication that the ΔK values associated with the upper cutoff of the power-law region are higher in tougher alloys. To account for crack growth in the instability region, it is suggested that the empirical equation of Forman, et al [33] be used since it has been applied successfully to Ti-6Al-4V (Feddersen and Hyler [5]). A modified form of Equation (C-1) is

$$\frac{\Delta a}{\Delta n} = \frac{\alpha \Delta K^m}{(1 - R)\frac{K_c}{\Delta K} - 1} \quad \text{(instability region)} \quad . \tag{C-3}$$

The upper cutoff of the power-law region is then found by equating Equations (C-1) and (C-3) so that the transition condition becomes

$$\frac{\Delta K}{K_c} = \frac{1 - R}{2} \quad . \tag{C-4}$$

The available data in Table C-5 are in fair agreement with Equation (C-4) so that it can be considered a reasonable, if not exact, criterion.

Discussion

Research in fatigue-crack growth over the past few years has revealed that microstructural variations can play a significant role. Depending on the ΔK level and on the composition/processing history, at least four different mechanisms are operative in Ti-6Al-4V: cleavage, dimpled rupture, striation formation, and secondary cracking. While not enough information is available

TABLE C-5. UPPER AND LOWER LIMITS OF THE POWER-LAW REGIME IN FATIGUE-CRACK GROWTH OF Ti-6Al-4V

Curve No.(a)	Lower Cutoff			Upper Cutoff			K_c	Reference
	$\Delta a/\Delta n$ (μm/cycle)	ΔK ($MNm^{-\frac{3}{2}}$)	K max ($MNm^{-\frac{3}{2}}$)	$\Delta a/\Delta n$ (μm/cycle)	ΔK ($MNm^{-\frac{3}{2}}$)	K max ($MNm^{-\frac{3}{2}}$)	($MNm^{-\frac{3}{2}}$)	
1	0.34	26	26	--	--	--	--	Bates & Clark [3]
2	0.04	9	13	--	--	--	--	Bucci, et al [4]
3	0.04	11	16	--	--	--	--	
4	0.22	22	22	9.0	69	69	>175	Crooker & Krause [1]
5	0.16	22	22	6.1	62	72	72	Crooker [32]
6	--	--	--	3.4	44	44	72	
7	0.28	22	22	3.4	44	44	68	
8	0.10	~10	~11	43	103	114	~297	Fedderson & Hyler [5]
9	0.13	10	17	38	88	147	~297	
11	--	--	--	1.5	29	31	--	Harrigan [6]
12	0.05	12	18	6.4	39	56	--	
13	0.05	12	18	--	--	--	--	
14	0.15	11	16	2.5	25	35	--	
15	0.02	9	25	--	--	--	--	Irving & Beevers [7]
16	0.02	9	25	--	--	--	--	
17	0.01	10	11	--	--	--	--	
18	0.02	9	25	--	--	--	--	
19	0.01	10	26	--	--	--	--	
20	0.38	22	24	--	--	--	--	Jones [8]
21	0.10	15	21	2.0	30	43	101	Paton, et al [9]
22	0.15	20	30	4.7	44	62	--	
23	--	--	--	3.4	24	34	--	
24	--	--	--	3.4	24	34	--	
26	0.03	8	24	>0.02	>14	>43	--	Robinson, et al [11]
27	0.08	10	30	>0.02	>18	>55	--	
28	0.10	19	21	--	--	--	78	Thompson [12]
29	0.13	21	24	--	--	--	84	
30	0.11	21	24	--	--	--	~83	
31	0.20	19	21	--	--	--	~75	
32	--	--	--	2.5	19	21	75	Thompson, et al [13]
33	0.04	8	9	--	--	--	84	
34	0.02	10	11	--	--	--	--	
35	0.09	15	17	--	--	--	--	Yoder, et al [14]
36	0.06	18	20	--	--	--	--	
41	--	--	--	0.25	15	50	66	Yuen, et al [2]

(a) See Table C-1.

on cleavage, it appears that the growth rates can be improved by promoting secondary cracking and inhibiting dimpled rupture. Also, it is reasonable to conclude that any crack-growth equation must take into account the micromechanism. For example, the value of K_{max} should enter into the equation in a different way when the fracture surface displays dimpled rupture than when it is completely striated.

Because of these microstructural variations, it is not yet possible to define a "master curve" for fatigue-crack growth in Ti-6Al-4V. Instead, equations of "typical behavior" are offered in Table C-6. The equations are useful for making preliminary estimates of the behavior of off-the-shelf pieces and provide a standard to decide whether a given microstructure displays outstandingly good or outstandingly poor behavior. Furthermore, it should be emphasized that the microstructural effect is sufficiently large that as of now actual crack-growth measurements are the only satisfactory method of accurately determining growth rate data in a given piece of this alloy.

Despite this, the relative insensitivity of growth rates via the striation mechanism to normalized stress intensity, $\Delta K_o/E$ (Table C-2), remains. This well-known phenomenon provides an unsolved problem and suggests some difficulties in attaining major improvements in growth-rate resistance.

References

1. Crooker, T. W., and Krause, D. J., "Fatigue Crack Growth Rates in Ti-6Al-4V Alloys at Various Yield Strength and Fracture Toughness Levels", First Progress Report, Naval Research Laboratory, 1972, p 18.

2. Yuen, A., Hopkins, S. W., Leverant, G. R., and Rau, C. A., "Correlations Between Fracture Surface Appearance and Fracture Mechanics Parameters for Stage II Fatigue Crack Propagation in Ti-6Al-4V", Met. Trans., Vol 5, 1974, p 1833.

3. Bates, R. C., and Clark, W. G., Jr., "Fractography and Fracture Mechanics", Transactions of American Society for Metals, Vol 62, 1969, p 380.

4. Bucci, R. J., Paris, P. C., Hertzberg, R. W., Schmidt, R. A., and Anderson, A. F., "Fatigue Threshold Crack Propagation in Air and Dry Argon for a Ti-6Al-4V Alloy", ASTM STP 513, American Society for Testing and Materials, p 125.

TABLE C-6. EQUATIONS DESCRIBING TYPICAL FATIGUE-CRACK-GROWTH BEHAVIOR IN Ti-6Al-4V

S.I. Units[a]	English Units[b]

In terms of stress-ratio, $R = K_{min}/K_{max}$

$$\frac{\Delta a}{\Delta n} = \frac{6.82 \times 10^{-6}}{f}\left(\frac{\Delta K}{1 - 0.4R}\right)^{3.4} = \frac{3.70 \times 10^{-4}}{f}\left(\frac{\Delta K}{1 - 0.4R}\right)^{3.4}$$

Provided

$\Delta K \geq 13\ MNm^{-\frac{3}{2}}$ $\qquad$ $\Delta K \geq 12\ ksi\sqrt{in.}$

$$f = \begin{cases} 1 \ ; \ \Delta K \geq \dfrac{(1 - R)\ K_c}{2} \\ \left[(1 - R)\ \dfrac{K_c}{\Delta K}\right] - 1 \ ; \ \Delta K \geq \dfrac{(1 - R)\ K_c}{2} \end{cases}$$

In terms of maximum stress intensity, K_{max}

$$\frac{\Delta a}{\Delta n} = \frac{3.87 \times 10^{-5}}{f}\left(\frac{\Delta K}{1 + \frac{2}{3}\frac{\Delta K}{K_{max}}}\right)^{3.4} = \frac{2.10 \times 10^{-3}}{f}\left(\frac{\Delta K}{1 + \frac{2}{3}\frac{\Delta K}{K_{max}}}\right)^{3.4}$$

Provided

$\Delta K \geq 13\ MNm^{-\frac{3}{2}}$ $\qquad$ $\Delta K \geq 12\ ksi\sqrt{in.}$

$$f = \begin{cases} 1 \ ; \ K_{max} \leq \dfrac{K_c}{2} \\ \dfrac{K_c}{K_{max}} - 1 \ ; \ K_{max} \geq \dfrac{K_c}{2} \end{cases}$$

(a) Growth rates in μm/cycle, stress intensities in $MNm^{-\frac{3}{2}}$.

(b) Growth rates in μin/cycle, stress intensities in $ksi\sqrt{in.}$

5. Feddersen, C. E., and Hyler, W. S., "Fracture and Fatigue-Crack-Propagation Characteristics of ½-Inch Mill-Annealed Ti-6Al-4V Titanium Alloy Plate", Final Report from Battelle's Columbus Laboratories to Naval Air Development Center, 1971.

6. Harrigan, M. J., "B-1 Fracture Mechanics Data for Air Force Handbook Usage", North American Rockwell Company, TFD-72-501-1, 1972.

7. Irving, P. E., and Beevers, C. J., "The Effect of Air and Vacuum Environments on Fatigue Crack Growth Rates in Ti-6Al-4V", Met. Trans., Vol 5, 1974, p 391.

8. Jones, R. E., "Fatigue Crack Growth Retardation After Single-Cycle Peak Overload in Ti-6Al-4V Titanium Alloy", Eng. Fract. Mech., Vol 5, 1973, p 585.

9. Paton, N. E., Williams, J. C., Chesnutt, J. C., and Thompson, A. W., "The Effects of Microstructure on the Fatigue and Fracture of Commercial Titanium Alloys", paper presented at NATO/AGARD Brussels Meeting, April 1975.

10. Pittinato, G. F., "Hydrogen-Enhanced Fatigue Crack Growth in Ti-6Al-4V ELI Weldments", Met. Trans., Vol 3, p 235.

11. Robinson, J. L., Irving, P. E., and Beevers, C. J., "An Analytic Approach to Low Stress Fatigue Crack Growth in Titanium", Third International Conference on Fracture, paper V-343, 1973.

12. Private communication to A. W. Thompson, Rockwell International Science Center, 1975.

13. Thompson, A. W., Frandsen, J. D., and Williams, J. C., "The Effect of Grain Size and Oxygen Content on the Fatigue Crack Growth Rate in Titanium", Metal Sci., Vol 9, No. 46, 1975.

14. Yoder, G. R., Cooley, L. A., and Crooker, T. W., "Fatigue Crack Propagation Resistance of Beta-Annealed Ti-6Al-4V Alloys of Differing Interstitial Oxygen Contents", Sixth Progress Report, Naval Research Laboratory, 1975.

15. Barsom, J. M., "Fatigue-Crack Propagation in Steels of Various Yield Strengths", paper presented at First National Congress on Pressure Vessels and Piping, ASME, San Francisco, California, 1971.

16. Rhodes, C. G., and Williams, J. C., "Observations of an Interface Phase in the α/β Boundaries in Titanium Alloys", Met. Trans., Vol 6A, 1975, p 1670.

17. Thompson, A. W., "Fatigue Crack Propagation in Austenitic Stainless Steels", Eng. Fract. Mech., Vol 7, 1975, p 61.

18. Hahn, G. T., and Simon, R., "A Review of Fatigue Crack Growth in High Strength Aluminum Alloys and the Relevant Metallurgical Factors", Eng. Fract. Mech., Vol 5, 1973, p 523.

19. Titanium Science & Technology, Edited by R. I. Jaffee and H. M. Burte, Plenum, New York (1973), "Some Observations on Fatigue Crack Growth in Alpha-Titanium" (J. L. Robinson and C. J. Beevers), p 1245.

20. "Commercial Supersonic Transport Program, Phase II-C Report", Boeing Company, FAA Contract FA-SS-66-5, 1966.

21. Amateau, M. F., Hanna, W. D., and Kendall, E. G., "The Effect of Microstructure on Fatigue Crack Propagation in Ti-6Al-6V-2Sn Alloy", Air Force Contract No. F04701-70-C-0059, 1970.

22. Crooker, T. W., "Factors Determining the Performance of High-Strength Structural Metals (Slope Transition Behavior of Fatigue Crack Growth Rate Curves)", Twelfeth Progress Report, Naval Research Laboratory, 1970, p 25.

23. Birkbeck, G., Inckle, A. E., and Waldron, G.W.J., "Aspects of Stage II Fatigue Crack Propagation in Low-Carbon Steel", J. Mater. Sci., Vol 6, 1971, p 319.

24. Richards, C. E., and Lindley, T. C., "The Influence of Stress Intensity and Microstructure on Fatigue Crack Propagation in Ferritic Materials", Eng. Fract. Mech., Vol 4, 1972, p 951.

25. Bathias, C., and Pelloux, R. M., "Fatigue Crack Propagation in Martensitic and Austenitic Steels", Met. Trans., Vol 4, 1973, p 1265.

26. Miller, G. A., "Fatigue Fracture Appearance and the Kinetics of Striation Formation in Some High-Strength Steels", Transactions of American Society for Metals, Vol 62, 1969, p 651.

27. Ritchie, R. O., and Knott, J. F., "Mechanisms of Fatigue Crack Growth in Low Alloy Steel", Acta Met., Vol 21, 1973, p 639.

28. Rosenfield, A. R., Rice, C. W., Martin, C. J., Thompson, D. S., and Zinkham, R. E., "Research on Synthesis of High Strength Aluminum Alloys", AFML-TR-74-129, Part I, 1974.

29. Garrett, G. G., and Knott, J. F., "On the Influence of Fracture Mechanisms on Fatigue Crack Propagation in Aluminum Alloys", Met. Trans., Vol 6A, 1975, p 1477.

30. Abdel-Raouf, H., Plumtree, A., and Topper, T. H., "Temperature and Strain Rate Dependence of Cyclic Deformation Response and Damage Accumulation in OFHC Copper and 304 Stainless Steel", Met. Trans., Vol 5, 1974, p 267.

31. Weiss, V., and Lal, D. N., "A Note on the Threshold Condition for Fatigue Crack Propagation", Met. Trans., Vol 5, 1974, p 1946.

32. Crooker, T. W., "The Role of Fracture Toughness in Low-Cycle Fatigue Crack Propagation for High-Strength Alloys", Eng. Fract. Mech., Vol 5, 1973, p 35.

33. Forman, R. G., Kearney, V. E., and Engle, R. M., "Numerical Analysis of Crack Propagation in Cyclic-Loaded Structures", Transactions of American Society of Mechanical Engineers, Vol 89, 1967, p 459.